NASA TECHNICAL NOTE

NASA TN D-6970

NASA TN D-6970

RANDOM RESPONSE OF RECTANGULAR PANELS TO THE PRESSURE FIELD BENEATH A TURBULENT BOUNDARY LAYER IN SUBSONIC FLOWS

by Wei J. Chyu and M. K. Au-Yang

Ames Research Center
Moffett Field, Calif. 94035

NATIONAL AERONAUTICS AND SPACE ADMINISTRATION • WASHINGTON, D. C. • OCTOBER 1972

1. Report No. NASA TN D-6970	2. Government Accession No.	3. Recipient's Catalog No.
4. Title and Subtitle RANDOM RESPONSE OF RECTANGULAR PANELS TO THE PRESSURE FIELD BENEATH A TURBULENT BOUNDARY LAYER IN SUBSONIC FLOWS		5. Report Date October 1972 6. Performing Organization Code
7. Author(s) Wei J. Chyu and M. K. Au-Yang		8. Performing Organization Report No. A-4382
9. Performing Organization Name and Address NASA Ames Research Center Moffett Field, Calif. 94035		10. Work Unit No. 134-14-07-05-00-21 11. Contract or Grant No.
12. Sponsoring Agency Name and Address National Aeronautics and Space Administration Washington, D.C. 20546		13. Type of Report and Period Covered Technical Note 14. Sponsoring Agency Code
15. Supplementary Notes		

16. Abstract

The response of a rectangular panel under the excitation of a turbulent boundary layer with a zero longitudinal mean pressure gradient in a subsonic flow was studied in detail. The method of normal mode was used together with the technique of spectral analysis. Both simply supported and clamped edge conditions of a panel were considered, and the displacement power spectral density of the panel response was computed. The results for the clamped edge panel compare favorably with existing data. Charts of structural acceptance, which provide a framework for estimating the response of other rectangular panels, are presented, and the physical significances of structural acceptances discussed.

17. Key Words (Suggested by Author(s))	18. Distribution Statement
Random vibration Turbulent boundary-layer excitation Normal mode analysis	Unclassified – Unlimited

19. Security Classif. (of this report)	20. Security Classif. (of this page)	21. No. of Pages	22. Price*
Unclassified	Unclassified	101	$3.00

* For sale by the National Technical Information Service, Springfield, Virginia 22151

TABLE OF CONTENTS

SYMBOLS

a	transition amplitude from the β mode to the α mode of vibration
A	surface area of the panel
A_m	normalization factor for ψ_m
b	$\frac{\omega}{U_c}$
c	damping coefficient
$C_{\alpha e}$	equivalent damping coefficient for the α mode
D	$\frac{Eh^3}{12(1-\sigma^2)}$, bending stiffness
E	Young's modulus
f	frequency
$f_\alpha(t)$	generalized force
$\frac{f\ell}{U_c}$	Strouhal number
F_1	$\frac{4f\ell_1}{U_c}$, $F_2 = \frac{4f\ell_2}{U_c}$
F_α	Fourier transform of f_α
$G(\underline{x},\omega)$	$2S(\underline{x},\omega)$ one-sided power spectral density function
$G(\underline{x}',\underline{x}'',\omega)$	$2S(\underline{x}',\underline{x}'',\omega)$ one-sided cross spectral density function
h	thickness of panel
$H_\alpha(\omega)$	frequency response function
$j_{\alpha\beta}(\omega)$	real part of acceptance
$j_{mr}(\omega)$	real part of longitudinal acceptance
$j'_{ns}(\omega)$	transversal acceptance
$J_{\alpha\beta}(\omega)$	acceptance

$k_{\alpha\beta}(\omega)$	negative of imaginary part of acceptance
$k_{mr}(\omega)$	negative of imaginary part of longitudinal acceptance
ℓ_1	panel length in x_1 direction
ℓ_2	panel length in x_2 direction
m_α	generalized mass for the α mode
M_∞	free-stream Mach number
$O_{S_p}(\underline{x}',\underline{x}'',\omega)$	operator corresponding to the pressure disturbance $S_p(\underline{x}',\underline{x}'',\omega)$
$p(\underline{x},t)$	pressure fluctuation acting on the panel
q_∞	dynamic pressure
$q_\alpha(t)$	generalized coordinates
$Q_\alpha(\omega)$	Fourier transform of q_α
$R(\underline{x}',\underline{x}'',\tau)$	cross correlation function
$S(\underline{x}',\underline{x}''\omega)$	two-sided cross spectral density function
$S(\underline{x},\omega)$	two-sided power spectral density function
t	time
T	averaging time
U_∞	free-stream velocity
$U_C(f)$	narrow-band convection velocity
$w(\underline{x},t)$	displacement normal to the panel surface
$W(\underline{x},\omega)$	Fourier transform of w
x_1	location on the panel in the longitudinal (or streamwise) direction
x_2	location on the panel in the lateral direction
$\underline{x}(x_1,x_2)$	coordinate referring to location on the panel
y_1	$\frac{x_1}{\ell_1}$

y_2	$\frac{x_2}{\ell_2}$
$\underline{y}(y_1, y_2)$	normalized coordinates referring to location on the panel
γ_m	roots of the transcendental equations (4) and (5)
δ	boundary-layer thickness
δ^*	displacement boundary-layer thickness
$\delta_{\alpha\beta}$	Kronecker delta
Δ^*	$\frac{\delta^*}{\ell}$
∇^4	$\frac{\partial^4}{\partial x_1^4} + 2\frac{\partial^2}{\partial x_1^2}\frac{\partial^2}{\partial x_2^2} + \frac{\partial^4}{\partial x_2^4}$
$\underline{\xi}$	$\underline{x}' - \underline{x}''$ coordinate referring to the separation distance of two points on the panel
η_1	$y_1' - y_1''$
η_2	$y_2' - y_2''$
$\underline{\eta}(\eta_1, \eta_2)$	$\underline{y}' - \underline{y}''$
μ	mass per unit area of the panel
ν_α	loss factor for the α mode
σ	Poisson ratio
ρ	correlation coefficient
τ	delay time
$\psi_\alpha(\underline{x})$	mode shape function of the panel
$\overline{\psi}_\alpha(\underline{y})$	mode shape function of a panel with unit dimensions
ω	angular frequency
ω_α	natural frequency of the α mode

Subscripts

$\alpha = (m,n)$	mode index
$\beta = (r,s)$	mode index
∞	quantity evaluated at the free stream
1	streamwise direction
2	lateral direction
p	quantities related to the excitation field
d	quantities related to panel displacement

RANDOM RESPONSE OF RECTANGULAR PANELS TO THE PRESSURE FIELD BENEATH A TURBULENT BOUNDARY LAYER IN SUBSONIC FLOWS

Wei J. Chyu and M. K. Au-Yang

Ames Research Center

SUMMARY

The response of a rectangular panel under the excitation of a turbulent boundary layer with a zero longitudinal mean pressure gradient in a subsonic flow was studied in detail. The method of normal mode was used together with the technique of spectral analysis. Simply supported and clamped edge boundary conditions of a panel were assumed. The response of the panel has been expressed in terms of displacement power spectral density. The mode number and frequency in the response computation were extended to 7 and 3000 Hz, respectively.

The results of response computation assuming a clamped edge condition compare favorably with existing experimental data with a clamped edge condition. The simply supported edge condition, however, overestimates the response. The effect of flow velocity on the response is to increase the higher frequency components of the power spectral density per unit excitation.

Charts of structural acceptances, which provide a framework for estimating the response of other rectangular panels, are presented as functions of dimensionless frequency and boundary-layer displacement thickness. Physical significances of the structural acceptances are also discussed, as regards the coincidence of the pressure and flexural waves and the probability of mode transition.

INTRODUCTION

The pressure fluctuations in regions of turbulent attached and separated boundary layers and shock waves adjacent to the surface of aerospace vehicles cause structural vibrations throughout atmospheric flight. The study of these vibrations is important in determining stress, fatigue, life of structures, and noise transmission into the interior of the vehicle. Unfortunately, the analysis of this type of vibration is complicated by the inherent random characteristics of the excitation pressure fields, and the difficulty of analytically describing the vibration of a realistic structure. For these reasons, early investigators of this problem considered only a hypothetical flow field and made the simplifying assumption that the structure, almost invariably either a beam or a rectangular panel, was infinitely large (refs. 1, 2, and 3). This assumption leads to a solution in terms of the mean square displacement of the panel as a whole, but not as a function of location on the panel.

In recent investigations the response of finite-size rectangular panels to the excitation of an attached turbulent boundary layer has been considered, but the panels were assumed to be simply supported (refs. 4 to 6). This assumption simplifies the algebra tremendously, permitting solutions to be expressed in closed forms. Although these theoretical results agree better with experiment than those obtained with the infinite panel assumption, they tend to overestimate the response of a realistic panel. Previous analysis also fails to predict the wave matching accurately between the flexural wave of a panel and the pressure wave. The estimation of this wave matching is important, particularly when the matching occurs at one of the resonant frequencies of the structure, and causes a large structural response. With the advent of modern high speed computers, a theoretical analysis of a finite rectangular panel with clamped edges under the excitation of a turbulent boundary layer is now feasible. Analytical integration in closed forms is not necessary, since numerical integration can be carried out with no algebraic simplification of the integrand. This digital computer oriented approach has the following additional advantages over an analytical approach: (1) The transparency of the problem is preserved, as often the physics of the problem is lost among a great length of closed-form mathematical formulas; (2) future developments are simplified, as the basic computer program can be modified to describe different flow fields and/or different structures.

A research program has therefore been undertaken to improve the analytical capability, and to develop practical computer programs for computing the displacement, velocity and stresses at different locations on realistic panel structures in different flow fields, including attached and separated flows at subsonic, transonic, and supersonic speeds. The first step in this process, discussed in this report, has been to consider the response of a clamped edge panel to the excitation of a subsonic attached turbulent boundary layer. The subsonic case was chosen because of the availability of corresponding excitation data (ref. 7) and response measurements (ref. 6). A similar analysis pertaining to attached and separated supersonic flow is in progress along with tests to obtain corresponding structural response data. For this reason, a computer program has been developed that is in modular form so that additions can be made to the program to accommodate different flow and structural conditions without affecting the rest of the program. The computer program pertaining to the analysis will be published separately.

METHOD OF ANALYSIS

Formulation of Displacement Power Spectral Density (DPSD)

The displacement $w(\underline{x},t)$ of a vibrating panel (fig. 1) is assumed to obey the classical thin plate equation:

$$\mu\ddot{w} + c\dot{w} + D\nabla^4 w = p(\underline{x},t) \tag{1}$$

In the present analysis a uniform plate is considered. Hence μ and D are constants and independent of $\underline{x}$. The above equation with c and p set equal to zero is the equation of free vibration of the plate, of which the solutions $\psi_\alpha(\underline{x})$ are called the natural normal modes of the plate. In the subsequent analysis, it will be assumed that the damping is so small that the natural normal modes and frequencies are not significantly changed. It is assumed further that $w(\underline{x},t)$ can be expanded in terms of $\psi_\alpha(\underline{x})$ as follows:

$$w(\underline{x},t) = \sum_{\alpha} q_{\alpha}(t)\psi_{\alpha}(\underline{x}) \tag{2}$$

Here ψ_{α} is assumed to be properly normalized:

$$\int_A \psi_{\alpha}(\underline{x})\psi_{\beta}(\underline{x})\, d\underline{x} = \delta_{\alpha\beta}$$

Furthermore, it will be assumed that $\psi_{\alpha}(\underline{x})$ can be obtained by separation of coordinates:

$$\psi_{\alpha}(\underline{x}) = \psi_m(x_1)\psi_n(x_2)$$

The term $\psi_{\alpha}(\underline{x})$ will be properly normalized if $\psi_m(x_1)$ and $\psi_n(x_2)$ are normalized:

$$\int_0^{\ell_1} \psi_m(x_1)\psi_n(x_1)dx_1 = \delta_{mn}$$

$$\int_0^{\ell_2} \psi_m(x_2)\psi_n(x_2)dx_2 = \delta_{mn}$$

It can be shown that, for a panel with simply supported edges

$$\psi_m(x_i) = \sqrt{\frac{2}{\ell_i}} \sin \frac{m\pi x_i}{\ell_i} \qquad i = 1, 2 \tag{3}$$

For a panel with clamped edges, ψ_m takes on different forms according to whether m is even or odd:

(a) If m is odd,

$$\psi_m(x_i) = \frac{1}{A_m\sqrt{\ell_i}} \left[\cos \gamma_m\left(\frac{x_i}{\ell_i} - \frac{1}{2}\right) + k_m \cosh \gamma_m\left(\frac{x_i}{\ell_i} - \frac{1}{2}\right)\right] \tag{4}$$

where γ_m are the roots of the equation

$$\tan \frac{\gamma_m}{2} + \tanh \frac{\gamma_m}{2} = 0$$

and

$$k_m = \frac{\sin \frac{\gamma_m}{2}}{\sinh \frac{\gamma_m}{2}}$$

(b) If m is even,

$$\psi_m(x_i) = \frac{1}{A_m\sqrt{\ell_i}}\left[\sin \gamma_m\left(\frac{x_i}{\ell_i} - \frac{1}{2}\right) + k_m \sinh \gamma_m\left(\frac{x_i}{\ell_i} - \frac{1}{2}\right)\right] \tag{5}$$

where γ_m are the roots of the equation

$$\tan \frac{\gamma_m}{2} - \tanh \frac{\gamma_m}{2} = 0$$

The orthogonality condition of the mode shape function can be used to find the normalization factors A_m.

$$A_m = \frac{\sqrt{2\gamma_m}}{Z_m}$$

where

$$Z_m = \gamma_m + \sin \gamma_m + k_m^2 \ (\sinh \gamma_m + \gamma_m) \qquad \text{if } m \text{ is odd}$$

$$= \gamma_m - \sin \gamma_m + k_m^2 \ (\sinh \gamma_m - \gamma_m) \qquad \text{if } m \text{ is even}$$

The numerical values of A_m and γ_m are:

m	A_m	γ_m
1	0.7133	4.730040
2	.7068	7.853202
3	.7071	10.995608
4	.7071	14.137164
5	.7071	17.278758
6	.7071	20.420352

Note that

$$A_m \simeq 0.7071 \qquad \text{for } m \geqslant 3$$

and

$$\gamma_m \simeq \gamma_6 + (m - 6)\,\pi \qquad \text{for } m \geqslant 7$$

The generalized coordinate $q_\alpha(t)$ satisfies the Lagrange equation

$$m_\alpha \ddot{q}_\alpha(t) + C_\alpha \dot{q}_\alpha(t) + K_\alpha q_\alpha(t) = f_\alpha(t)$$

where the generalized mass

$$m_\alpha = \mu \int \psi_\alpha{}^2(\underline{x})d\underline{x} = \mu$$

in view of the orthonormality condition of $\psi_\alpha(\underline{x})$.

Similarly,

$$C_\alpha = c$$

$$K_\alpha = m_\alpha \omega_\alpha{}^2$$

and

$$f_\alpha(t) = \int p(\underline{x},t)\psi_\alpha(\underline{x})d\underline{x} \tag{6}$$

The above Lagrange equation is valid only for viscous damping. With structural damping the corresponding Lagrange equation (ref. 6) takes the form:

$$m_\alpha \ddot{q}_\alpha(t) + K_\alpha(1 + i\nu_\alpha')q_\alpha(t) = f_\alpha(t)$$

where ν_α' is the loss factor corresponding to structural damping. For harmonic solution the above equation can be cast into viscous damping form because $q = (1/i\omega)\dot{q}$. Therefore

$$m_\alpha q_\alpha(t) + C'_{\alpha e} q_\alpha(t) + K_\alpha q_\alpha(t) = f_\alpha(t)$$

where $C'_{\alpha e} = (K_\alpha \nu_\alpha'/\omega)$ is the equivalent viscous damping coefficient. In practice, both viscous and structural damping are present, and the Lagrange equation takes the final form

$$m_\alpha \ddot{q}_\alpha(t) + C_{\alpha e} q_\alpha(t) + K_\alpha q_\alpha(t) = f_\alpha(t) \tag{7}$$

where

$$C_{\alpha e} = C'_{\alpha e} + C_\alpha$$

is the equivalent damping coefficient that takes into account the effect of both viscous and structural damping. The viscous loss factor δ_α' is usually defined by the following relation:

$$C_\alpha = \frac{2K_\alpha \delta_\alpha'}{\omega_\alpha}$$

Hence,

$$C_{\alpha e} = \frac{K_\alpha \nu_\alpha'}{\omega} + \frac{2K_\alpha \delta_\alpha'}{\omega_\alpha}$$

If the combined damping is small, so that the PSD curve is sharply peaked at the natural frequencies, only the frequencies around the neighborhood of the natural frequencies are of interest. Therefore

$$\omega \approx \omega_\alpha$$

and

$$C_{\alpha e} = \frac{K_\alpha}{\omega} (2\delta_\alpha' + \nu_\alpha')$$

$$= \frac{K_\alpha \nu_\alpha}{\omega}$$

where

$$\nu_\alpha = \nu_\alpha' + 2\delta_\alpha'$$

is the combined loss factor for both structural and viscous damping.[1] It is this combined loss factor ν_α that is measured experimentally. The natural frequency ω_α will be computed by the method of Hearman (ref. 8).

The Fourier transform of the Lagrange equation (7) takes the form:

$$Q_\alpha(\omega) = H_\alpha(\omega) F_\alpha(\omega) \tag{8}$$

where[2]

$$H_\alpha(\omega) = \frac{1}{m_\alpha[(\omega_\alpha{}^2 - \omega^2) + i\nu_\alpha \omega_\alpha{}^2]} \tag{9}$$

Equations (2) and (8) together give

$$W(\underline{x},\omega) = \sum_\alpha H_\alpha(\omega) F_\alpha(\omega) \psi_\alpha(\underline{x}) \tag{10}$$

The displacement power spectral density is related to $W_T(\underline{x},\omega)$ by

$$S_d(\underline{x},\omega) = \lim_{T\to\infty} \frac{\pi}{T} W_T{}^*(\underline{x},\omega) W_T(\underline{x},\omega) \tag{11}$$

---

[1] The loss factor ν_α takes into account the effect of hysteretic damping as well as viscous damping. The latter includes the interaction of panel motion on the flow field within and outside the boundary layer, and the effect of acoustical radiation into the interior of the structure (cavity), and into the exterior flow field. The present state of art requires that ν_α be measured experimentally. Development of analytical and experimental methods for the determination of loss factor are in progress.

[2] One can alternatively write $C_{\alpha e} \approx 2K_\alpha \delta_\alpha / \omega_\alpha$ where $2\delta_\alpha = 2\delta_\alpha' + \nu_\alpha'$. This will give $H(\omega) = 1/m_\alpha[(\omega_\alpha{}^2 - \omega^2) + 2i\delta_\alpha \omega_\alpha \omega]$ instead of equation (9). The two expressions are equal at $\omega = \omega_\alpha$.

where W_T is the truncated Fourier transform of w. Equations (7), (8), (10), and (11) together give

$$S_d(\underline{x},\omega) = \sum_{\alpha}\sum_{\beta} H_\alpha(\omega)H_\beta^*(\omega)\psi_\alpha(\underline{x})\psi_\beta(\underline{x})$$

$$\cdot \lim_{T\to\infty} \frac{1}{T}\frac{1}{4\pi} \int_A\int_A\int_{-T}^{T}\int_{-T}^{T} \psi_\alpha(\underline{x}')\psi_\beta(\underline{x}'')p(\underline{x}',t')p(x'',t'')e^{-i\omega(t''-t')}$$

$$\cdot dt'\, dt''\, d\underline{x}'\, d\underline{x}''$$

The excitation cross correlation function $R_p(\underline{x}',\underline{x}'',t)$ and the cross spectral density $S_p(\underline{x}',\underline{x}'',\omega)$ are defined by:

$$R_p(\underline{x}',\underline{x}'',\tau) = \lim_{T\to\infty} \frac{1}{2T}\int_{-T}^{T} p(\underline{x}',t')p(\underline{x}'',t'+\tau)dt' \tag{12}$$

$$S_p(\underline{x}',\underline{x}'',\omega) = \frac{1}{2\pi}\int_{-\infty}^{\infty} R_p(\underline{x}',\underline{x}'',\tau)e^{-i\omega\tau}d\tau \tag{13}$$

Equations (12) and (13) can be used to derive the following expression for S_d:

$$S_d(\underline{x},\omega) = AS_p(\omega)\sum_{\alpha}\psi_\alpha{}^2(\underline{x})|H_\alpha(\omega)|^2 J_{\alpha\alpha}(\omega)$$

$$+ 2AS_p(\omega)\sum_{\alpha\neq\beta}\psi_\alpha(\underline{x})\psi_\beta(\underline{x})H_\alpha(\omega)H_\beta^*(\omega)J_{\alpha\beta}(\omega) \tag{14}$$

α,β counted once

where

$$J_{\alpha\beta}(\omega) = \frac{1}{AS_p(\omega)}\int_A\int_A \psi_\alpha(\underline{x}')\psi_\beta(\underline{x}'')S_p(\underline{x}',\underline{x}'',\omega)d\underline{x}'\, d\underline{x}'' \tag{15}$$

is the familiar structural acceptance first introduced by Powell (ref. 9). Note that it is dimensionless. An empirical formula for $S_p(\underline{x}',\underline{x}'',\omega)$ is given in appendix A, and in appendix B the structural acceptance $J_{\alpha\beta}$ is shown to be equal to the transition amplitude per unit area per unit excitation between the α and β mode of vibration.

Separation Into Real and Imaginary Parts and Factorization of Acceptance

Since $S_p(\underline{x}',\underline{x}'',\omega)$ is a complex function (see appendix A), the structural acceptance is generally complex. Therefore it can be written as

$$J_{\alpha\beta} = j_{\alpha\beta} - ik_{\alpha\beta} \tag{16}$$

Furthermore, with the assumption that both the mode shape function and the excitation can be factored into their respective coordinate components, the acceptances can be factored in the following forms:

$$j_{\alpha\beta} = j'_{ns} j_{mr}$$

$$k_{\alpha\beta} = j'_{ns} k_{mr}$$

for homogeneous turbulence

$$j_{mr}(\omega) = \frac{1}{\ell_1} \int_0^{\ell_1} \int_0^{\ell_1} \psi_m(x_1')\psi_r(x_1'')|\rho_p(\xi_1,0,\omega)|\cos b\xi_1 \; dx_1' \; dx_1''$$

$$j'_{ns}(\omega) = \frac{1}{\ell_2} \int_0^{\ell_2} \int_0^{\ell_2} \psi_n(x_2')\psi_s(x_2'')|\rho_p(0,\xi_2,\omega)|dx_2' \; dx_2''$$

$$k_{mr}(\omega) = \frac{1}{\ell_1} \int_0^{\ell_1} \int_0^{\ell_1} \psi_m(x_1')\psi_r(x_1'')|\rho_p(\xi_1,0,\omega)|\sin b\xi_1 \; dx_1' \; dx_1''$$

Since the correlation coefficients $\rho_p(\xi_1,0,\omega)$ and $\rho_p(0,\xi_2,\omega)$ do not depend on the signs of ξ_1 and ξ_2, that is,

$$\rho_p(\xi_1,0,\omega) = \rho_p(|\xi_1|,0,\omega)$$

$$\rho_p(0,\xi_2,\omega) = \rho_p(0,|\xi_2|,\omega)$$

The above expressions for the acceptances can be simplified considerably if the region of integration is divided into two triangles bounded by the straight lines $x'' = 0$, $x' = \ell$ and $x' = x''$; $x' = 0$, $x'' = \ell$ and $x'' = x'$ and the symmetry property of the mode shape function is used:

$$\psi_m(x) = (-1)^{m+1} \psi_m(\ell - x)$$

The final results are:

$$\left.\begin{aligned} j_{mr}(\omega) &= \frac{2}{\ell_1} \int_0^{\ell_1} \int_0^{x_1''} \psi_m(x')\psi_r(x'')|\rho_p(\xi_1,0,\omega)|\cos b\xi_1 \; dx_1' \; dx_1'' && \text{if } m+r \text{ even} \\ &= 0 && \text{if } m+r \text{ odd} \end{aligned}\right\} \tag{17}$$

$$j'_{ns}(\omega) = \frac{2}{\ell_2} \int_0^{\ell_2} \int_0^{x_2''} \psi_n(x_2')\psi_s(x_2'')|\rho_p(0,\xi_2,\omega)|dx_2'\,dx_2'' \qquad \text{if } n+s \text{ even}$$

$$= 0 \qquad \text{if } n+s \text{ odd} \qquad (18)$$

$$k_{mr}(\omega) = \frac{2}{\ell_1} \int_0^{\ell_1} \int_0^{x_1''} \psi_m(x_1'')\psi_r(x_1'')|\rho_p(\xi_1,0,\omega)|\sin b\xi_1\, dx_1'\,dx_1'' \qquad \text{if } m+r \text{ odd}$$

$$= 0 \qquad \text{if } m+r \text{ even} \qquad (19)$$

A physical argument leading to the second identity of the above equations will be given in appendix B.

Two-Parameter Formulation of Acceptance

As formulated above, the acceptances depend on the panel dimension ℓ_1, ℓ_2, the convection velocity U_c, the frequency ω, and the boundary-layer displacement thickness δ^*. Previous mathematical procedure requires recomputation of acceptances when any one of the above four parameters is changed. Since this recomputation is extremely time consuming, the acceptances have been reformulated as follows so that they do not depend on all of the above parameters. Define:

$$F_i = \frac{4f\ell_i}{U_c}$$

$$y_i = \frac{x_i}{\ell_1}$$

$$\eta_i = y_i' - y_i''$$

$$\Delta_i^* = \frac{\delta^*}{\ell_i}$$

where

$$i = 1, 2$$

The acceptances then take the form:

$$j_{mr}(F_1) = 2 \int_0^1 \int_0^{y_1''} \bar{\psi}_m(y_1')\bar{\psi}_r(y_1'')\left|\rho_p\left(\eta_1,0,\frac{\pi F_1}{2}\right)\right|\cos\frac{\pi F_1 \eta_1}{2}\, dy_1'\,dy_1'' \qquad \text{if } m+r \text{ even}$$

$$= 0 \qquad \text{if } m+r \text{ odd} \qquad (20)$$

$$j'_{ns}(F_2) = 2\int_0^1 \int_0^{y_2''} \bar{\psi}_n(y_2')\bar{\psi}_s(y_2'')\left|\rho_p\left(0,\eta_2,\frac{\pi F_2}{2}\right)\right| dy_2'\, dy_2'' \qquad \text{if } n+s \text{ even}$$

$$= 0 \qquad \text{if } n+s \text{ odd} \qquad (21)$$

$$k_{mr}(F_1) = 2\int_0^1 \int_0^{y_1''} \bar{\psi}_m(y_1')\bar{\psi}_r(y_1'')\left|\rho_p\left(\eta_1,0,\frac{\pi F_1}{2}\right)\right| \sin\frac{\pi F_1 \eta_1}{2}\, dy_1'\, dy_1'' \qquad \text{if } m+r \text{ odd}$$

$$= 0 \qquad \text{if } m+r \text{ even} \qquad (22)$$

Here $\bar{\psi}_m(y)$ are the normalized mode shape functions (eqs. (4) and (5)) with ℓ replaced by unity; the pressure correlation coefficients $|\rho_p(\eta_1, 0, \pi F_1/2)|$, $|\rho_p(0, \eta_2, \pi F_2/2)|$ are as defined in appendix A. In equations (20) to (22), the acceptances now depend on only two parameters, F_i and Δ_i^*. As long as Δ_i^* remains constant, the same acceptance curves can be used to compute the displacement power spectral density of different rectangular panels at different free-stream velocities.

In terms of these new acceptances, the displacement power spectral density takes the form:

$$S_d(\underline{y},f) = S_p(f)\sum_{\alpha} \bar{\psi}_\alpha^2(\underline{y})|H_\alpha(2\pi f)|^2 j_{mm}(F_1) j'_{nn}(F_2)$$

$$+ 2S_p(f)\sum_{\alpha\neq\beta} \frac{\bar{\psi}_\alpha(\underline{y})\bar{\psi}_\beta(\underline{y}) j'_{ns}(F_2)[g_{\alpha\beta} j_{mr}(F_1) + h_{\alpha\beta} k_{mr}(F_1)]}{m_\alpha m_\beta (g_{\alpha\beta}^2 + h_{\alpha\beta}^2)} \qquad (23)$$

where

$$g_{\alpha\beta} = (\omega_\alpha^2 - \omega^2)(\omega_\beta^2 - \omega^2) + \nu_\alpha \nu_\beta \omega_\alpha^2 \omega_\beta^2 \qquad (24)$$

$$h_{\alpha\beta} = \nu_\alpha \omega_\alpha^2 (\omega_\beta^2 - \omega^2) - \nu_\beta \omega_\beta^2 (\omega_\alpha^2 - \omega^2) \qquad (25)$$

Acceptance charts based on equations (20) to (22) have been developed for the case of a rectangular panel under excitation of a turbulent boundary layer in a subsonic flow with a zero-longitudinal mean pressure gradient. The application of these charts in displacement PSD computation is described in appendix C.

RESULTS

The first part of the results from the present analysis includes the response of a clamped edge panel to turbulent flow excitation applied on one side of the panel. The panel properties and flow parameters used for an illustrative computation are given in table 1. The results are shown in figures 2 to 9 along with some results of an identical panel with simply supported edges. Figures 2 to 6 show the structural acceptances for a boundary layer with $\delta^*/\ell_1 = 0.04468$ and

$\delta^*/\ell_2 = 0.06499$, for which the corresponding response data are available from Wilby's experiment (ref. 6). Figure 6 shows the variation of acceptance with boundary-layer displacement thickness. Figure 7 shows the calculated DPSD at the quarter- and midpoints of the panel, together with the corresponding experimental results. Figure 8 depicts the perspective view of the distribution of displacement PSD components at each mode on the panel. Figure 9(a) shows the variation of the displacement PSD with longitudinal distance x_1/ℓ_1, evaluated at the lateral position x_2/ℓ_2 for which the PSD is a maximum for a given mode shown in figure 8. Similarly, figure 9(b) shows the variation of the displacement PSD with lateral distance x_2/ℓ_2 evaluated at the longitudinal position x_1/ℓ_1 for which the PSD is a maximum. PSD results are obtained by truncating the series in equation (23) after the seventh mode. It is found that decreasing the mode number to five, or increasing the mode number to nine, has a negligible effect on the results.

The second part of the results (figs. 10 to 12) are charts of acceptances plotted against the frequency parameter F_i for various Δ_i^*. These charts, together with equation (23), enable the displacement PSD of the response of a clamped edge panel to be computed for attached turbulent boundary-layer excitations in subsonic flow.

DISCUSSION

Structural Acceptances

Coincidence of structural and pressure waves– The response of a panel to a spatial-temporal correlated random pressure fluctuation caused by a turbulent boundary layer is characterized by wave-length matchings between the pressure wave and the flexural waves of the panel; a condition often referred to as "coincidence." It is this peak coincidence that gives rise to large response if it occurs at one of the resonant frequencies of the structure. Coincidence frequencies are identified by peaks of the longitudinal joint acceptance curves (fig. 2). They occur at F (or $4f\ell/U_c$) $\simeq 2m$ for both simply supported and clamped edge panels.

Figure 2 shows that the degree of wavelength matching is highest in the first mode, and decreases with increase of mode number for both boundary conditions. A simply supported panel exhibits a higher degree of matching than a clamped edge panel. Since the joint terms (the first sum on the right-hand side of eq. (23)) involving the joint acceptances account for almost all of the $S_d(\underline{x},\omega)$, it follows that a simply supported panel will undergo a larger mean square displacement than a clamped edge panel.

In the case of a simply supported panel, the peaks occur at $F < 2m$ because of the finiteness of the panel. This means that the flexural wavelength of the panel is shorter than the matching wavelength of the pressure wave. As the mode number is increased, the peaks approach $F = 2m$, the matching condition of an infinite panel, because the panel appears to be infinite when compared with the small wavelengths of the pressure waves at higher mode numbers.

When the panel edges are clamped, the panel boundary has two effects, one due to the finiteness of the panel as stated above, and the other due to the rigidity of the clamped boundary, For a nonresponsive region of a clamped-edge panel the effect appears to be small when compared

with the long pressure waves at the lower modes, and large when compared with the short pressure waves at higher modes. Thus, the effect of the clamped edges is negligible at lower mode matchings. The acceptance curves (fig. 2) show that the peaks at lower mode numbers occur at $F < 2m$, because finiteness of the panel dominates. At higher mode numbers the opposite effect of the nonresponsive part of the panel edges begins to dominate and the peaks shift to $F > 2m$. It is significant that the peaks shift a half wavelength larger than $2m$. Thus, the generally accepted assumption that wave matching always occurs at $F = 2m$ is not true for a finite panel.

Structural acceptances as transition amplitudes– Suppose an arbitrary external force is applied on a structure initially vibrating in the β normal mode. The structure will generally transit into another mode (the α mode) of vibration, which can be a normal mode or a linear superposition of normal modes of vibration. The probability of this transition is called the transition amplitude between the β normal mode, and the α mode when the structure is excited by the specific force in question. It is shown in appendix B that the structural acceptance $J_{\alpha\beta}(\omega)$ is equal to the transition amplitude per unit area per unit excitation from the β to the α mode of vibration when the panel is excited by randomly fluctuating pressure forces.

In the case of two-dimensional panel vibration the transition amplitude is regarded as a product of longitudinal and lateral acceptances. The longitudinal acceptance $j_{mr} - ik_{mr}$ corresponds to the transition amplitude between the mth and the rth mode of vibration of a one-dimensional structure (a beam) under the excitation of the longitudinally correlated component of the pressure force or $|\rho(\xi_1, 0, \omega)|e^{-i\omega\xi_1/U_c}$ in equation (A1). The in-phase part of this longitudinal component of the pressure force gives rise to the real part j_{mr} of the longitudinal acceptance and the out-of-phase part to the imaginary part k_{mr}. The lateral transition amplitude j'_{ns} corresponds to the transition amplitude of another one-dimensional structure under the excitation of the laterally correlated component of the pressure force or $|\rho(0,\xi_2,\omega)|$.

Several interesting characteristics of the transition amplitudes are disclosed by the acceptances in figures 3, 4, and 5. Figures 3 and 4 show that longitudinal transition amplitudes j_{mn} and k_{mn} are typically maximum when $m = n$. In case $m \neq n$ the magnitude decreases with increasing order of the sum of m and n. This implies that the probability of the initial mode remaining in the same mode is the highest and that there is less probability of transition to other modes. The figures also show that the acceptances have maxima at F$\simeq$twice the lower mode number of m or n, indicating that the maximum transitions occur also at coincidence frequencies of the lower mode numbers of m or n.

Figure 5 shows that the lateral acceptances j'_{ns} are small compared with the longitudinal acceptances in figures 3 and 4, particularly at high mode numbers. Since the pressure field is less correlated in the lateral direction, it follows that the lateral acceptances should contribute less to the panel response than longitudinal acceptances (see eq. (23)). The appearance of wave matching in the lateral acceptances is not possible because of the lack of convection velocity in the lateral direction.

Acceptance as a function of F and Δ^*– Typical acceptances as shown in figure 6 vary significantly with $\Delta_1{}^*$ at low Strouhal number F_1, and their dependence on $\Delta_1{}^*$ gradually disappears as F_1 increases. The reduction in dependency on $\Delta_1{}^*$ occurs because high values of F_1 correspond to high frequencies and short pressure wavelengths, and the boundary layer therefore appears to be infinitely thick in comparison with the short pressure waves. This factor was also taken into account when the empirical formulas for the correlation coefficients were derived as shown in

appendix A, where the correlation coefficients are independent of $\Delta_1{}^*$ at high frequencies. This same variation of wavelength with F_1 relative to $\Delta_1{}^*$ causes the acceptances for lower modes to vary more significantly with $\Delta_1{}^*$ than those involving higher modes. This variation can be seen by comparing typical acceptance j_{22} with j_{77} in figures 6(a) and 6(b), respectively.

Structural Response

Displacement PSD as function of frequency– Figures 7(a) and 7(b) show the results of the computed displacement power spectral density (DPSD) at the quarter point of the panel at M_∞ = 0.3 and 0.5, and their comparisons with Wilby's measurements (ref. 6). Results are shown for both clamped edge and simply supported panels. The dimensions and material properties of the panel are listed in table 1. Figure 7(c) shows the results of the calculated panel response at the midpoint of the panel, where no experimental data are available for comparison.

The study of figure 7 discloses that the peaks of the response curve always occur at, or very near, the natural frequencies. The envelope of the peaks in the spectra decays rapidly with frequency to justify the normal mode approach used in the present analysis. The response computation based on the clamped edge boundary condition (figs. 7(a) and 7(b)) agrees better with Wilby's measurements (ref. 6) than with the computations based on the simply supported boundary condition. The results also show that the joint terms (the first sum of eq. (23)) account for almost all of the contribution to DPSD at the peaks. The contribution of the cross terms (the second sum of eq. (23)) to DPSD is completely negligible except at some valleys of the DPSD curve. Powell (ref. 9) showed that because of the orthogonality condition of the mode shape functions, the cross-term contribution to a uniformly loaded surface will be zero when averaged over the entire surface. However, he also pointed out that the cross terms cannot be neglected if damping is appreciable or if the force is applied to a localized area.

When the Mach number is changed from 0.3 to 0.5 (figs. 7(a) and 7(b), the overall shape of the DPSD curve does not change, but the displacement per unit excitation increases at higher frequencies. The corresponding rms displacement per unit pressure input increases by about 11 percent at the quarter point and 17 percent at the midpoint of the panel. This increase in response is attributed to the increase in the spatial correlation of the pressure field at high frequencies as the Mach number is increased. Since pressure excitation also increased with velocity ($\sqrt{p^2} \simeq 0.006\, q_\infty$), the rms displacement of the panel will increase, as a result of both the increase in pressure excitation $S_p(f)$ and the increase in DPSD per unit pressure excitation, $S_d(\underline{x},f)/S_p(f)$.

The computed DPSD at the midpoint of the panel (fig. 7(c)) does not have peaks at natural frequencies, which correspond to antisymmetric modes, because the panel midpoint is a node point for the antisymmetric modes.

Displacement PSD distribution on a panel– Computer programs capable of displaying the perspective view of displacement PSD on a panel were also developed. The displacement PSD on a panel is necessary information for the assessment of the distribution of stress. Typical results given in figure 8 show the distribution of PSD components on a clamped edge panel at natural frequencies corresponding to modes (1-1), (2-1), (1-2), (3-1), and (2-2). Figure 9 shows the variation of maximum displacement PSD with longitudinal and lateral coordinates. Note that when mode m or $n > 1$, the peaks of the PSD next to the panel edge do not occur at exactly

$\ell/2m$ from the edge, as they would in the case of a simply supported panel. The fact that the peaks of the PSD occur at distances greater than $\ell/2m$ from the edge is due to the rigidity of the panel at the clamped edge. Note also that when mode m or $n > 1$ and the mode number is odd (for instance $m = 3$ in fig. 9(a)), the PSD in the middle region of the panel is symmetric, but the PSD next to the panel edge is asymmetric about the respective peaks.

CONCLUSIONS

The study on the response of a rectangular panel under the excitation of a turbulent boundary layer discloses the following:

1. The matching between the pressure wave and the flexural wave of a panel does not occur exactly at even integer values of the reduced frequency $F = 4f\ell/U_c$, as it would when the panel is infinite for two reasons; (a) the finiteness of the panel significantly affects the low frequency matchings, and (b) the rigidity of the clamped boundary significantly affects the high frequency matchings.

2. The structural acceptance $J_{\alpha\beta}$ is equal to the probability of transition, or transition amplitude, from the β mode to α mode of vibration, per unit excitation power spectral density per unit area of the panel, when the panel is excited by the random pressure. The longitudinal transition amplitudes (j_{mn} and k_{mn}) exhibit a general behavior, being maximal when $m = n$. When $m \neq n$, the magnitude decreases with increasing order of the sum of m and n. This decrease implies that the probability of preserving the same mode is higher than the probability of transiting to different modes.

3. An expression that depends only on the dimensionless frequency F_i and boundary layer thickness Δ_i^* can be derived for the structural acceptance. Corresponding acceptance charts were therefore prepared which make possible a quick estimation of the response of any rectangular panel to excitation of a turbulent boundary layer in subsonic flow with a zero longitudinal mean gradient.

4. The lateral acceptances are small compared with the longitudinal acceptances. Since pressure field is less correlated in the lateral direction, the lateral acceptances contribute less to the panel response than longitudinal acceptances.

5. The response computation based on the clamped edge boundary condition of a panel is in better agreement with the measurements than previous results obtained by investigators who used a simply supported boundary condition in the acceptance calculation.

6. As the Mach number is increased within the subsonic range, the response of a panel is also increased in its high frequency components of vibration. The increase is attributed to two factors: the increase in the spatial correlation of the pressure field at high frequencies; and the increase of the magnitude of pressure excitations.

7. The variation of boundary-layer thickness affects only the low frequency component of the response through the structural acceptances, which vary significantly near the low frequency, particularly where the wave matching occurs.

Ames Research Center
National Aeronautics and Space Administration
Moffett Field, Calif. 94035, July 7, 1972

APPENDIX A

RANDOM EXCITATION BY SURFACE PRESSURE FLUCTUATIONS

The pressure fluctuations that occur on a surface adjacent to a turbulent boundary layer have been shown by many investigators (refs. 7 and 10 to 16) to be spatially and temporarily correlated. For homogeneous turbulence, as attached flow, the cross spectral density of the fluctuating pressure depends only on the separation distance and can be expressed in the following form:

$$\frac{S_p(\xi_1,\xi_2,\omega)}{S_p(\omega)} = |\rho(\xi_1,\xi_2,\omega)|e^{-i\omega\xi_1/U_c} \tag{A1}$$

where $|\rho_p(\xi_1, \xi_2, \omega)|$ is the cross correlation coefficient between two points separated by distances of ξ_1 and ξ_2 in the x_1 and x_2 directions. Experimental data also show that the correlation coefficient can be separated in coordinates as follows:

$$|\rho_p(\xi_1,\xi_2,\omega)| = |\rho_p(\xi_1,0,\omega)|\ |\rho_p(0,\xi_2,\omega)| \tag{A2}$$

In the case of a turbulent boundary layer at a zero longitudinal pressure gradient in a subsonic flow, empirical formulas have been constructed for $|\rho_p(\xi_1,0,\omega)|$ and $|\rho_p(0,\xi_2,\omega)|$ based on Bull's experimental data (ref. 7):

$$\left|\rho_p\left(\eta_1,0,\frac{\pi F_1}{2}\right)\right| = e^{-\alpha_1 \frac{\pi F_1}{2}|\eta_1|} \qquad \text{if } \frac{\pi F_1}{2}\Delta_1{}^* \geqslant k_1$$

$$= e^{-\alpha_2|\eta_1|/\Delta_1{}^*} \qquad \text{if } \frac{\pi F_1}{2}\Delta_1{}^* < k_1$$

$$\left|\rho_p\left(0,\eta_2,\frac{\pi F_2}{2}\right)\right| = e^{-\alpha_3\frac{\pi F_2}{2}|\eta_2|} \qquad \text{if } |\eta_2| \geqslant -\left[9.1 \log\left(\frac{\pi F_2}{2}\Delta_2{}^*\right) + 5.45\right]\Delta_2{}^*$$

$$= c + de^{-\alpha_4|\eta_2|/\Delta_2{}^*} \qquad \text{if } |\eta_2| < -\left[9.1 \log\left(\frac{\pi F_2}{2}\Delta_2{}^*\right) + 5.45\right]\Delta_2{}^*$$

where

$\alpha_1 = 0.1$ $\quad$ $c = 0.28$

$\alpha_2 = 0.037$ $\quad$ $d = 0.72$

$\alpha_3 = 0.715$ $\quad$ $k_1 = 0.37$

$\alpha_4 = 0.547$

The convection velocity, U_C, in this mathematical model is given by,

$$U_C = (\kappa_1 + \kappa_2 e^{-\alpha_5 \omega \delta^*/U_\infty})U_\infty \tag{A3}$$

where

$$\kappa_1 = 0.59$$

$$\kappa_2 = 0.30$$

$$\alpha_5 = 0.89$$

APPENDIX B

ACCEPTANCE AS TRANSITION AMPLITUDES BETWEEN TWO NORMAL MODES OF VIBRATION AND ITS SIGNIFICANCE IN PANEL VIBRATION

In view of the importance of acceptances in predicting structural response to random forces, a physical meaning of acceptances is derived below. Suppose a structure is vibrating initially in the β normal mode. If an arbitrary external force is applied, the structure will in general transit into another mode of vibration which can be a linear superposition of normal modes or a pure normal mode. The probability of this transition is called the transition amplitude between the β normal mode and the final mode when the structure is excited by the specific force in question. Since the final mode is, in general, a linear superposition of the normal modes, it can be expressed as $\sum_{\alpha} a_{\alpha\beta}\psi_{\alpha}$, where $a_{\alpha\beta}$ is the transition amplitude between the α and β normal mode.

To show the relationship between the transition amplitude and the acceptance, a mathematical formulation of the above discussion is necessary. In the language of linear algebra, the method of normal mode analysis assumes that the normalized mode shape functions ψ_{α} form an orthonormal basis in a linear space, S, which is the space of all possible vibration modes of the structure. Any mode of vibration is a vector in S and therefore can be expressed as a linear sum of ψ_{α}. The orthonormal condition of ψ_{α} can be expressed mathematically as:

$$\int_A \psi_{\alpha}(\underline{x})\psi_{\beta}(\underline{x})d\underline{x} = \delta_{\alpha\beta} \tag{B1}$$

where the integration is over the entire structure, or in the present case, the area of the rectangular panel. This suggests that the scalar product between two vectors A, B in S can be defined as:

$$\langle A|B\rangle = \int_A A(\underline{x})B(\underline{x})d\underline{x} \tag{B2}$$

In this linear space, a disturbance such as $S_p(\underline{x}',\underline{x}'',\omega)$ is described mathematically by a linear operator $O_{S_p}(\underline{x}',\underline{x}'',\omega)$ in S with the property that if A is a vector in S,

$$O_{S_p}(\underline{x}',\underline{x}'',\omega)A \equiv \int_A d\underline{x}''\, S_p(\underline{x}',\underline{x}'',\omega)A(\underline{x}'') \tag{B3}$$

in accordance with the definition of scalar product in equation (B2). By definition of O_{S_p}, $O_{S_p}A$ is also in S. In particular, when $A = \psi_{\beta}(\underline{x})$, $O_{S_p}\psi_{\beta}$ is also in S. Therefore it can be expanded as follows:

$$O_{S_p}(\underline{x}',\underline{x}'',\omega)\psi_{\beta}(\underline{x}'') = \sum_{\gamma} a_{\gamma\beta}\psi_{\gamma}(\underline{x}')$$

In the case of a flat panel, each of α,β,γ contains two indices such as (1,1), (1,2) . . . (∞,∞). The coefficients $a_{\alpha\beta}$ can be obtained by forming the scalar product between ψ_α and $O_{S_p}(\underline{x}',\underline{x}'',\omega)$ as follows,

$$\left.\begin{aligned}\langle\psi_\alpha(\underline{x}')|O_{S_p}(\underline{x}',\underline{x}'',\omega)\psi_\beta(\underline{x}'')\rangle &= \langle\psi_\alpha(\underline{x}')|\sum_\gamma a_{\gamma\beta}\psi_\gamma(\underline{x}')\rangle \\ &= \sum_\gamma a_{\gamma\beta}\,\langle\psi_\alpha(\underline{x}')|\psi_\gamma(\underline{x}')\rangle \\ &= \sum_\gamma a_{\gamma\beta}\delta_{\alpha\gamma} \\ &= a_{\alpha\beta}\end{aligned}\right\} \tag{B4}$$

By definition of equations (B2) and (B3),

$$\langle\psi_\alpha(\underline{x}')|O_{S_p}(\underline{x}',\underline{x}'',\omega)\psi_\beta(\underline{x}'')\rangle = \int_A\int_A \psi_\alpha(\underline{x}')S_p(\underline{x}',\underline{x}'',\omega)\psi_\beta(\underline{x}'')d\underline{x}'\,d\underline{x}'' \tag{B5}$$

Comparing equations (B4) and (B5) with the definition of the acceptance $J_{\alpha\beta}$,

$$J_{\alpha\beta}(\omega) = \frac{1}{S_p(\omega)A}\iint\psi_\alpha(\underline{x}')S_p(\underline{x}',\underline{x}'',\omega)\psi_\beta(\underline{x}'')d\underline{x}'\,d\underline{x}''$$

the following identification can be established:

$$J_{\alpha\beta}(\omega) = \frac{1}{S_p(\omega)A}a_{\alpha\beta}$$

Thus the acceptance $J_{\alpha\beta}$ is just the transition amplitude per unit PSD of excitation per unit area from the β to the α normal mode of vibration when the structure is excited by the disturbance described by $S_p(\underline{x}',\underline{x}'',\omega)$.

In the case of two-dimensional panel vibration the transition amplitude is a product of longitudinal and lateral acceptances (see equations (14) and (23)). The longitudinal acceptance j_{mr}-ik_{mr} corresponds to the transition amplitude between the m and the r mode of vibration of a one-dimensional structure under the excitation of the longitudinal correlated components of the pressure force. The amplitude of a final mode r formed from initial modes 1, 2, . . . n is proportional to the following sum:

$$\sum_{m=1}^{n}(j_{mr} + k_{mr})$$

where the first sum represents the transitions caused by the in-phase pressure fluctuations, and the second sum by the out-of-phase pressure fluctuations. When any two of the above acceptances

have the same sign at a given frequency, the transition is such that they reinforce each other, giving rise to constructive interference. If they have opposite signs, they cancel each other, giving rise to destructive interference.

During a transition, the parity of the mode must be conserved if the excitation has even parity or symmetry in space, and must change if the excitation has odd parity or antisymmetry in space. Since j_{mr} is proportional to transition amplitude caused by the in-phase pressure force, which is symmetric in space (it contains a cosine term in eq. (20)), j_{mr} must be zero if $m + r$ is odd. On the other hand, since k_{mr} is proportional to the transition amplitude caused by the out-of-phase pressure force, which is antisymmetric in space (it contains a sine term in eq. (22)), k_{mr} must be zero if $m + r$ is even. For the same reason j'_{mr} must be zero if $m + r$ is odd. The physical significance of equations (20) to (22) is thus shown in terms of the parity of modal transition.

APPENDIX C

APPLICATION OF ACCEPTANCE CHARTS IN DISPLACEMENT PSD COMPUTATION

Values of $j_{mr}(F_1)$, $k_{mr}(F_1)$, and $j'_{ns}(F_2)$ up to the seventh mode have been computed and plotted in figures 10 through 12 for F up to 15.0, and Δ_i* ranging from 0.015 to 0.08 in increments of 0.01, for a clamped edge rectangular panel under boundary layer excitations. These charts, together with equation (23), enable the displacement PSD be computed for a clamped edge rectangular panel exposed to a subsonic freestream velocity. The procedure is to compute the U_C first, using equation (A3). Then, knowing the dimensions of the panel and the boundary layer displacement thickness, the two parameters F_i and Δ_i* can be computed. The corresponding acceptances can be read from the charts and substituted into equation (23) with natural frequencies and loss factors which can be determined experimentally or analytically. The method of linear interpolation can be used if Δ_i* does not coincide exactly with one of the values at which the acceptances are evaluated.

REFERENCES

1. Corcos, G. M,; and Liepmann, H. W.: On the Contribution of Turbulent Boundary Layers to the Noise Inside a Fuselage. NACA TM 1420, 1956.

2. Ribner, H. S.: Boundary-Layer-Induced Noise in the Interior of Aircraft, University of Toronto. U.T.I.A. Rep. 37, 1956.

3. Kraichnan, R. H.: Noise Transmission From Boundary Layer Pressure Fluctuations. J. Acoust. Soc. Amer., vol. 29, no. 1, Jan. 1957, pp. 65-80.

4. Strawdermann, Wayne A.: Turbulent-Induced Plate Vibrations: An Evaluation of Finite and Infinite-Place Models, J. Acoust. Soc. Amer., vol. 46, no. 5, pt. 2, 1969, pp. 1294-1307.

5. Bozich, Daniel J.: Spatial Correlation in Acoustic-Structural Coupling. J. Acoust. Soc. Amer., vol. 36, no. 1, Jan. 1964, pp. 52-58.

6. Wilby, John F.: The Response of Simple Panels to Turbulent Boundary Layer Excitation. AFFDL-TR-67-70 Oct. 1967.

7. Bull, M. K.: Wall-Pressure Fluctuations Associated with Subsonic Turbulent Boundary Layer Flow. J. Fluid Mech., vol. 28, pt. 4, 22 June 1967, pp. 719-754.

8. Hearman, R. F. S.: The Frequency of Flexural Vibration of Rectangular Orthotropic Plates with Clamped or Supported Edges, J. Appl. Mech. vol. 26, Ser. E, no. 4, Dec. 1959, pp. 537-540.

9. Powell, Alan: On the Fatigue Failure of Structures Due to Vibrations Excited by Random Pressure Fields, J. Acoust. Soc. Amer., vol. 30, no. 12, Dec. 1958, pp. 1130-1135.

10. Harrison, Mark: Pressure Fluctuations on the Wall Adjacent to a Turbulent Boundary Layer. David Taylor Model Basic Rep. 1260, Dec. 1958.

11. Serafini, John S.: Wall-Pressure Fluctuations and Pressure-Velocity Correlations in a Turbulent Boundary Layer. NASA TR R-165, 1963.

12. Willmarth, W. W.; and Wooldridge, C. E.: Measurements of the Fluctuating Pressure at the Wall Beneath a Thick Turbulent Boundary Layer. J. Fluid Mech., vol. 14, pt. 2, Oct. 1962, pp. 187-210.

13. Kistler, A. L.; and Chen W. S.: The Fluctuating Pressure Field in a Supersonic Turbulent Boundary Layer. J. Fluid Mech. vol. 16, pt. 1, May 1963, pp. 41-64.

14. Speaker, W. V.; and Ailman, C. M.: Spectra and Space-Time Correlations of the Fluctuating Pressures at a Wall Beneath a Supersonic Turbulent Boundary Layer Perturbed by Steps and Shock Waves. NASA CR-486, 1966.

15. Coe, Charles F.: Surface-Pressure Fluctuations Associated with Aerodynamic Noise. NASA SP-207, 1969, pp. 409-424.

16. Chyu, Wei J.; and Hanly Richard D.: Power- and Cross-Spectra and Space-Time Correlations of Surface Fluctuating Pressures at Mach Numbers Between 1.6 and 2.5. NASA TN D-5440, 1969.

TABLE 1.– PANEL PROPERTIES AND FLOW PARAMETERS

[Ref. 6]

Mild steel panel	
ℓ_1	0.1016 m (4 in.)
ℓ_2	0.06985 m (2.75 in.)
h	0.000381 m (0.015 in.)
E	0.2323×10^{12} N/m^2 (33.7×10^6 lb/in.^{2})
σ	0.3
ν	0.009
Density	
	7473 kg/m^3 (0.27 lb/in.^{3})
Flow parameters	
M_∞	0.3 and 0.5
δ^*	0.00454 m (0.179 in.)

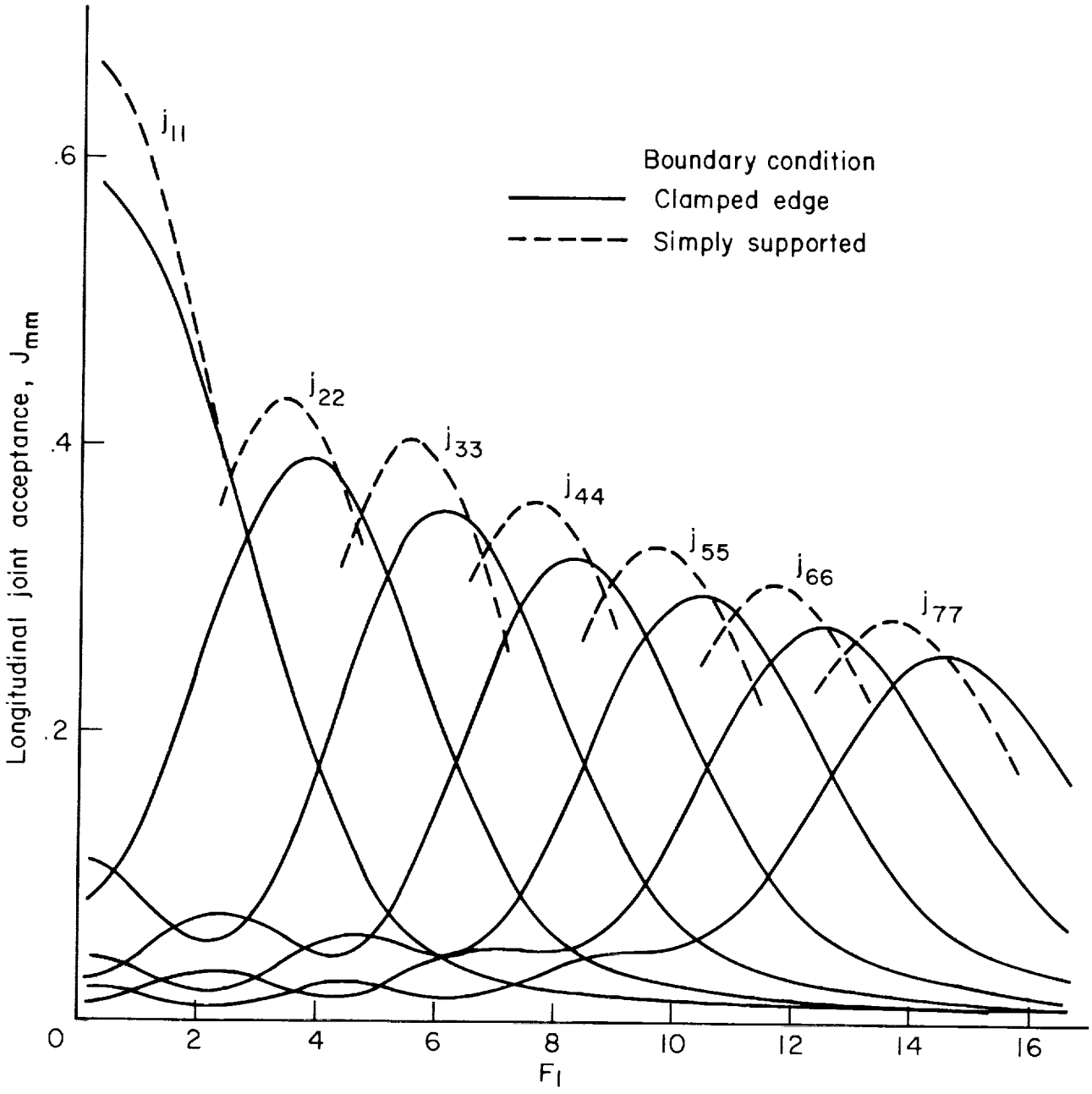

Figure 2.– Longitudinal joint acceptances of clamped and simply supported panel for $\Delta_1^* = 0.04468$.

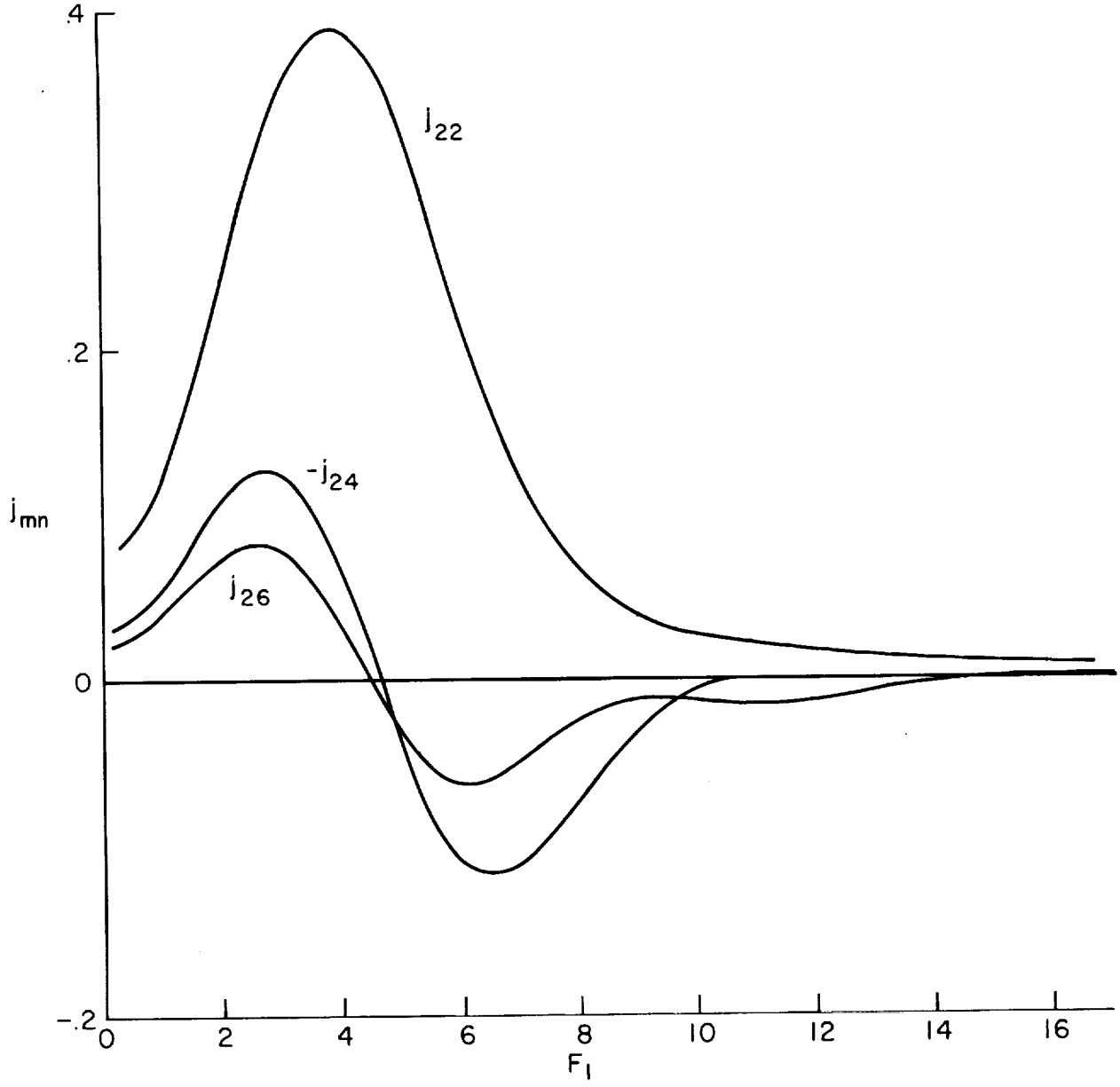

(a) j_{22}, $-j_{24}$, j_{26}

Figure 3.– Real part of longitudinal acceptances of clamped edge panels for $\Delta_1^* = 0.04468$.

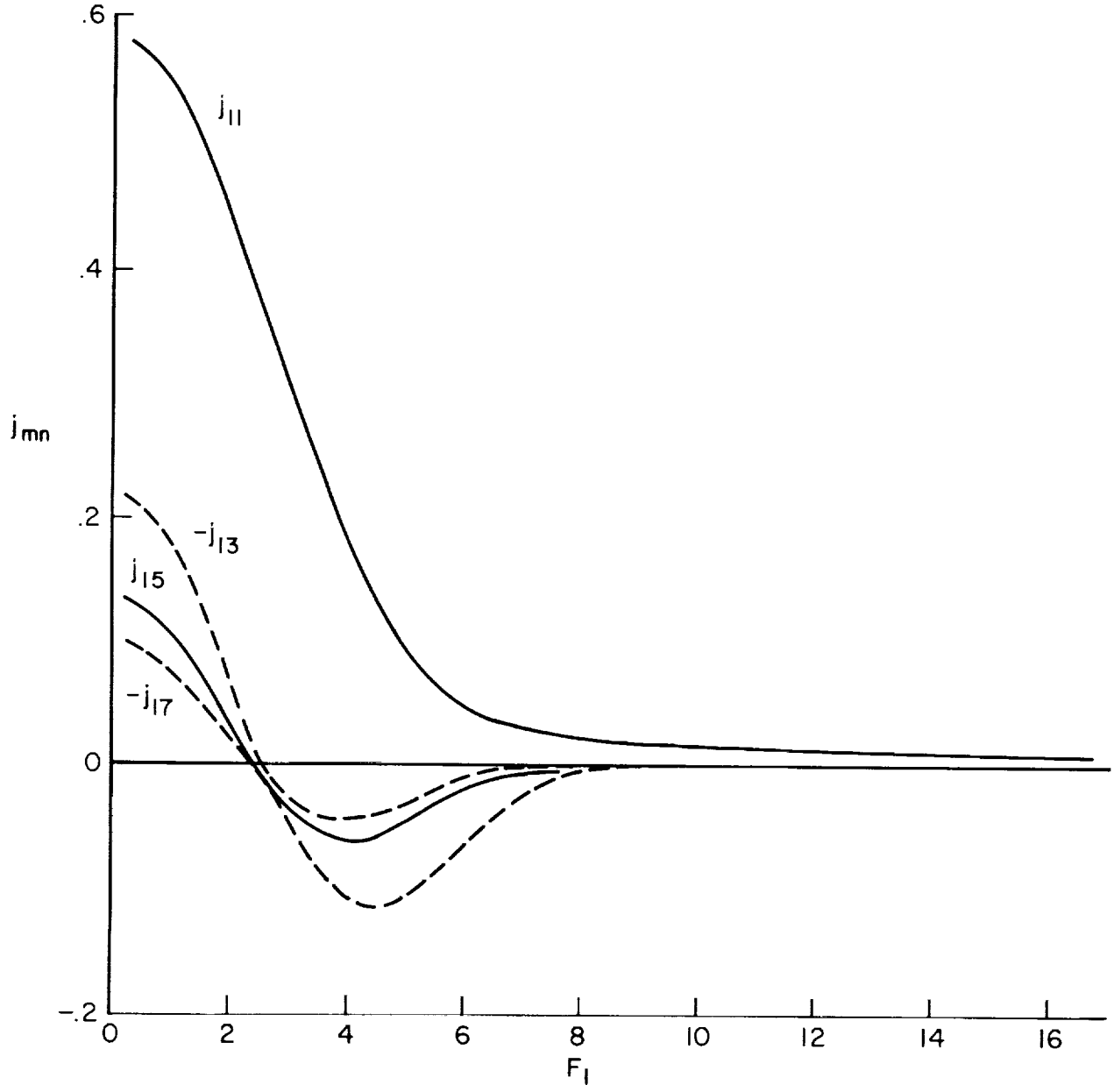

(b) j_{11}, $-j_{13}$, j_{15}, $-j_{17}$

Figure 3. – Continued.

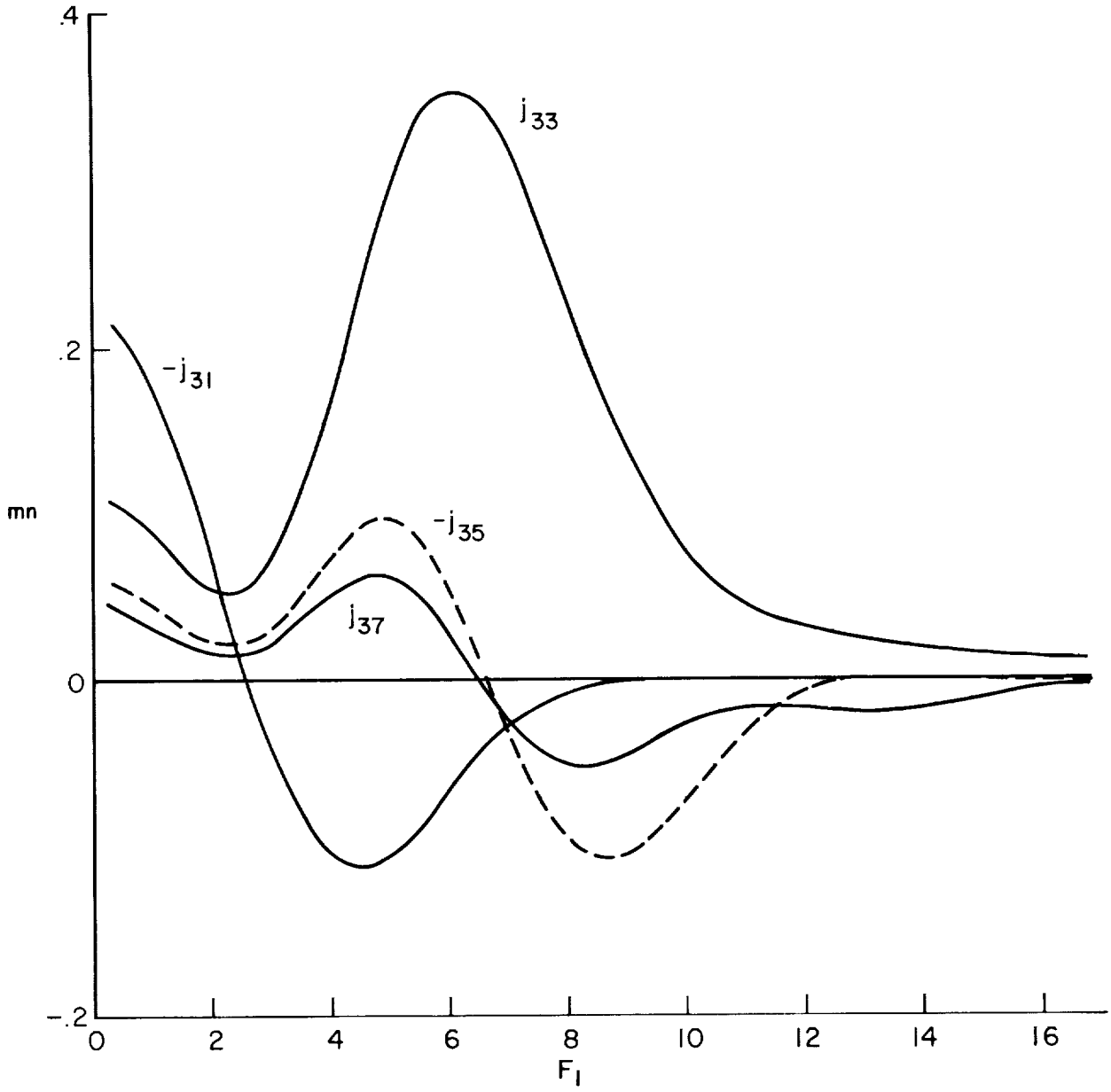

(c) $-j_{31}, j_{33}, -j_{35}, j_{37}$

Figure 3. – Continued.

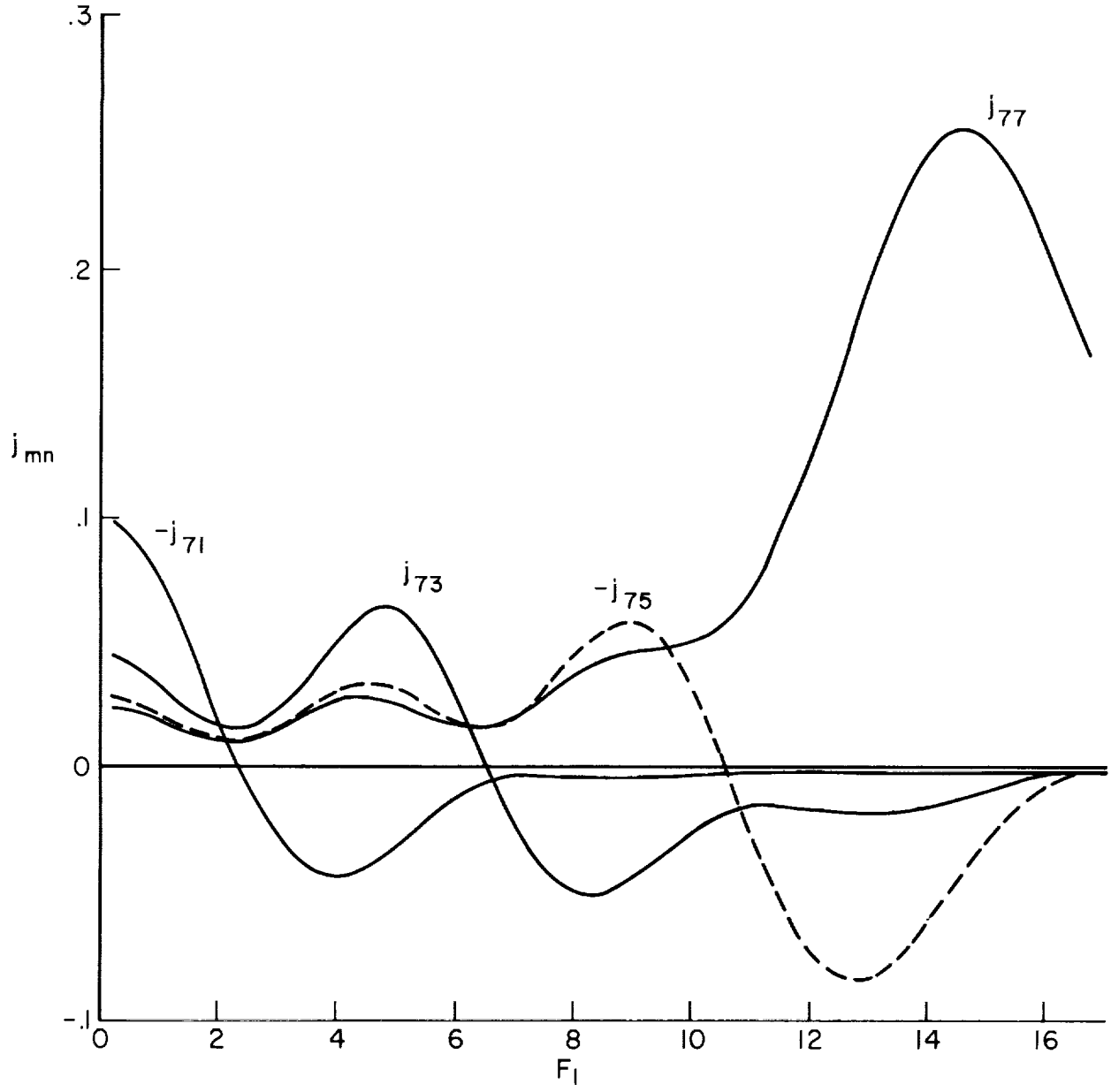

(d) $-j_{71}$, j_{73}, $-j_{75}$, j_{77}

Figure 3. – Concluded.

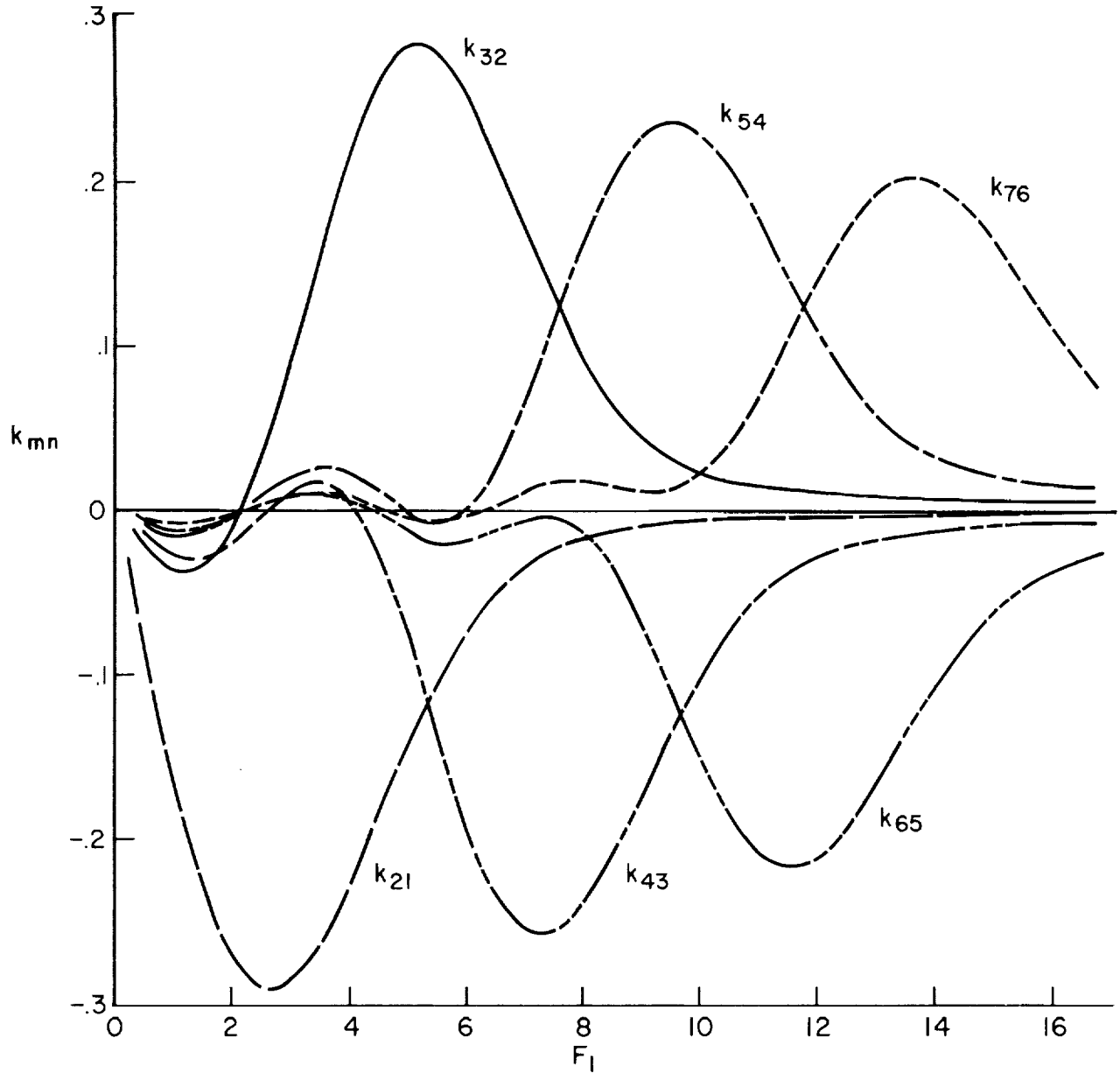

(a) k_{32}, k_{54}, k_{76}, k_{21}, k_{43}, k_{65}

Figure 4.– Imaginary part of longitudinal acceptances of clamped edge panels for $\Delta_1^* = 0.04468$.

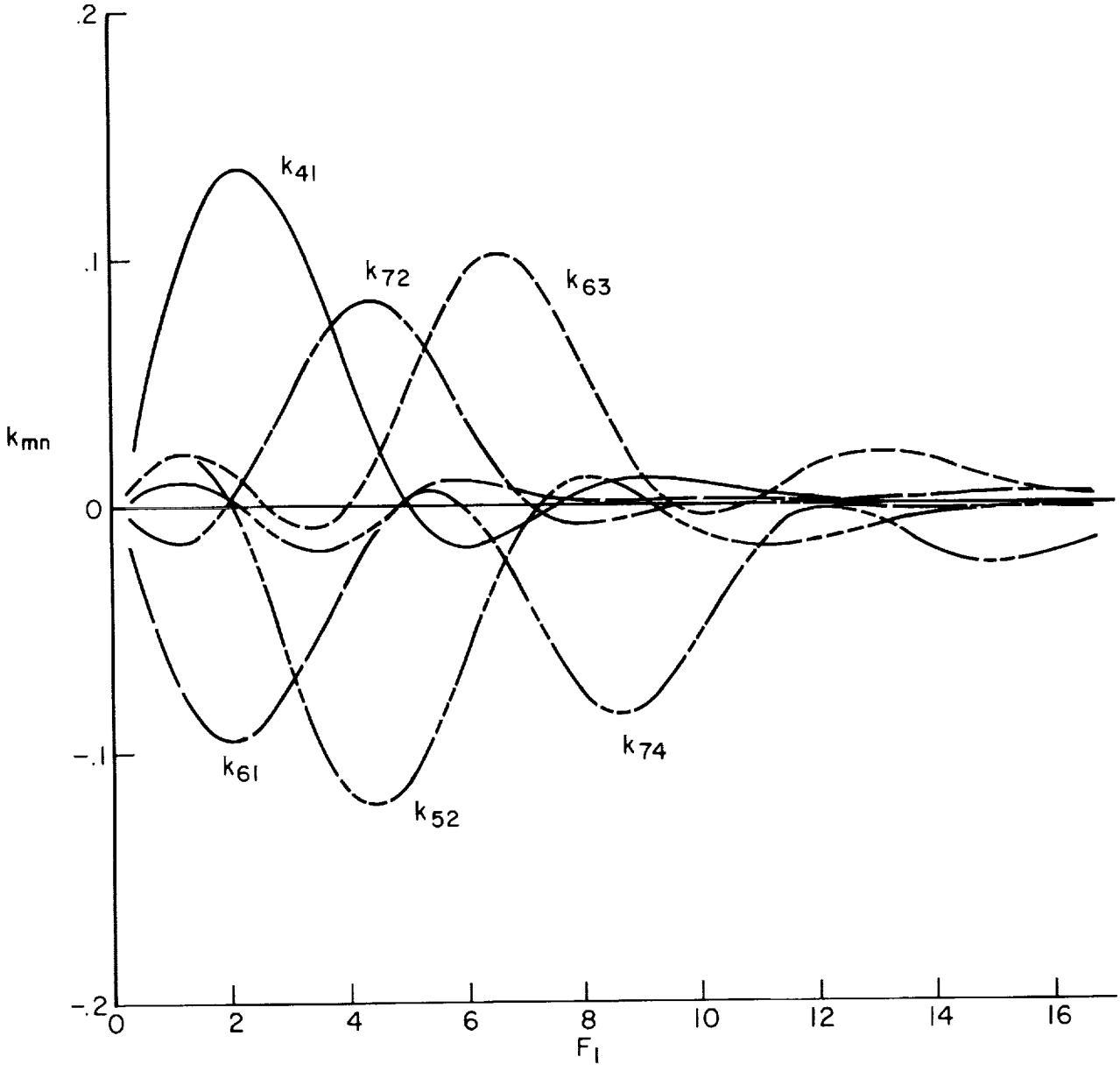

(b) k_{41}, k_{72}, k_{63}, k_{61}, k_{52}, k_{74}

Figure 4. – Continued.

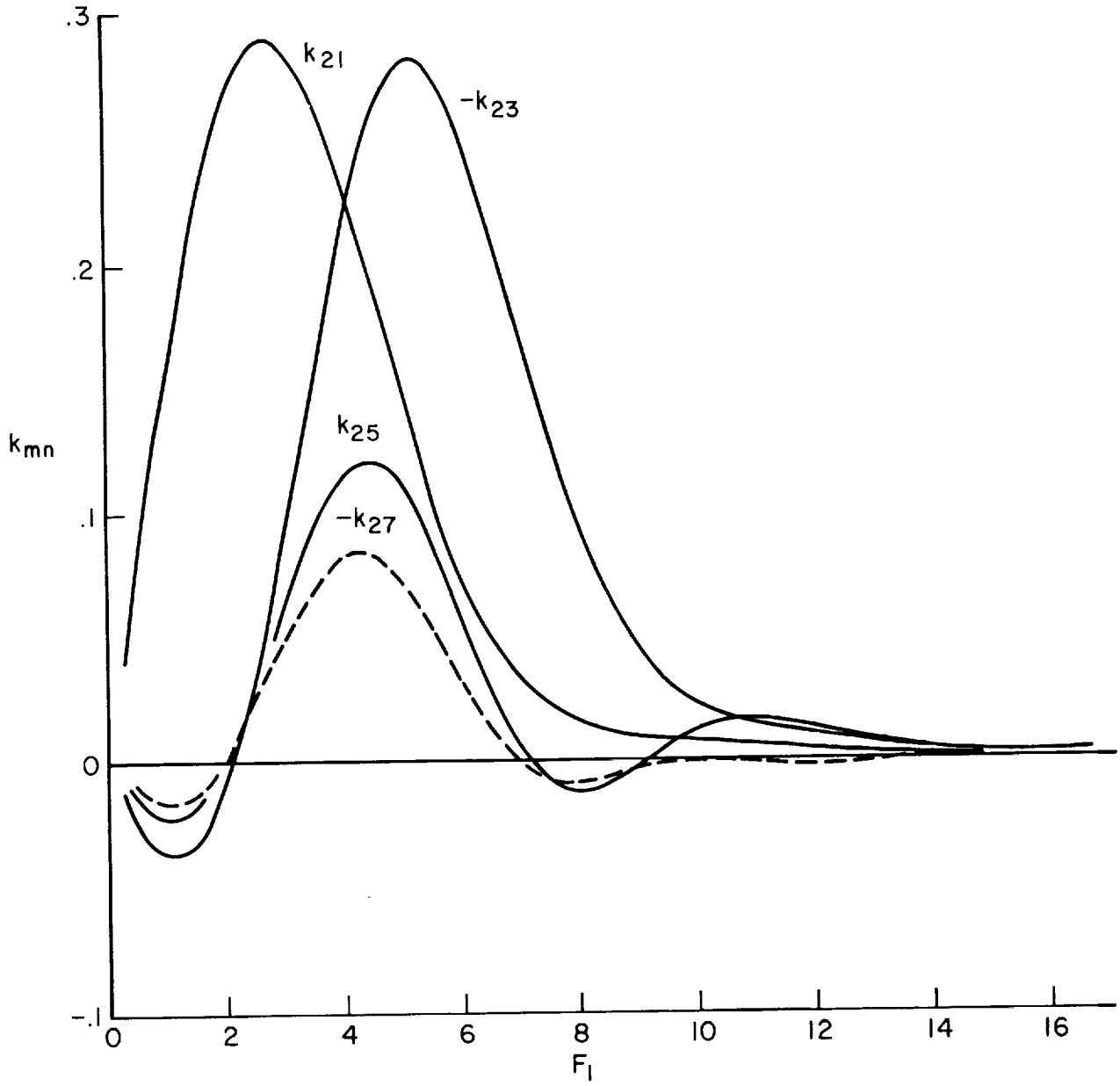

(c) k_{21}, $-k_{23}$, k_{25}, k_{27}

Figure 4. – Concluded.

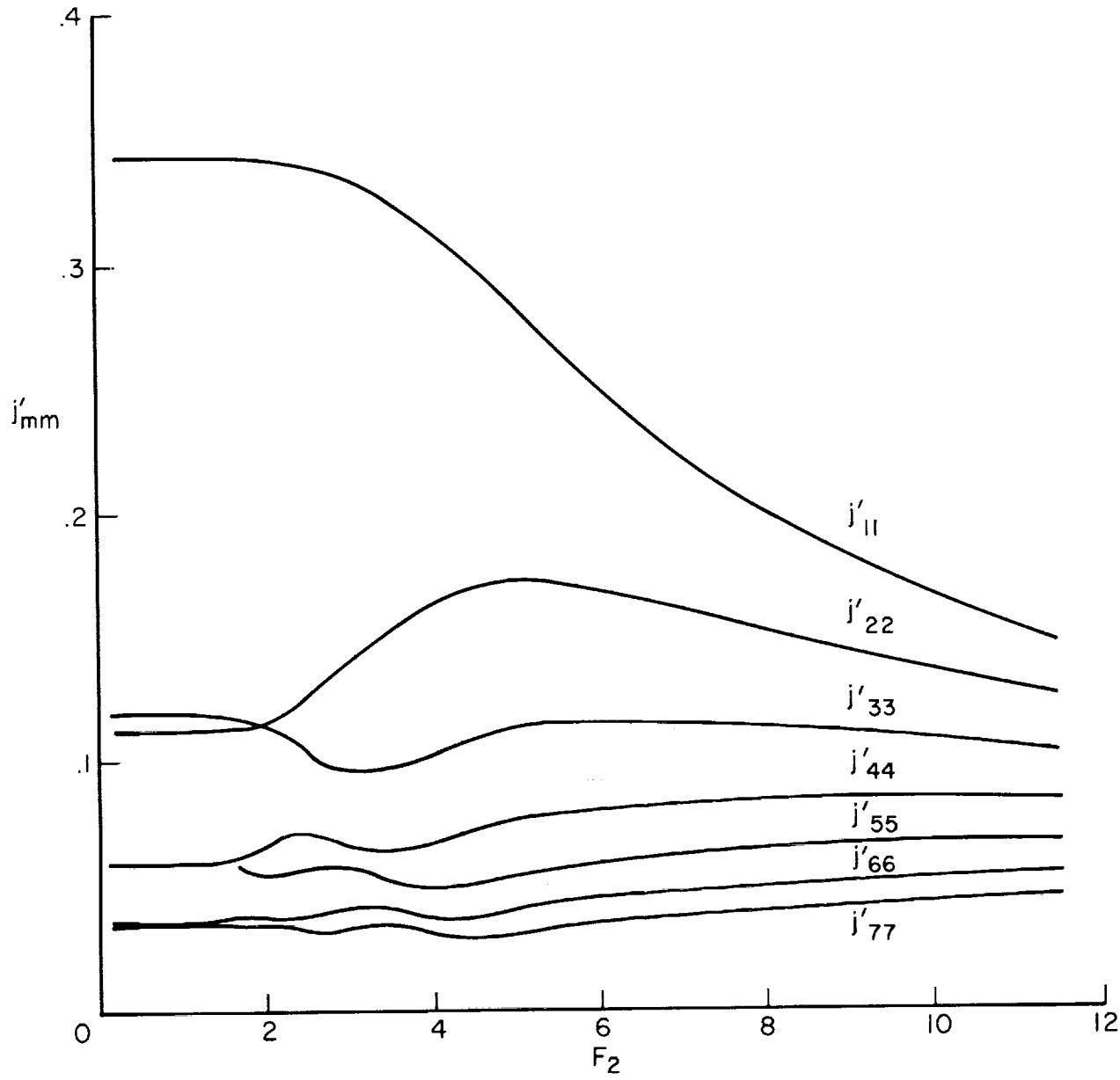

(a) j'_{11}, j'_{22}, j'_{33}, j'_{44}, j'_{55}, j'_{66}, j'_{77}

Figure 5. – Lateral acceptances of clamped edge panels for $\Delta_1^* = 0.06499$.

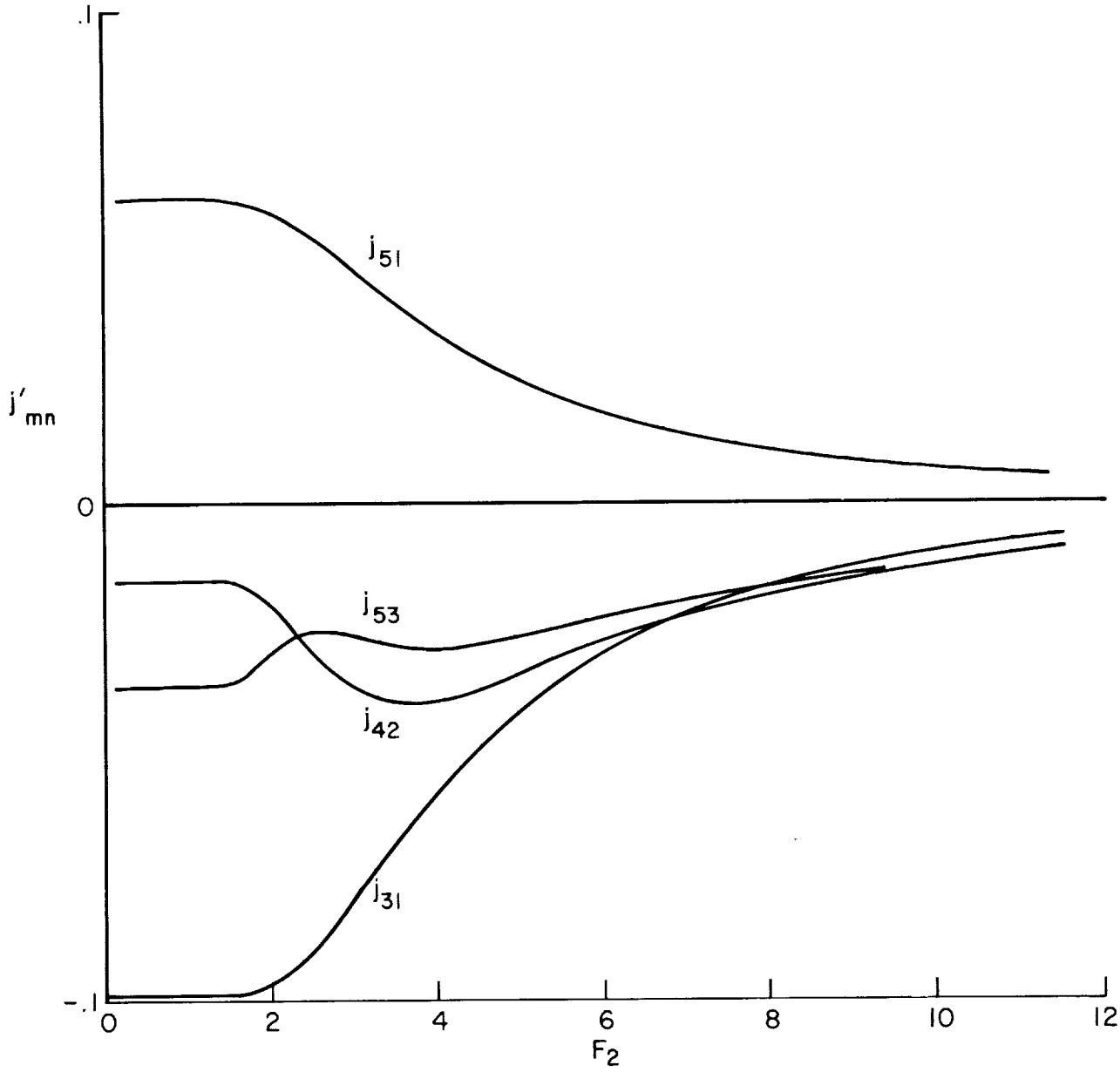

(b) j'_{51}, j'_{53}, j'_{41}, j'_{31}

Figure 5. – Concluded.

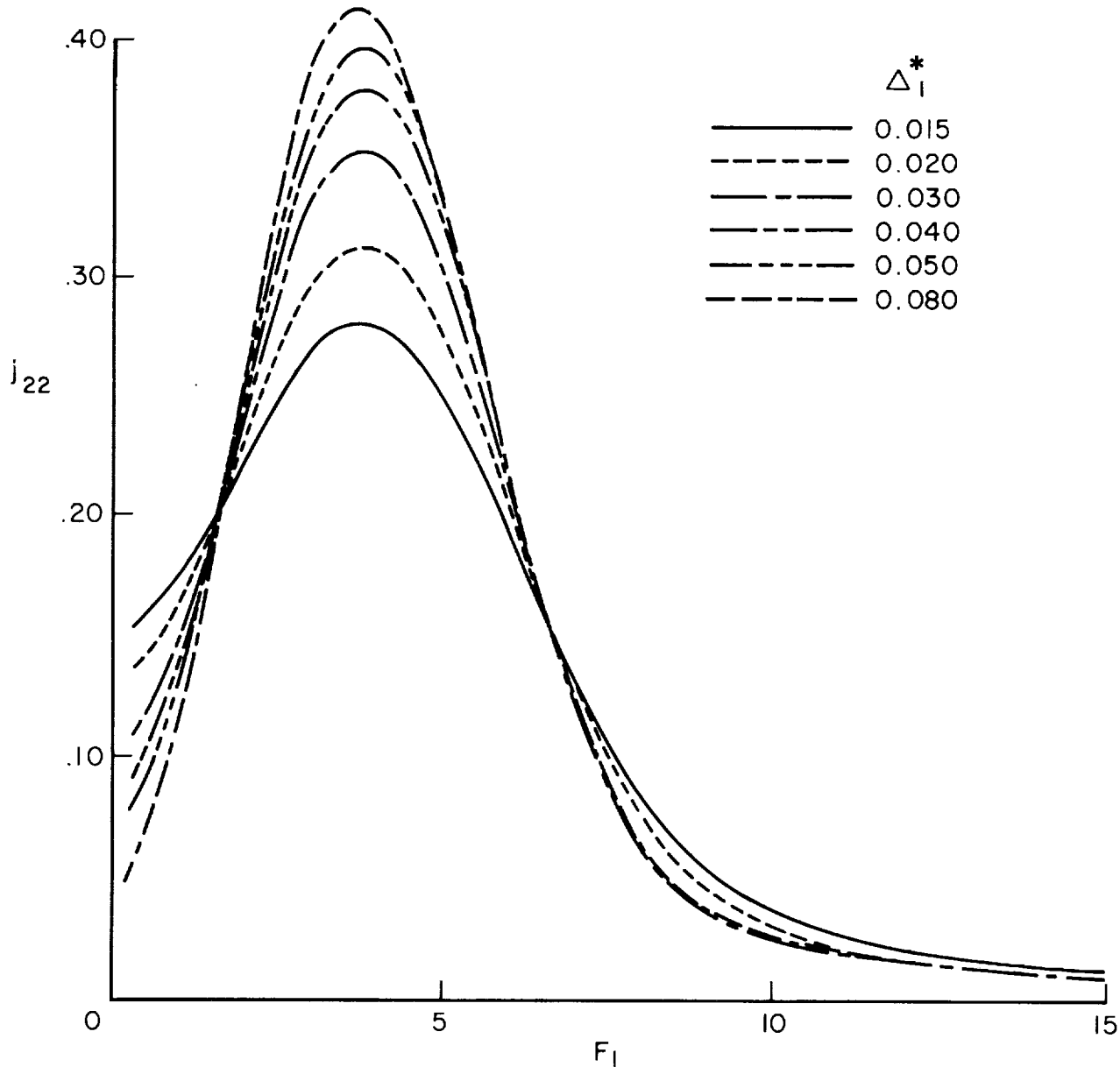

(a) j_{22}

Figure 6. – Variations of acceptances with Δ_1^*.

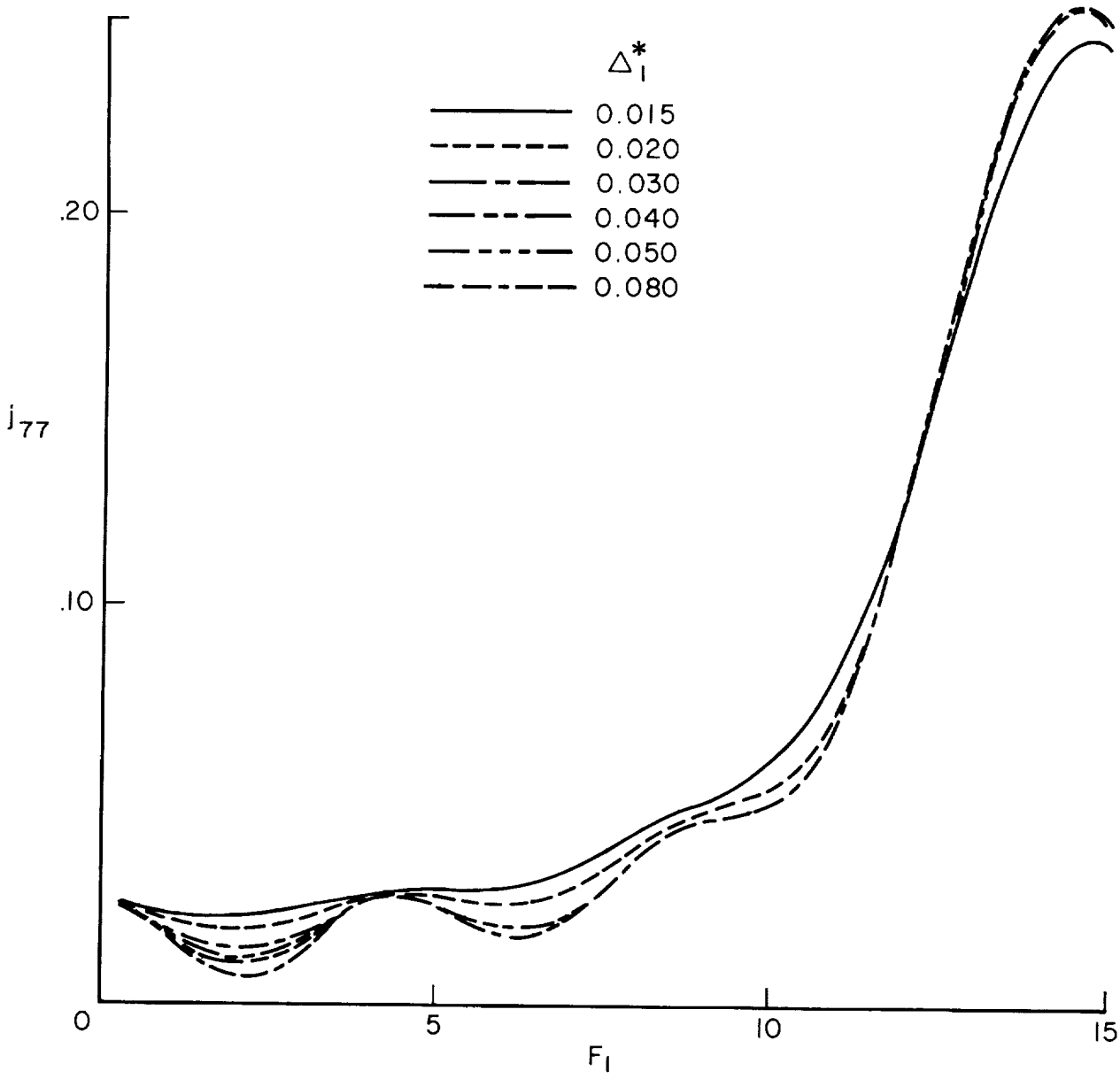

(b) j_{77}

Figure 6. – Continued.

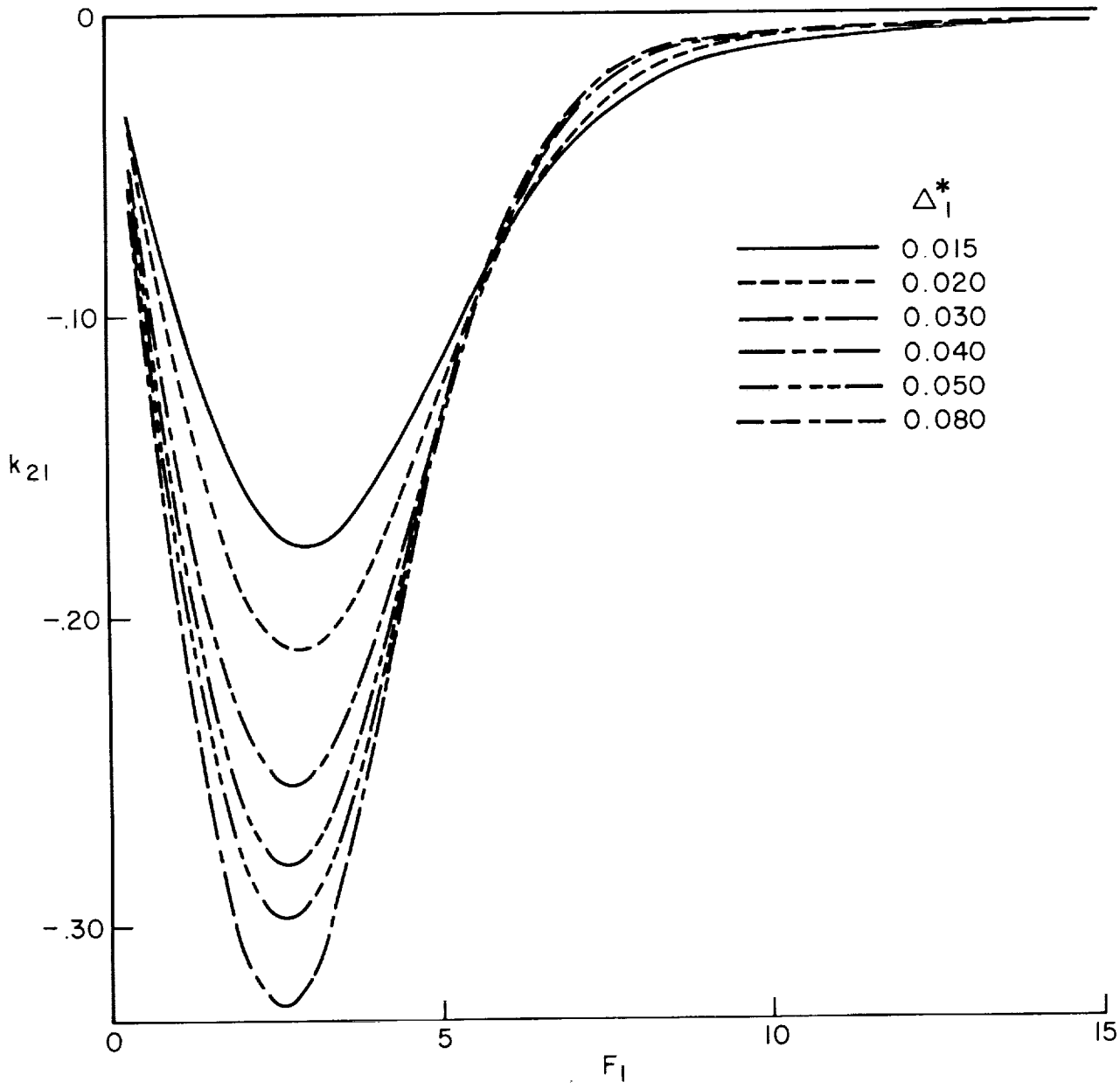

(c) k_{21}

Figure 6. – Concluded.

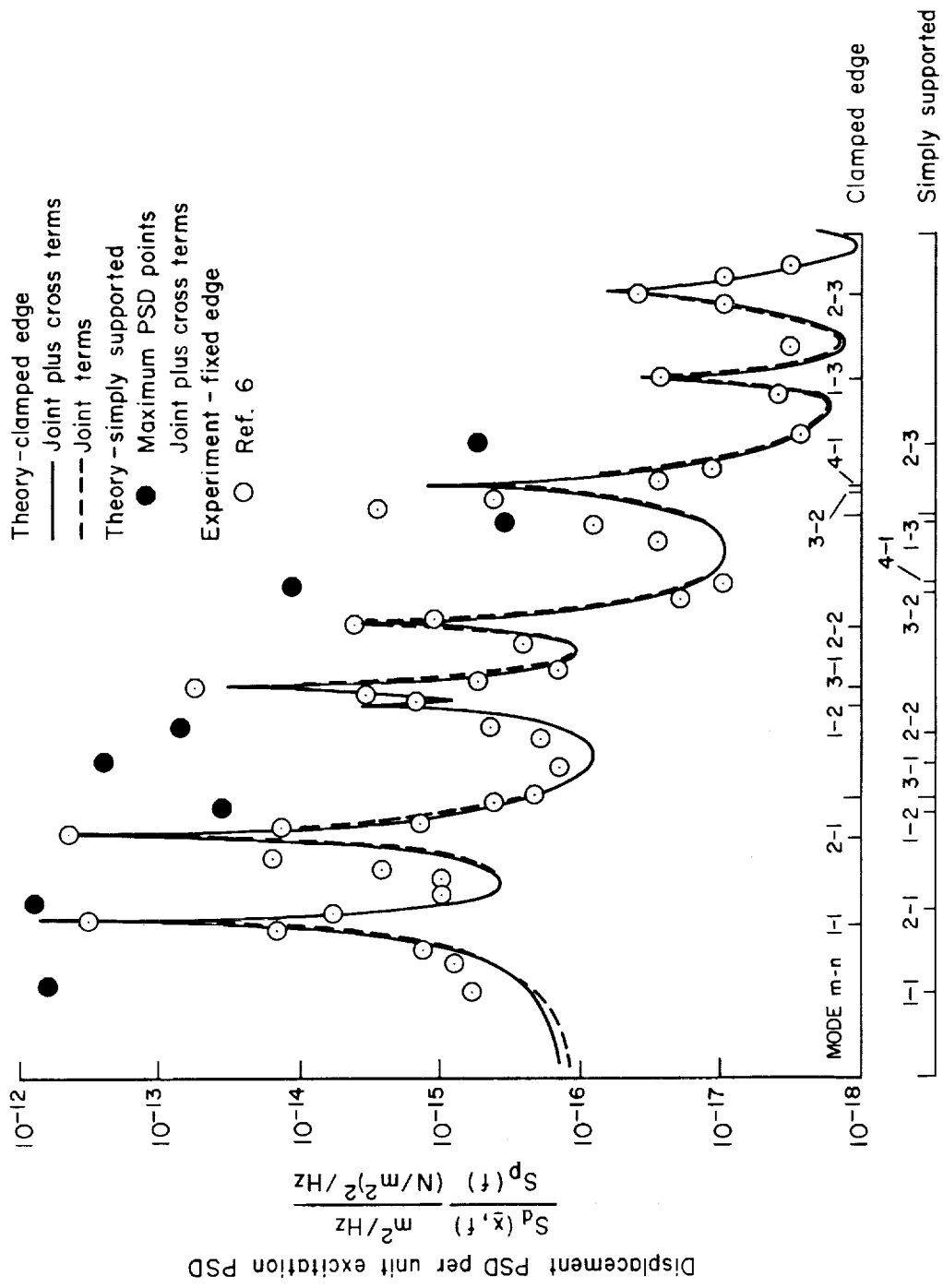

(a) Response at panel quarter point, $M_\infty = 0.3$.

Figure 7. — Displacement PSD of the panel response to unit excitation PSD.

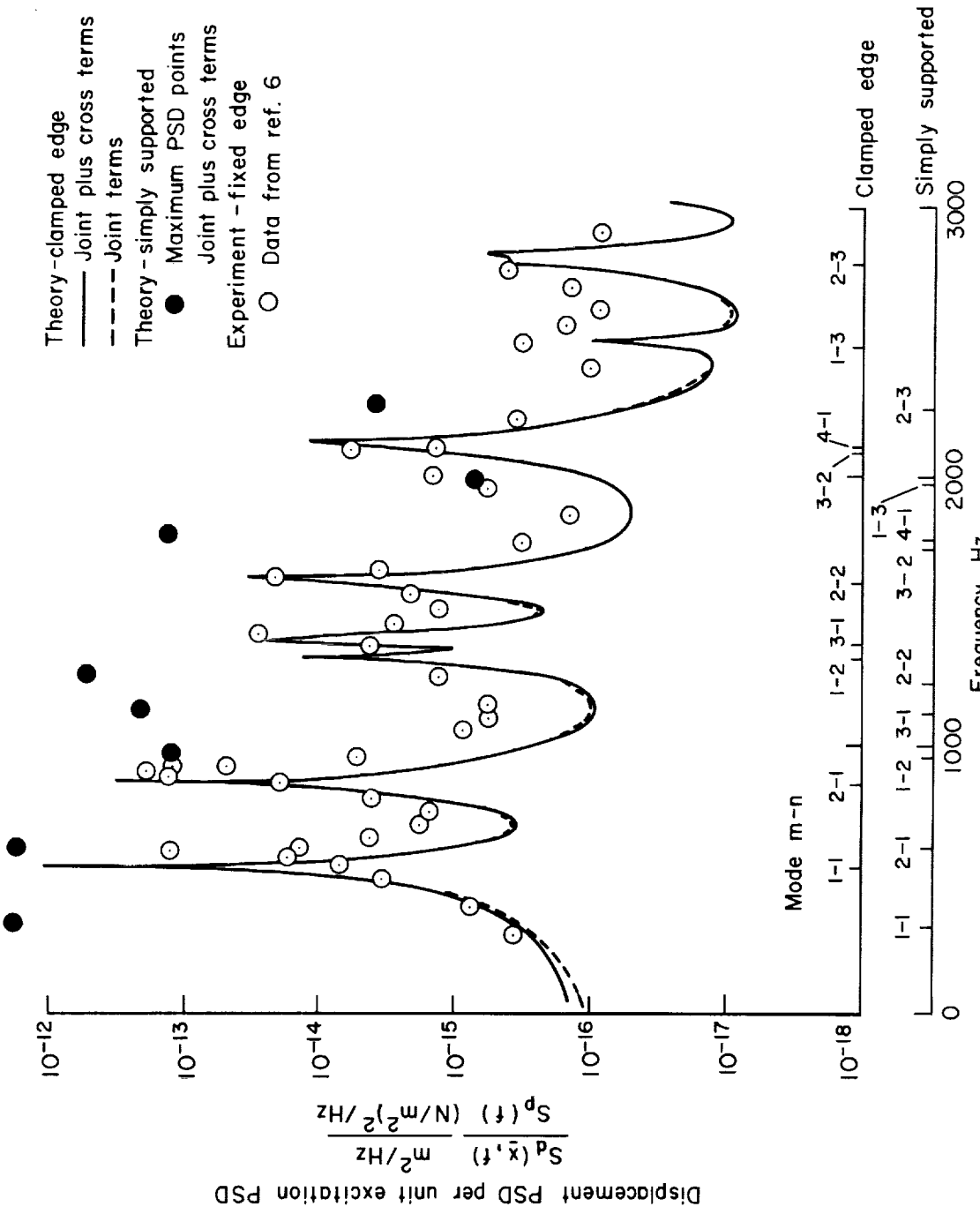

(b) Response at panel quarter point, $M_\infty = 0.5$.

Figure 7. — Continued.

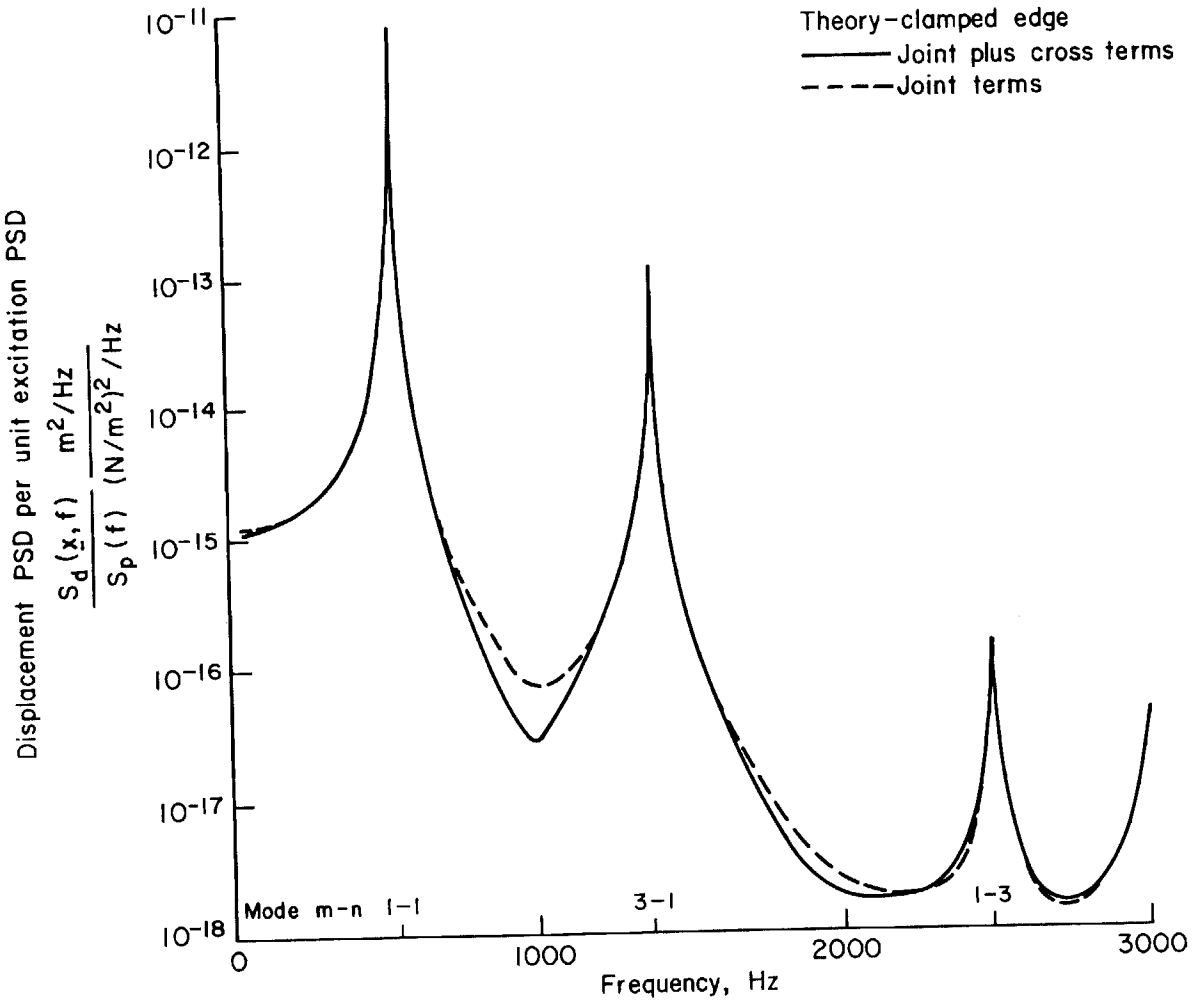

(c) Response at the midpoint of the clamped edge panel, $M_\infty = 0.3$.

Figure 7. – Concluded.

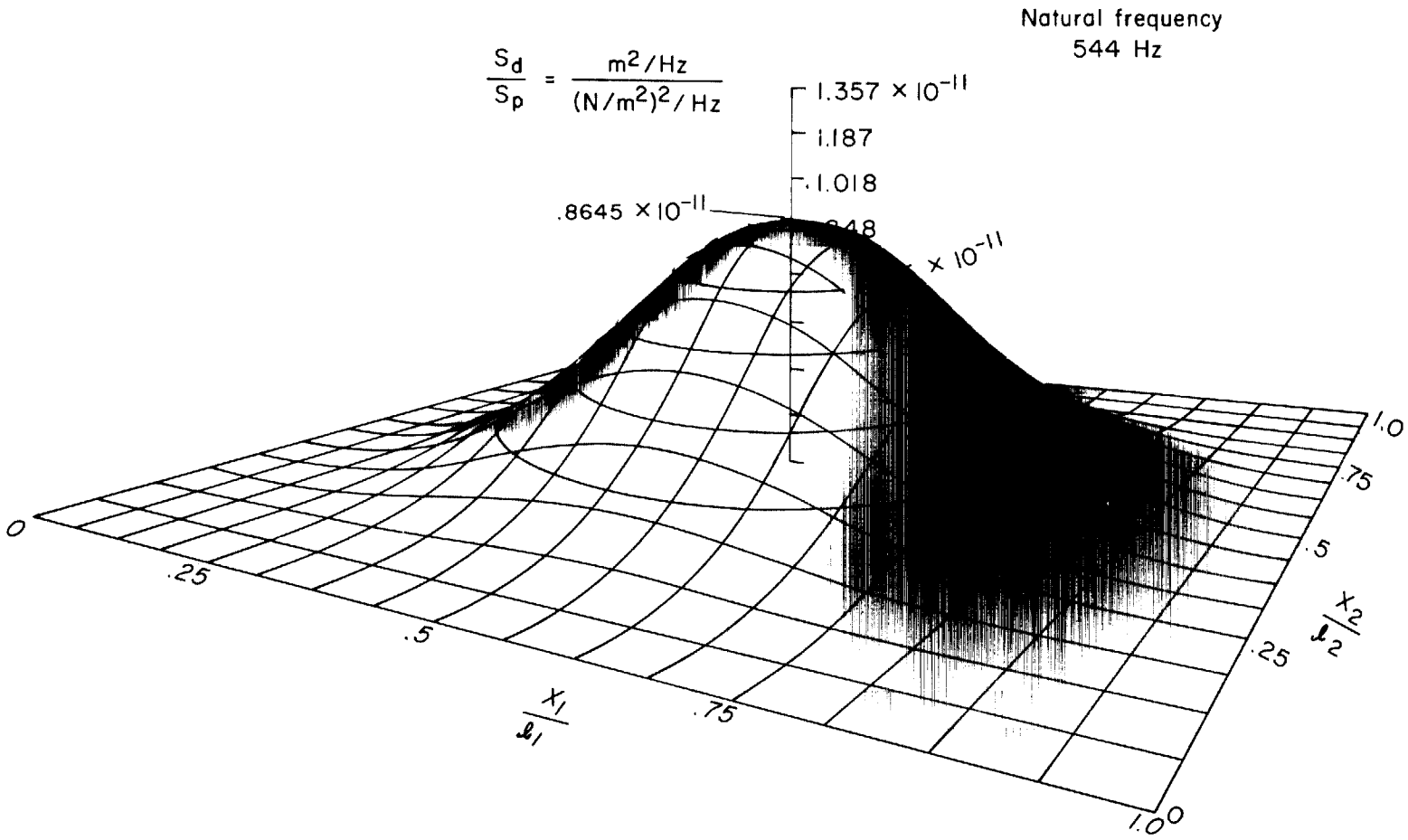

(a) Mode (1–1)

Figure 8.– Perspective view of displacement PSD of the response of clamped edge panel to unit excitation at $M = 0.3$.

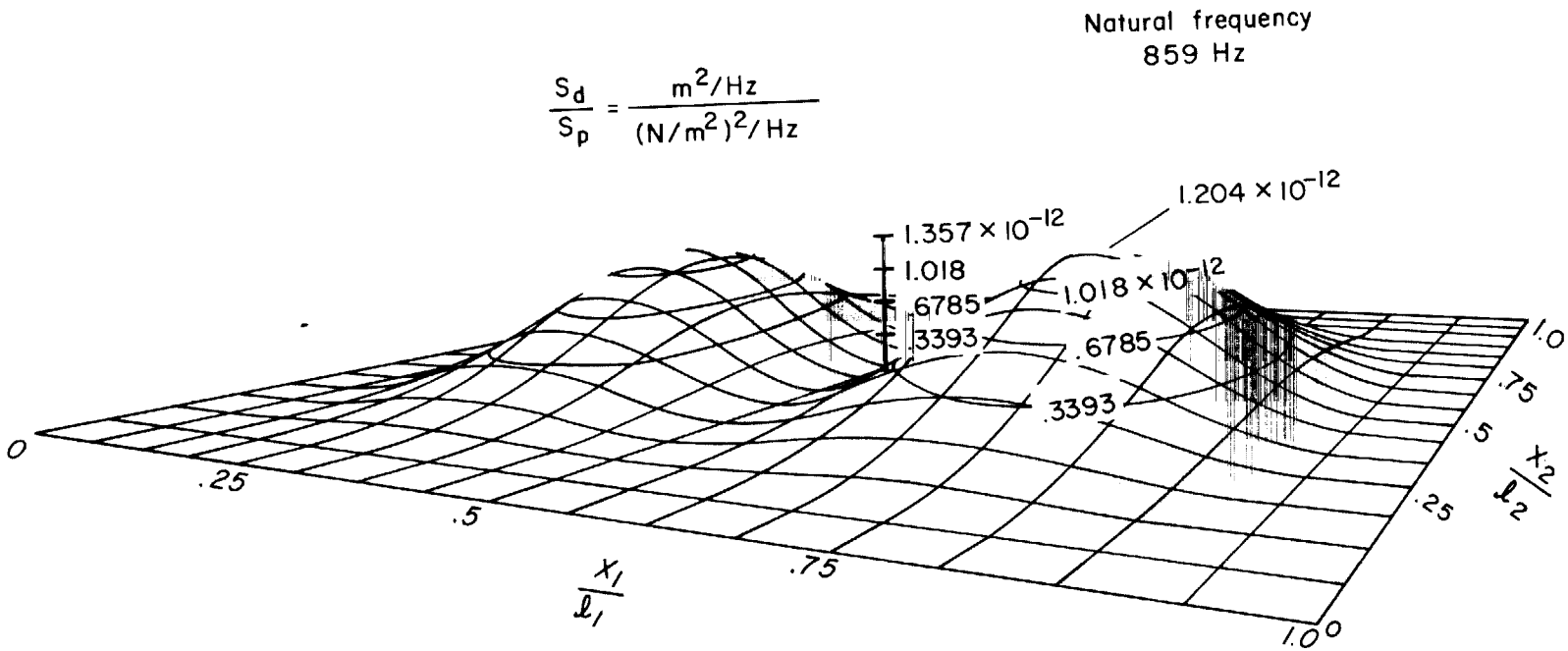

(b) Mode (2–1)

Figure 8. – Continued.

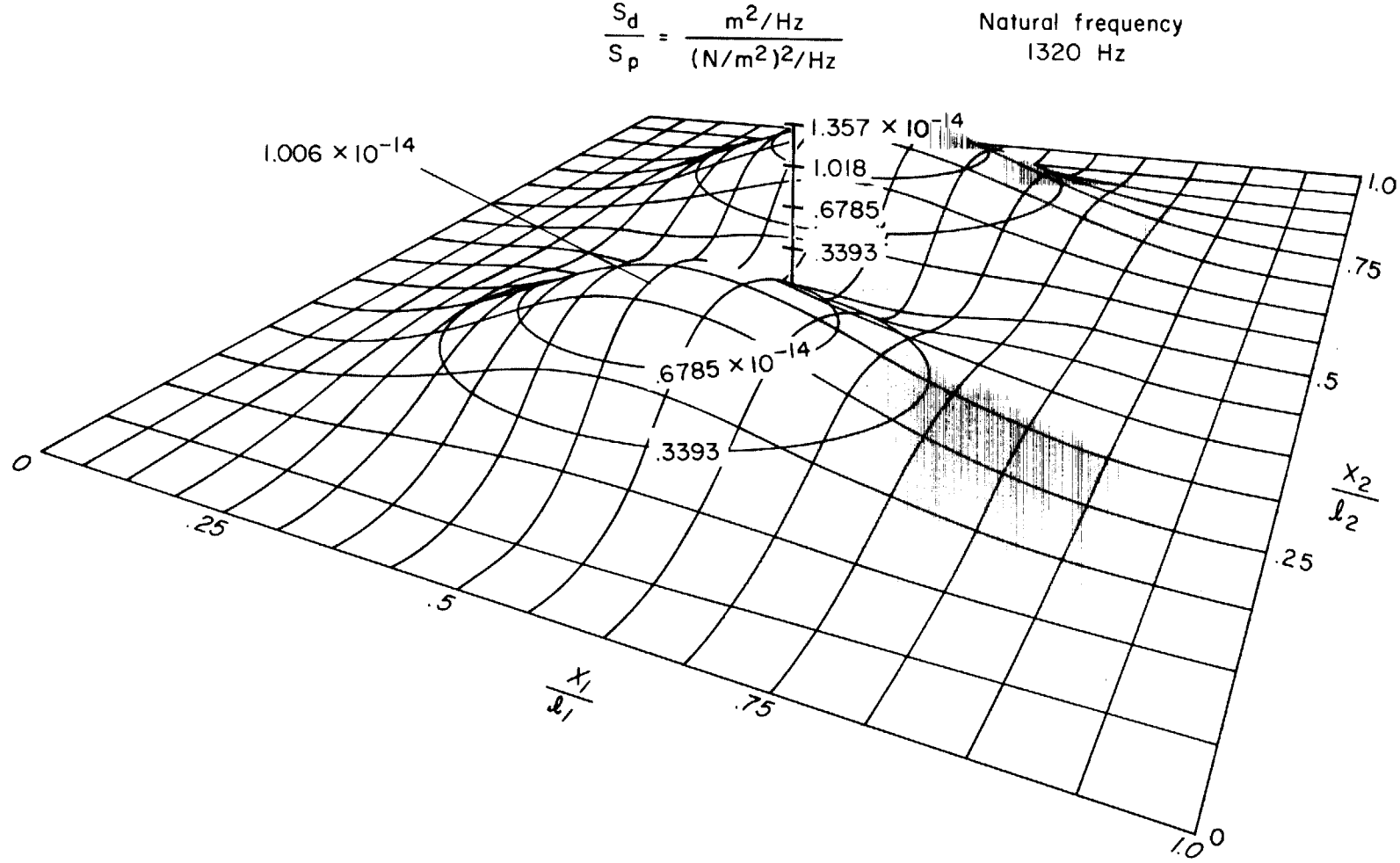

(c) Mode (1-2)

Figure 8. – Continued.

$$\frac{S_d}{S_p} = \frac{m^2/Hz}{(N/m^2)^2/Hz}$$

Natural frequency
1387 Hz

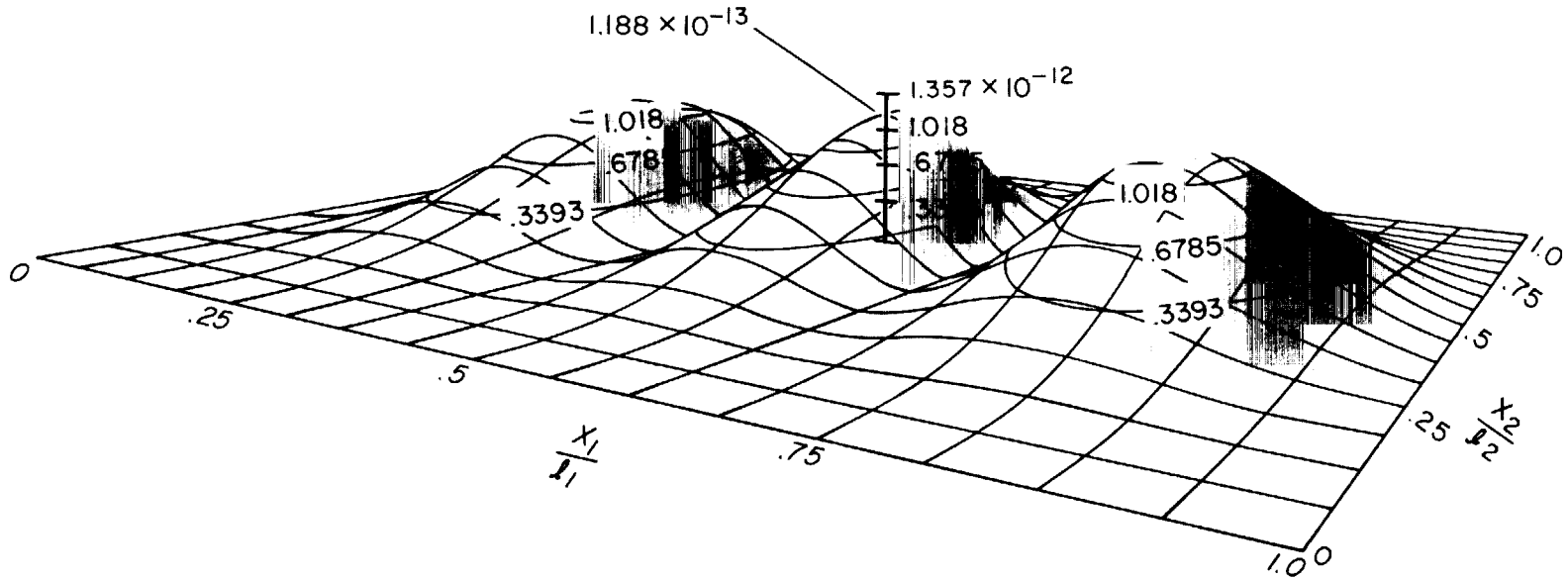

(d) Mode (3-1)

Figure 8. – Continued.

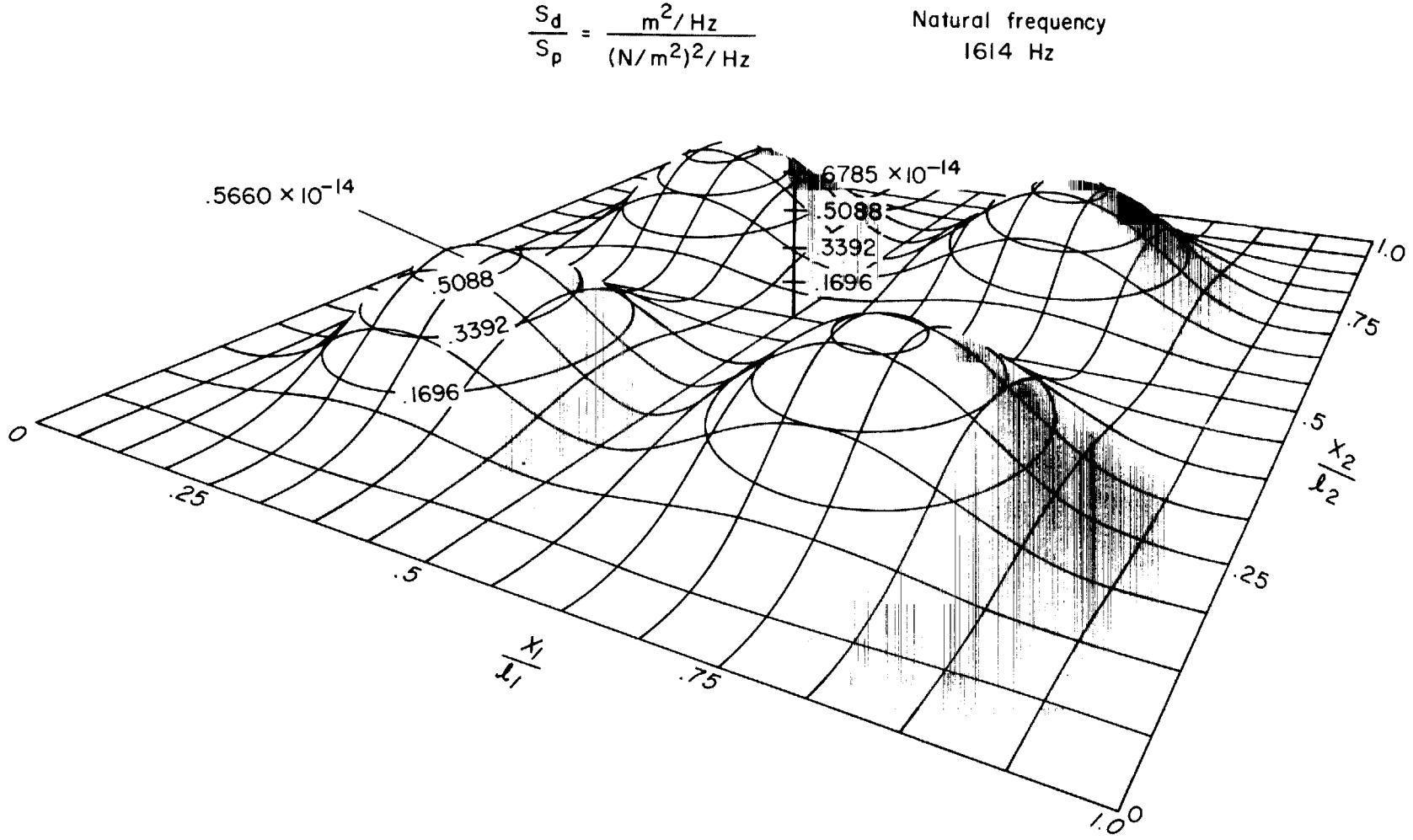

(e) Mode (2–2)

Figure 8. – Concluded.

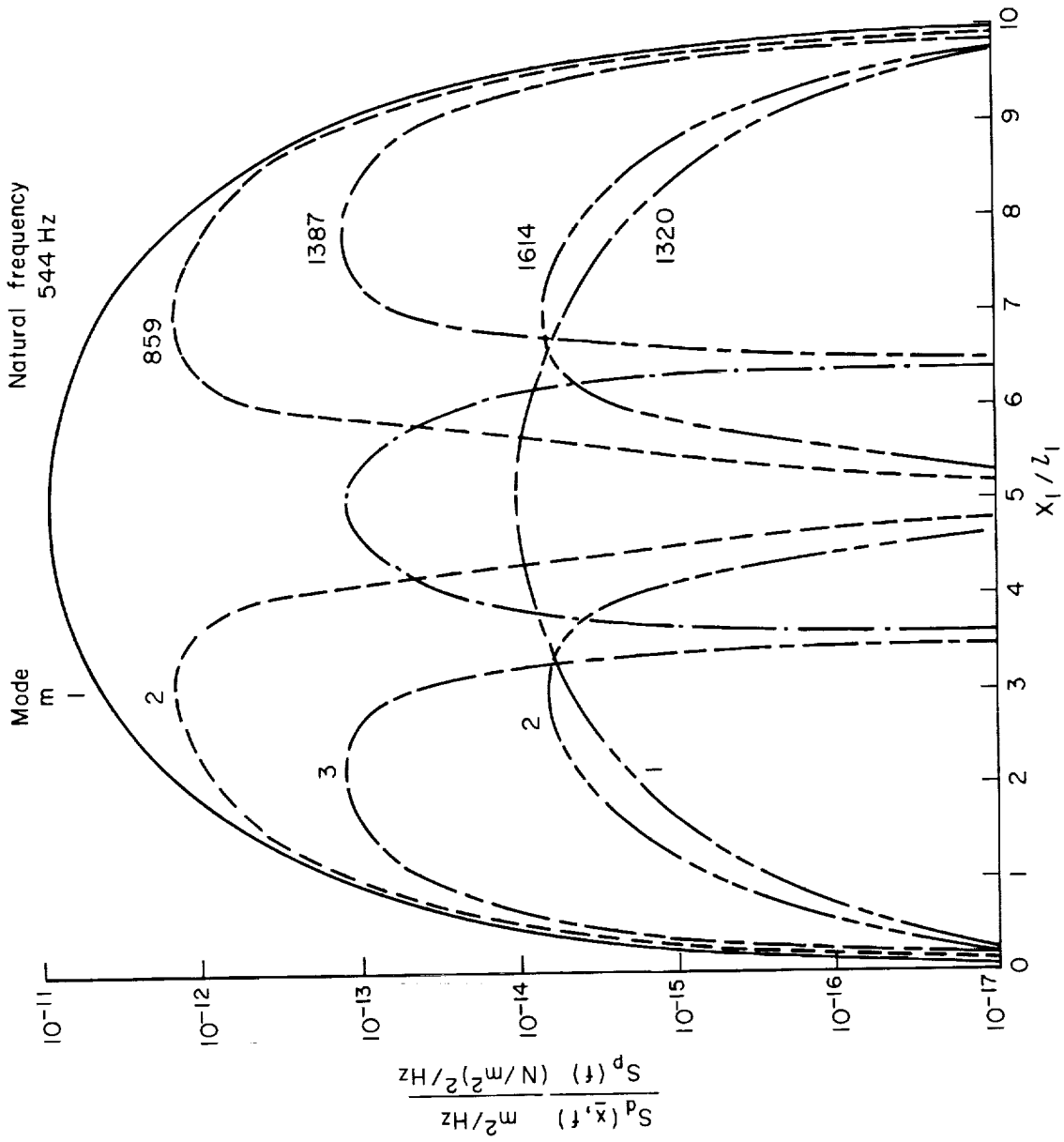

(a) Variation with longitudinal coordinate.

Figure 9. – Variation of maximum displacement PSD with coordinates of the panel.

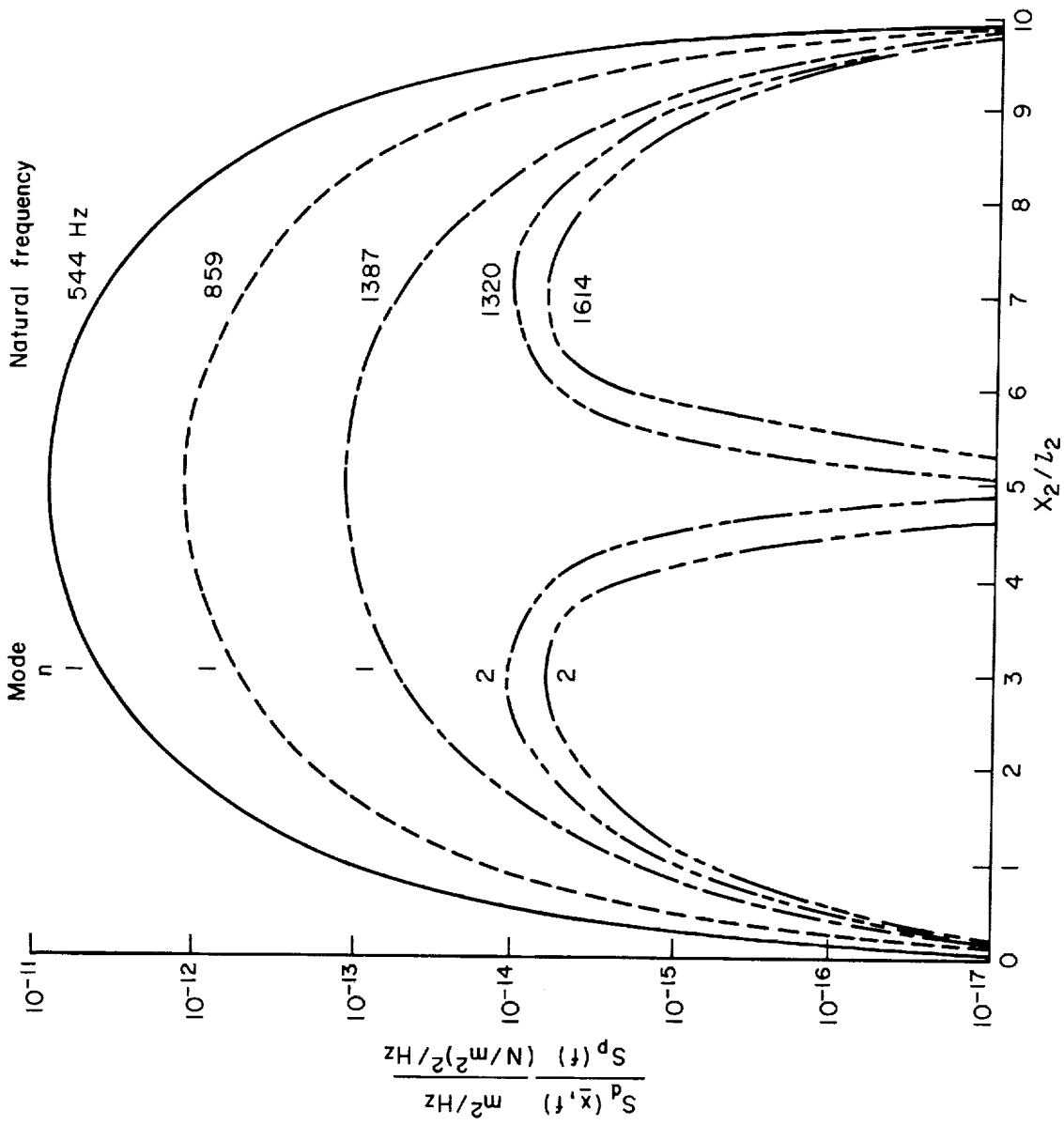

(b) Variation with lateral coordinates.

Figure 9. – Concluded.

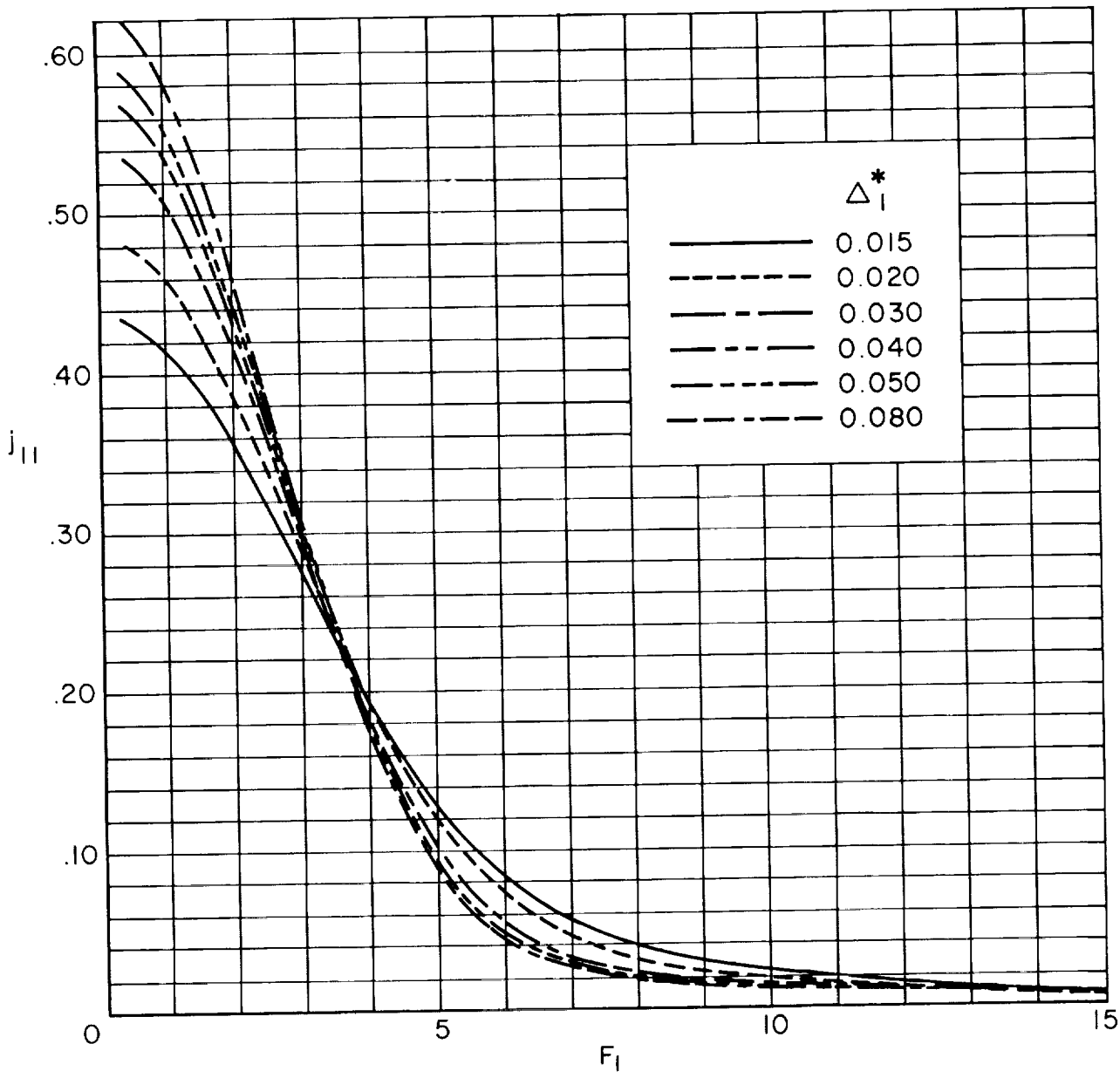

(a) j_{11}

Figure 10. – Real part of longitudinal acceptance of clamped edge panels.

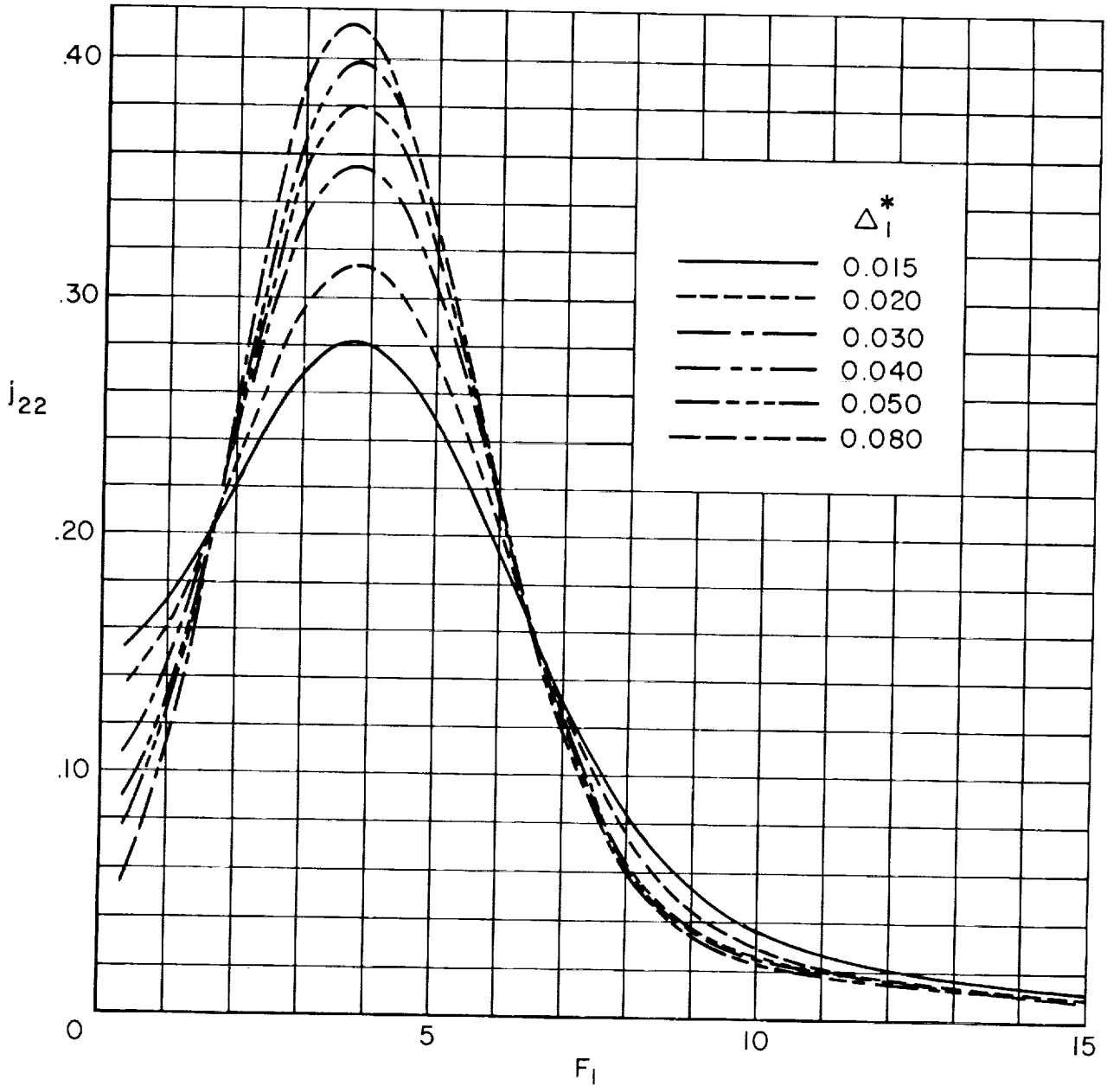

(b) j_{22}

Figure 10. – Continued.

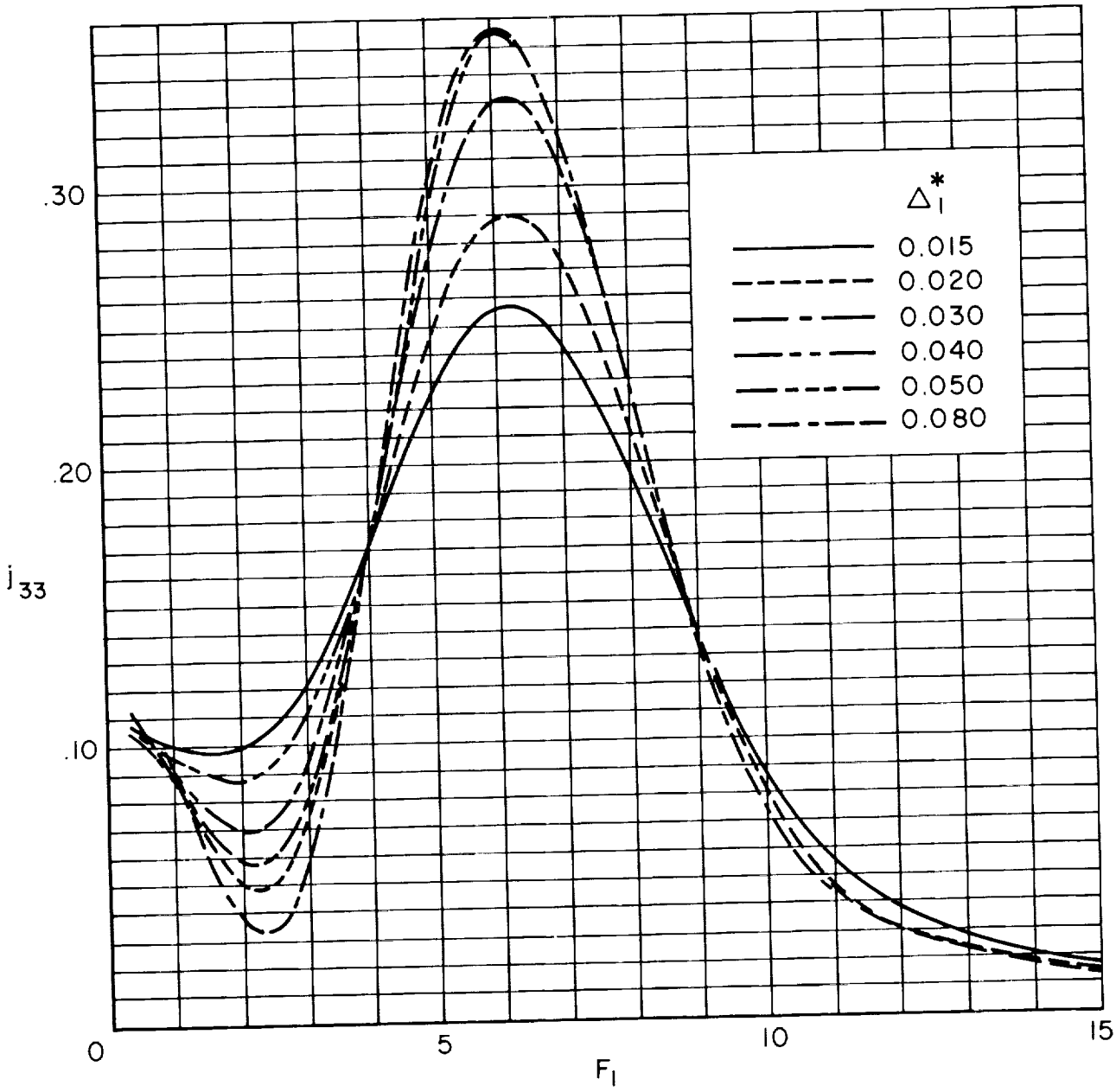

(c) j_{33}

Figure 10. – Continued.

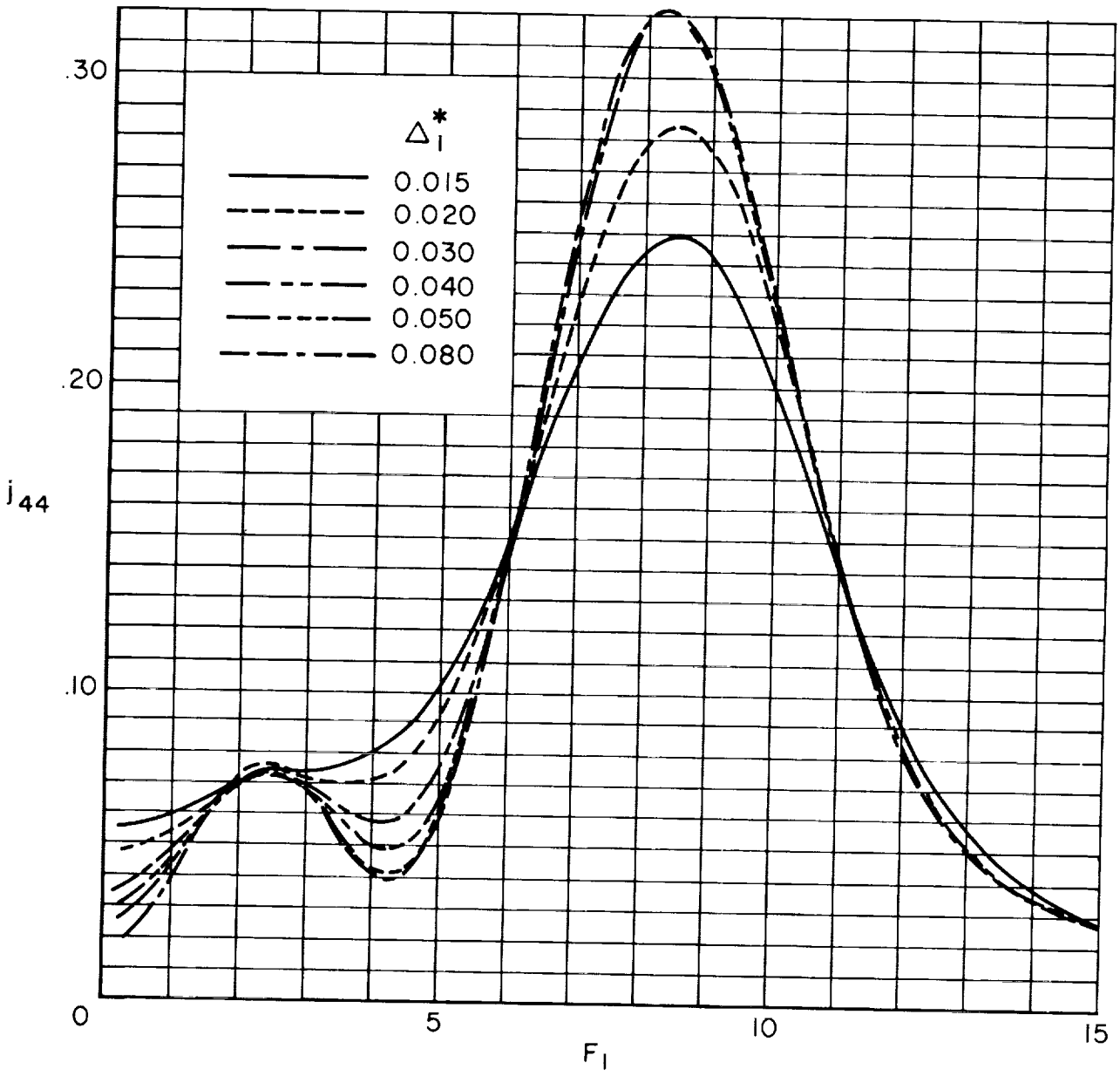

(d) j_{44}

Figure 10. – Continued.

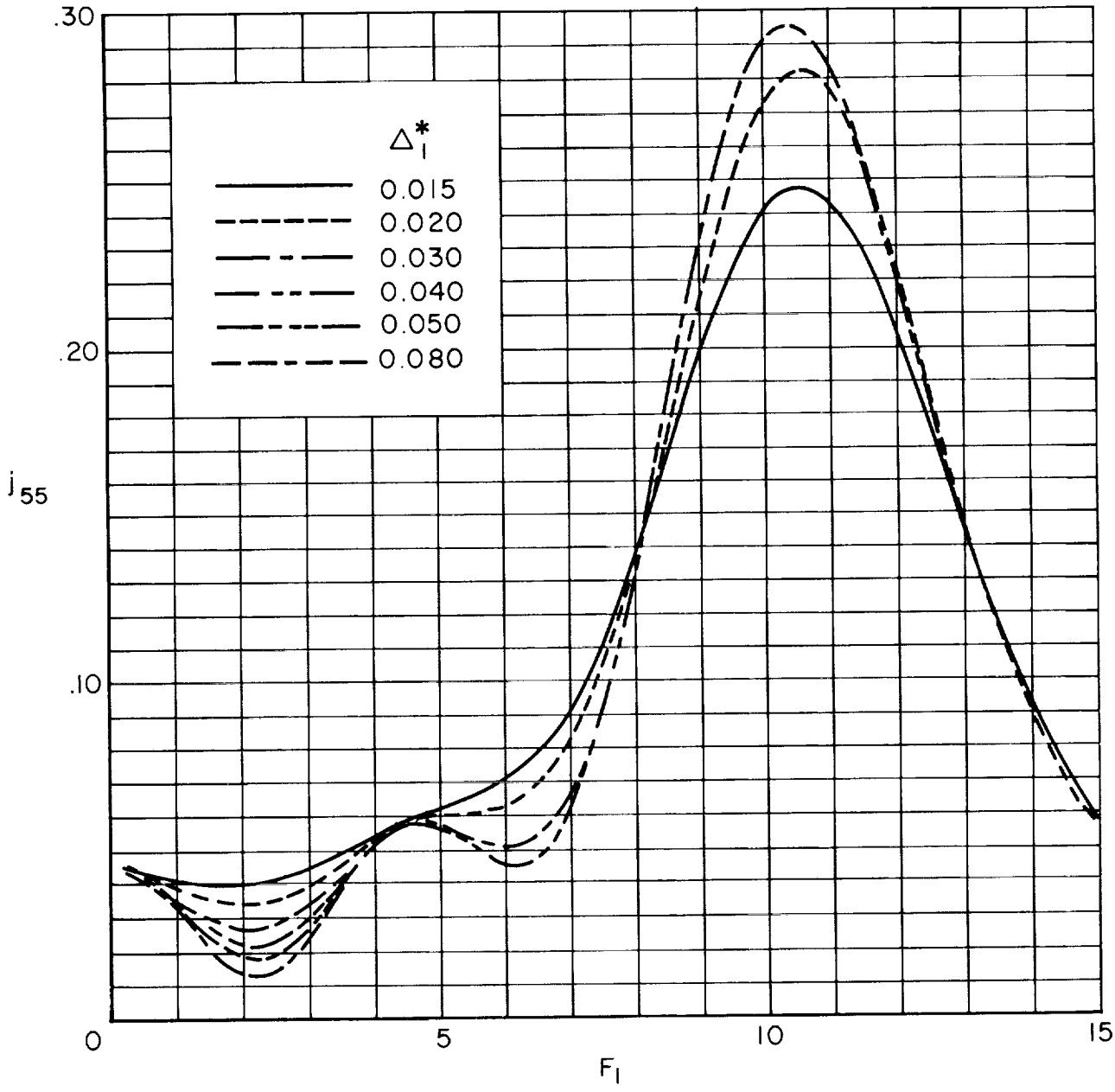

(e) j_{55}

Figure 10. – Continued.

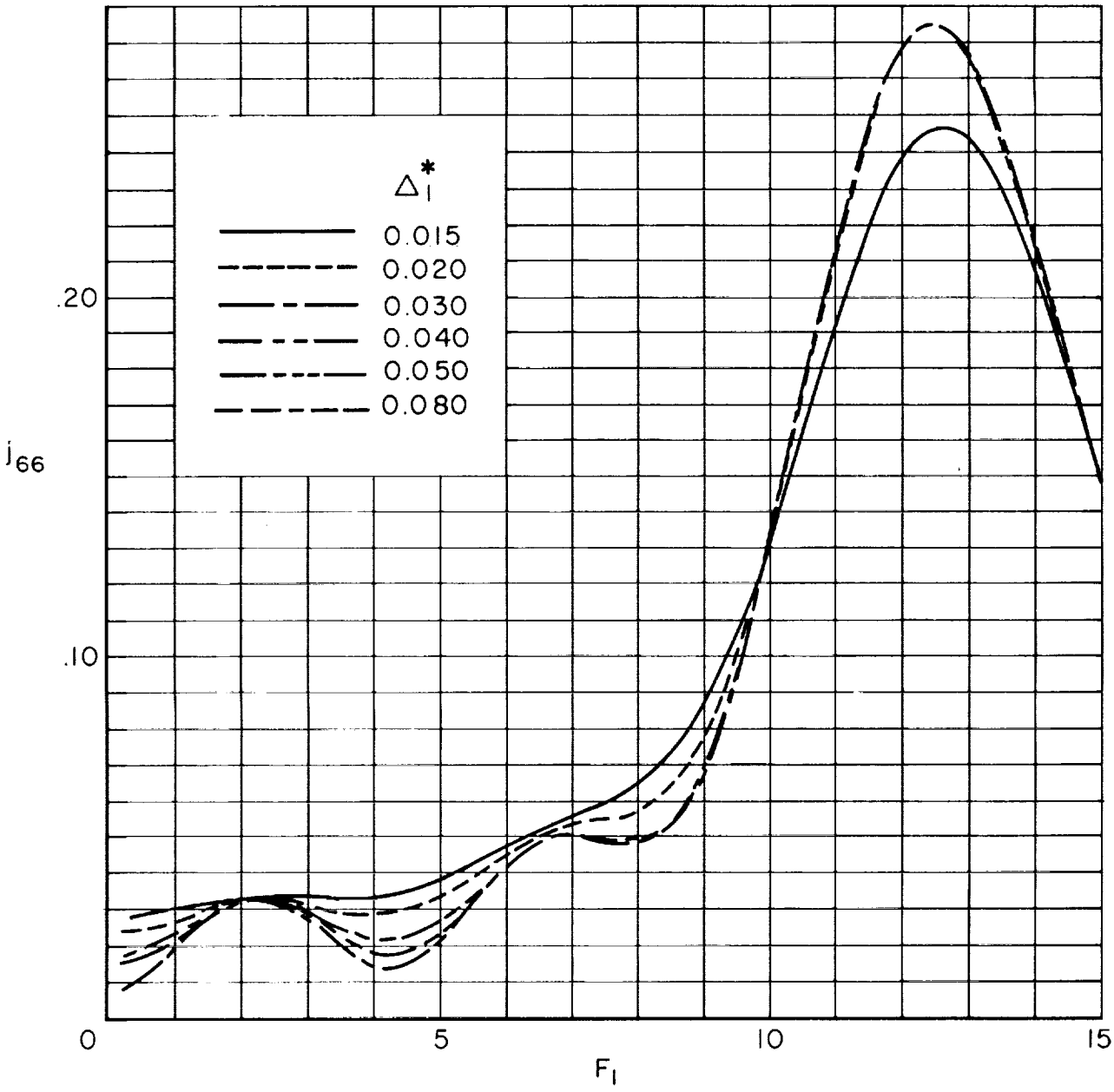

(f) j_{66}

Figure 10. – Continued.

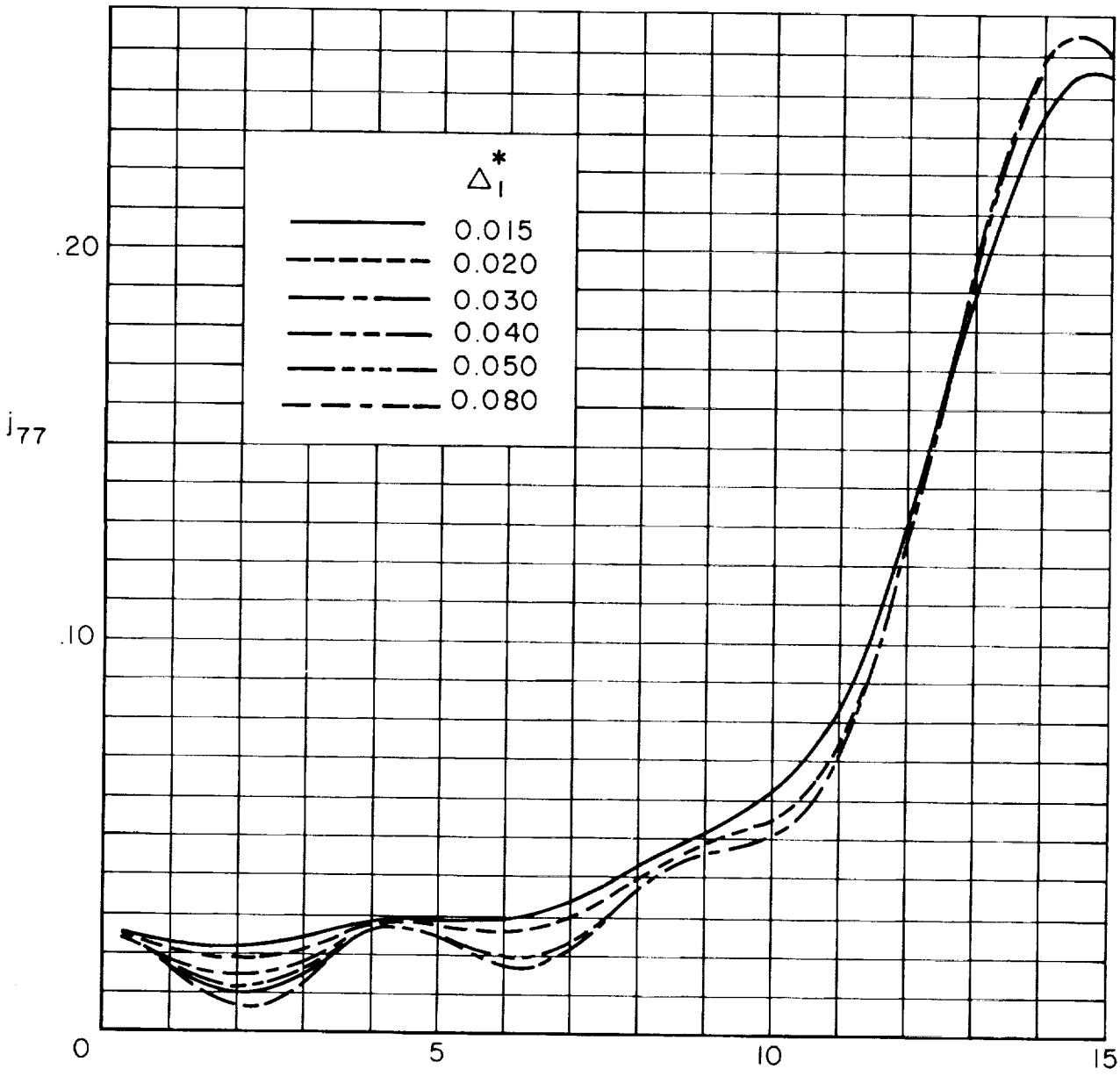

(g) j_{77}

Figure 10. – Continued.

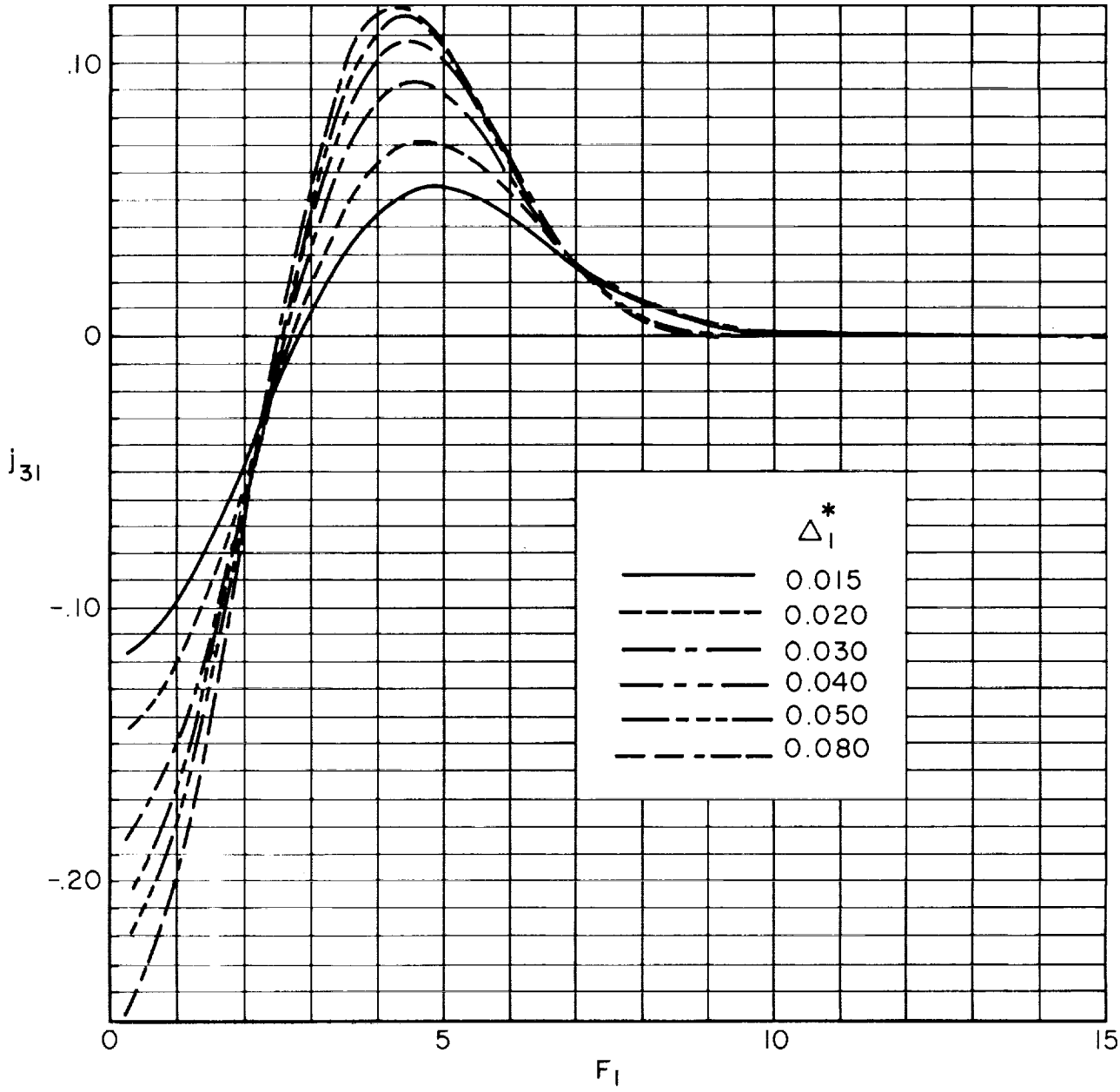

(h) j_{31}

Figure 10. – Continued.

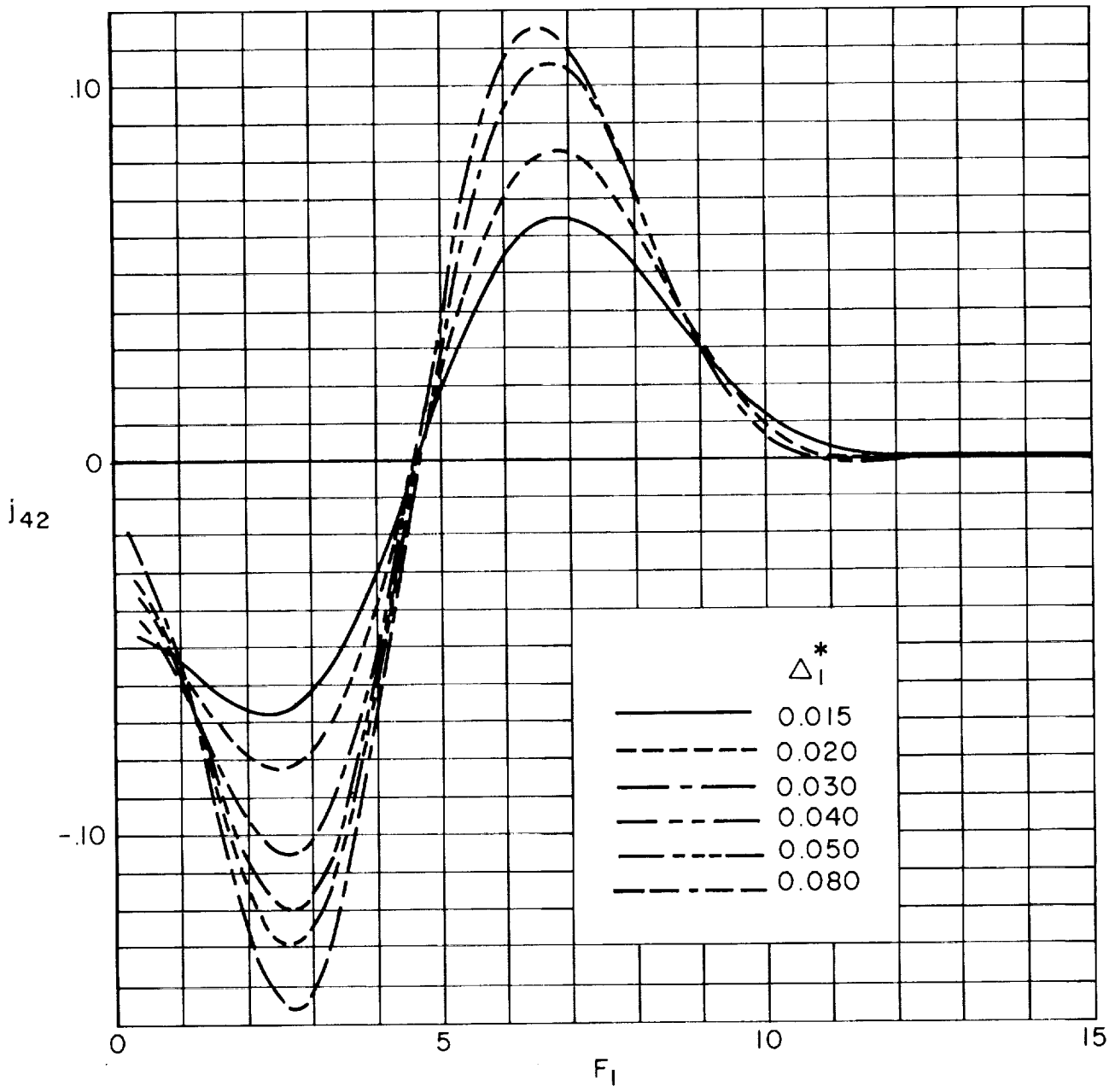

(i) j_{42}

Figure 10. – Continued.

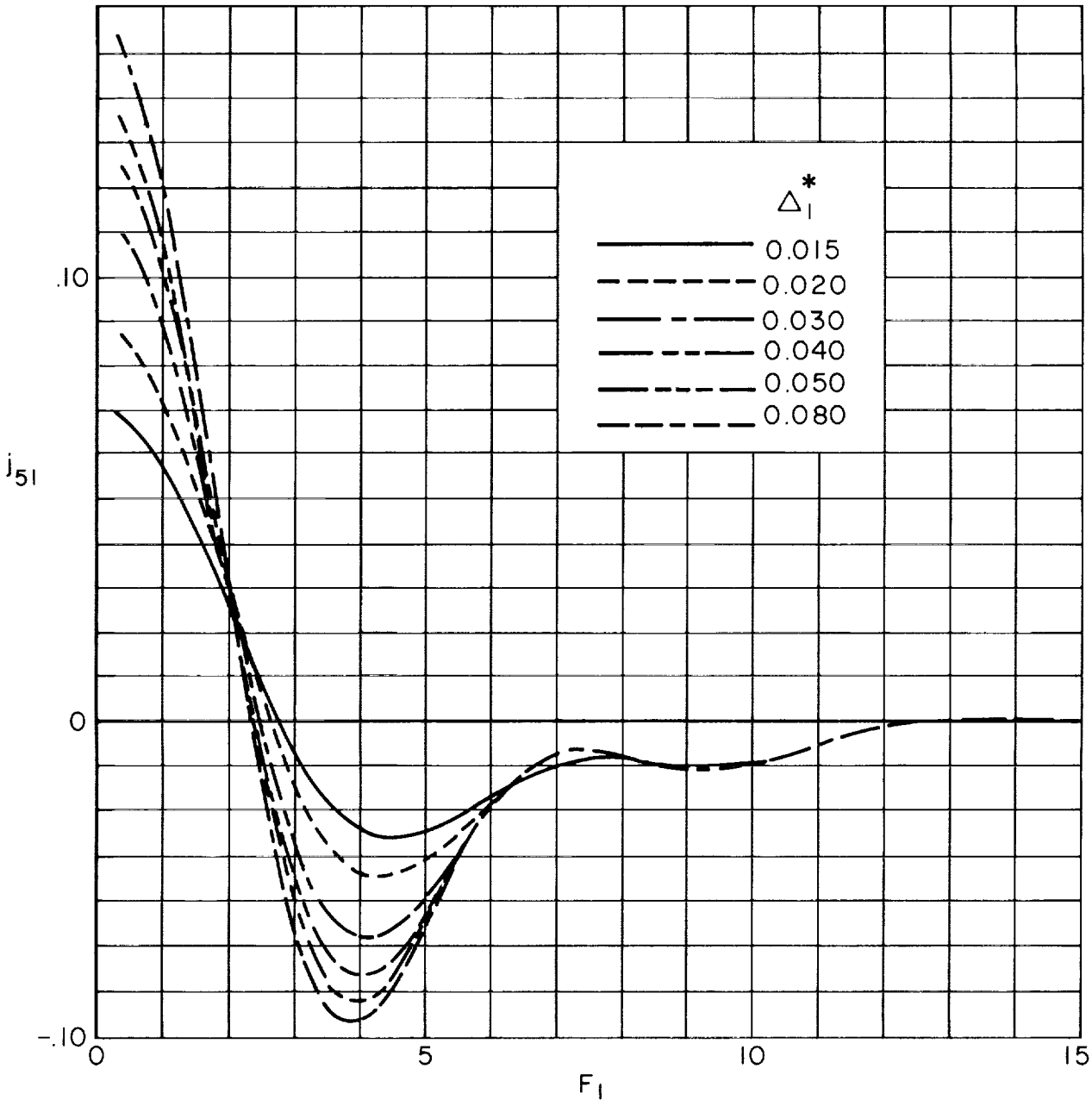

(j) j_{51}

Figure 10. – Continued.

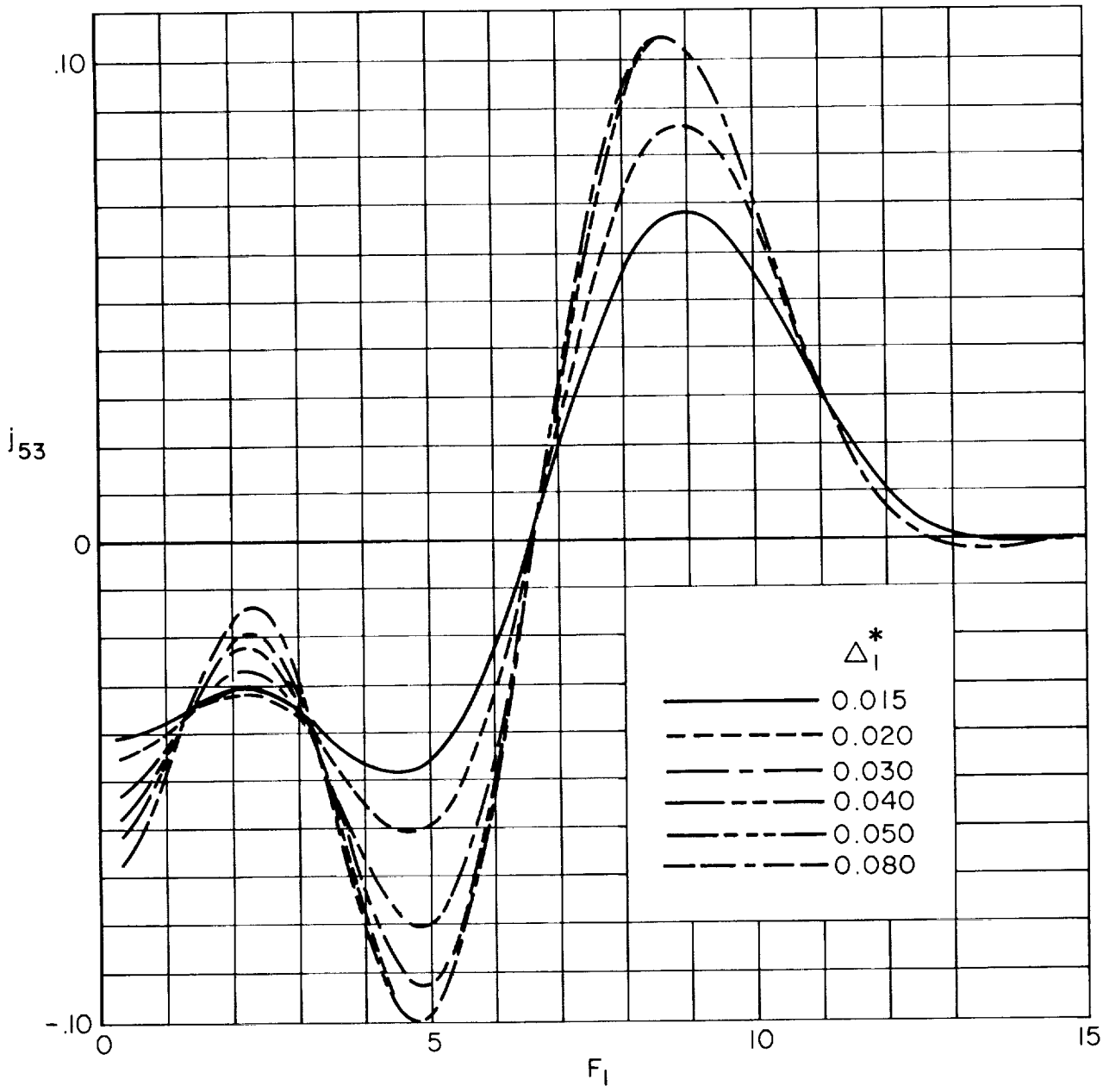

(k) j_{53}

Figure 10. – Continued.

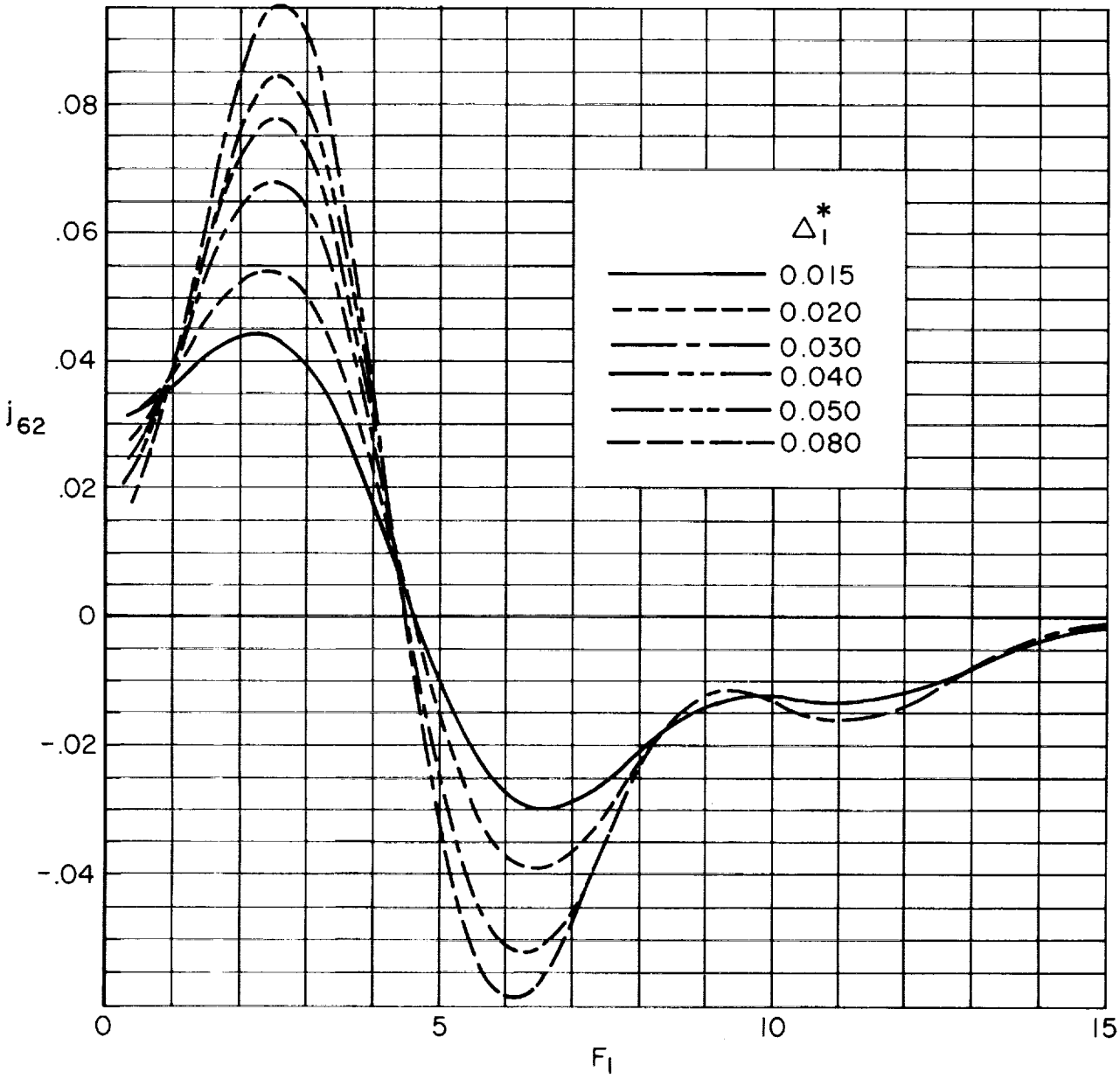

(l) j_{62}

Figure 10. – Continued.

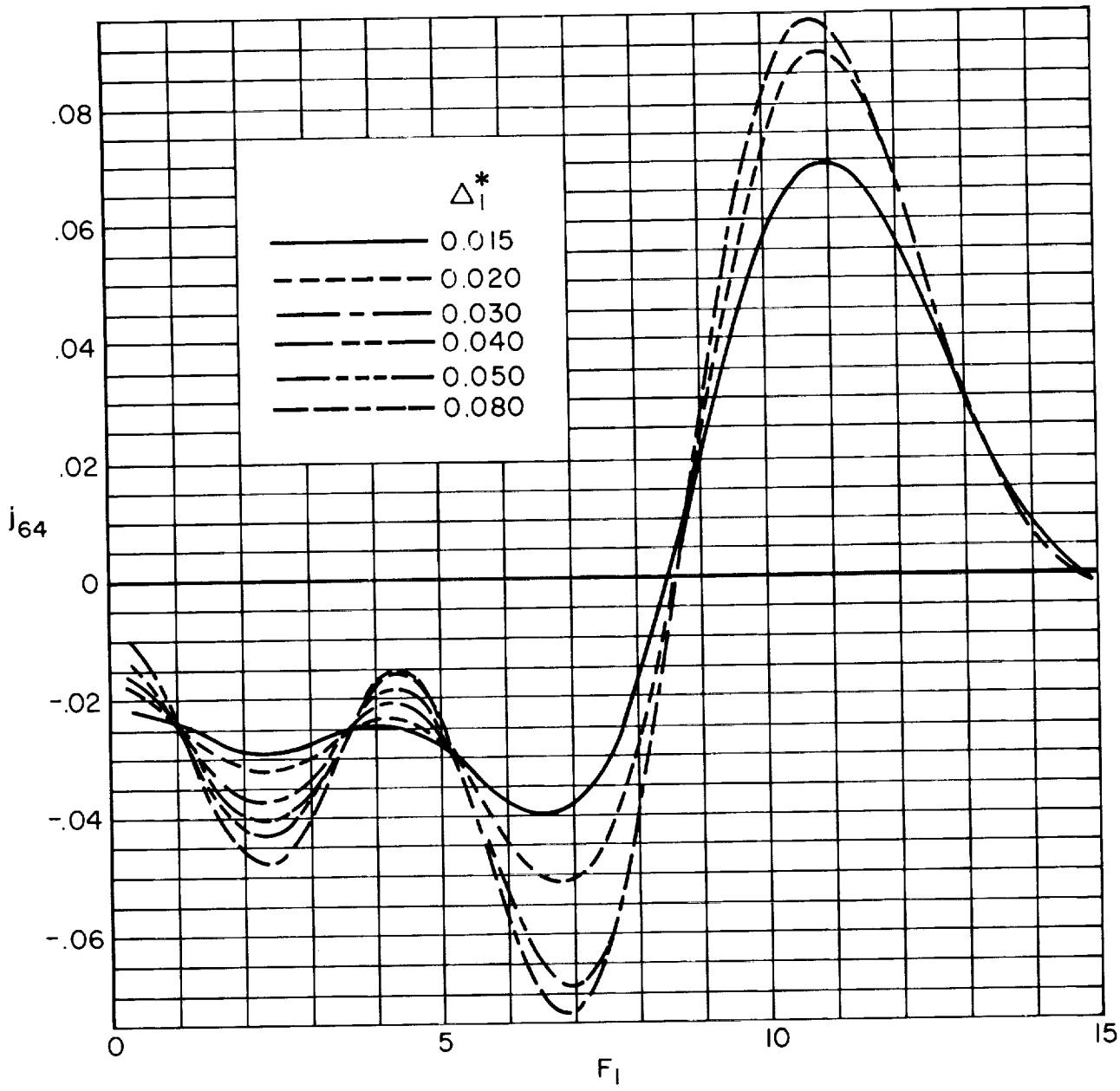

(m) j_{64}

Figure 10. – Continued.

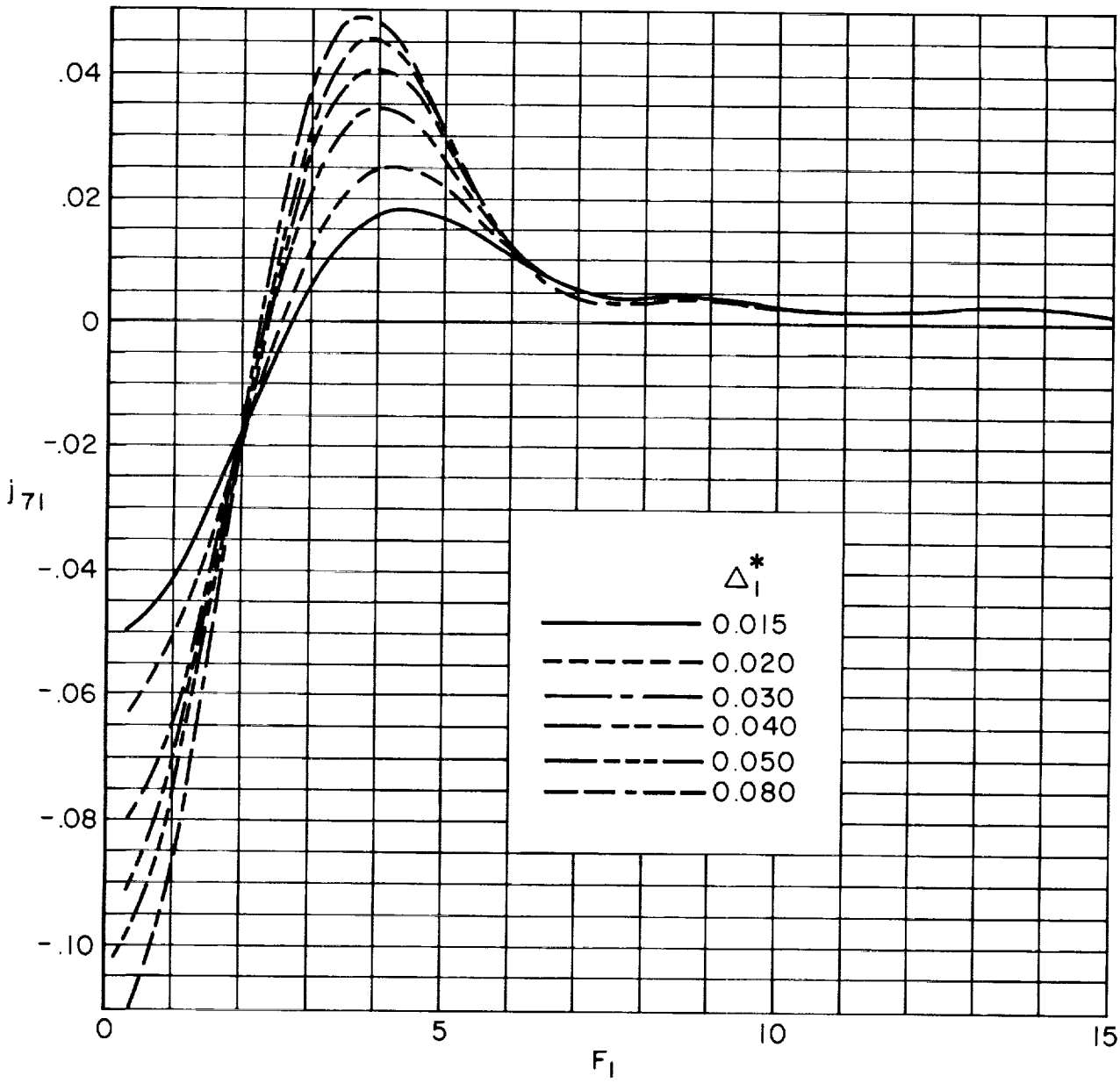

(n) j_{71}

Figure 10. – Continued.

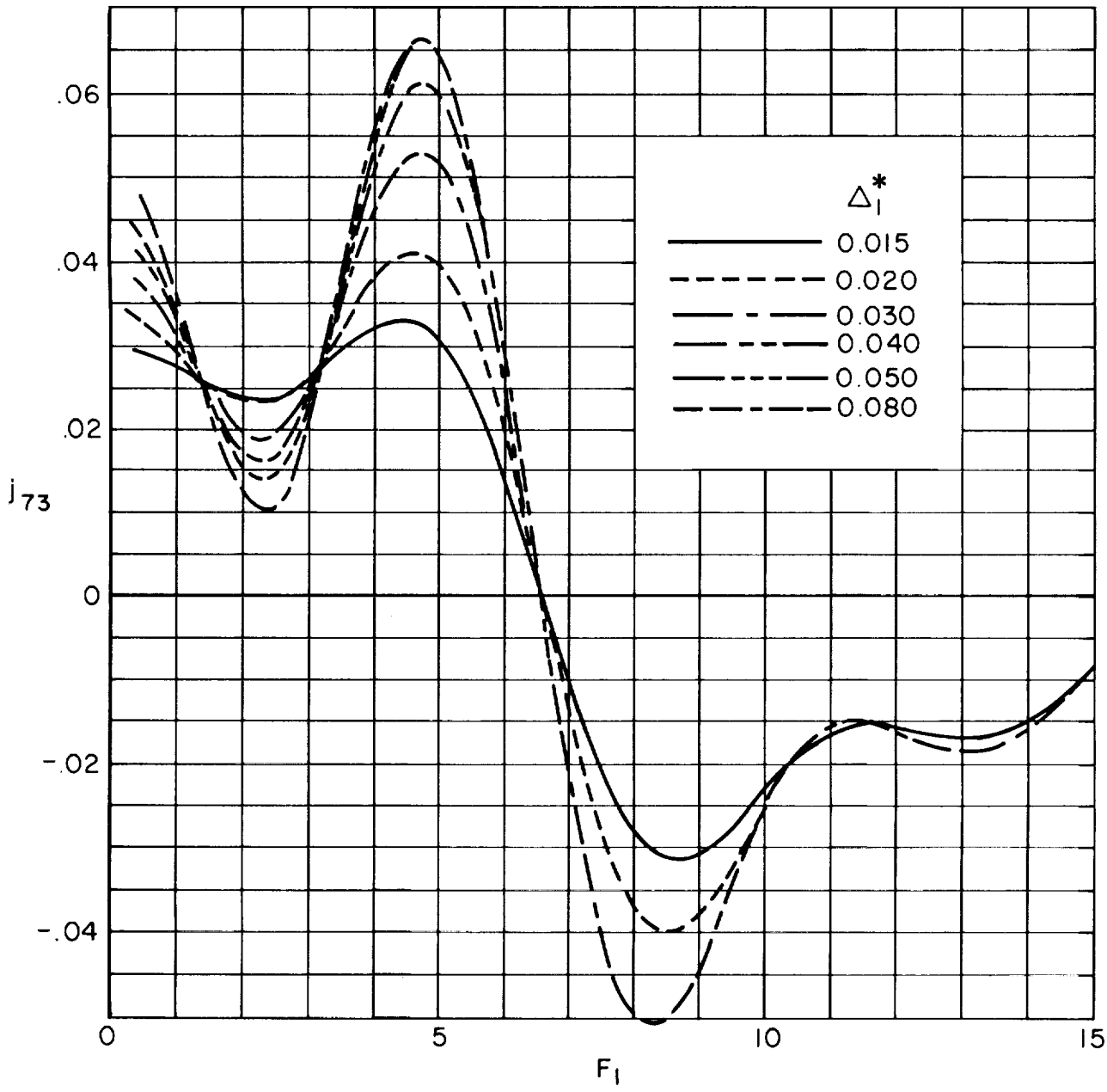

(o) j_{73}

Figure 10. – Continued.

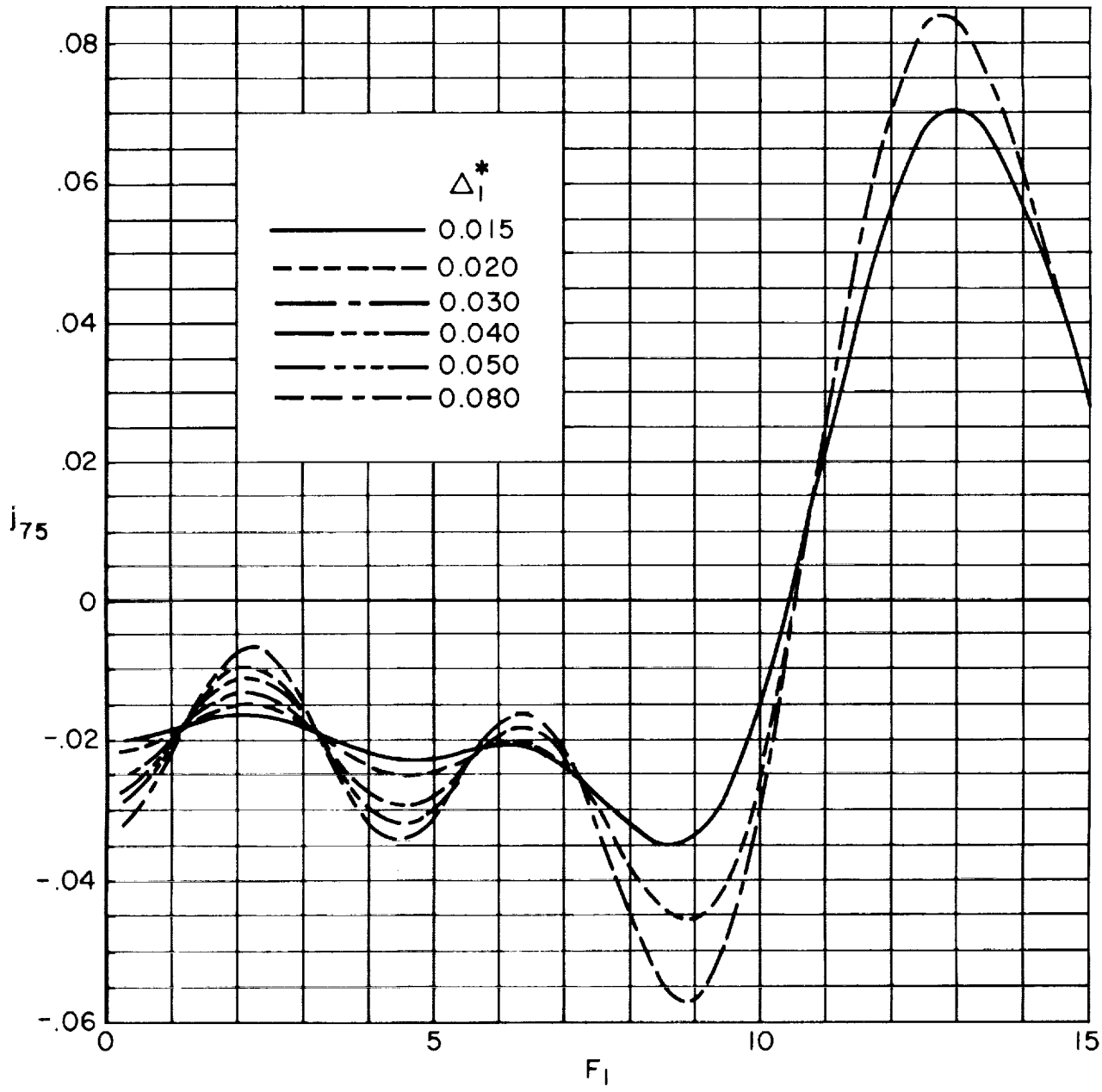

(p) j_{75}

Figure 10. – Concluded.

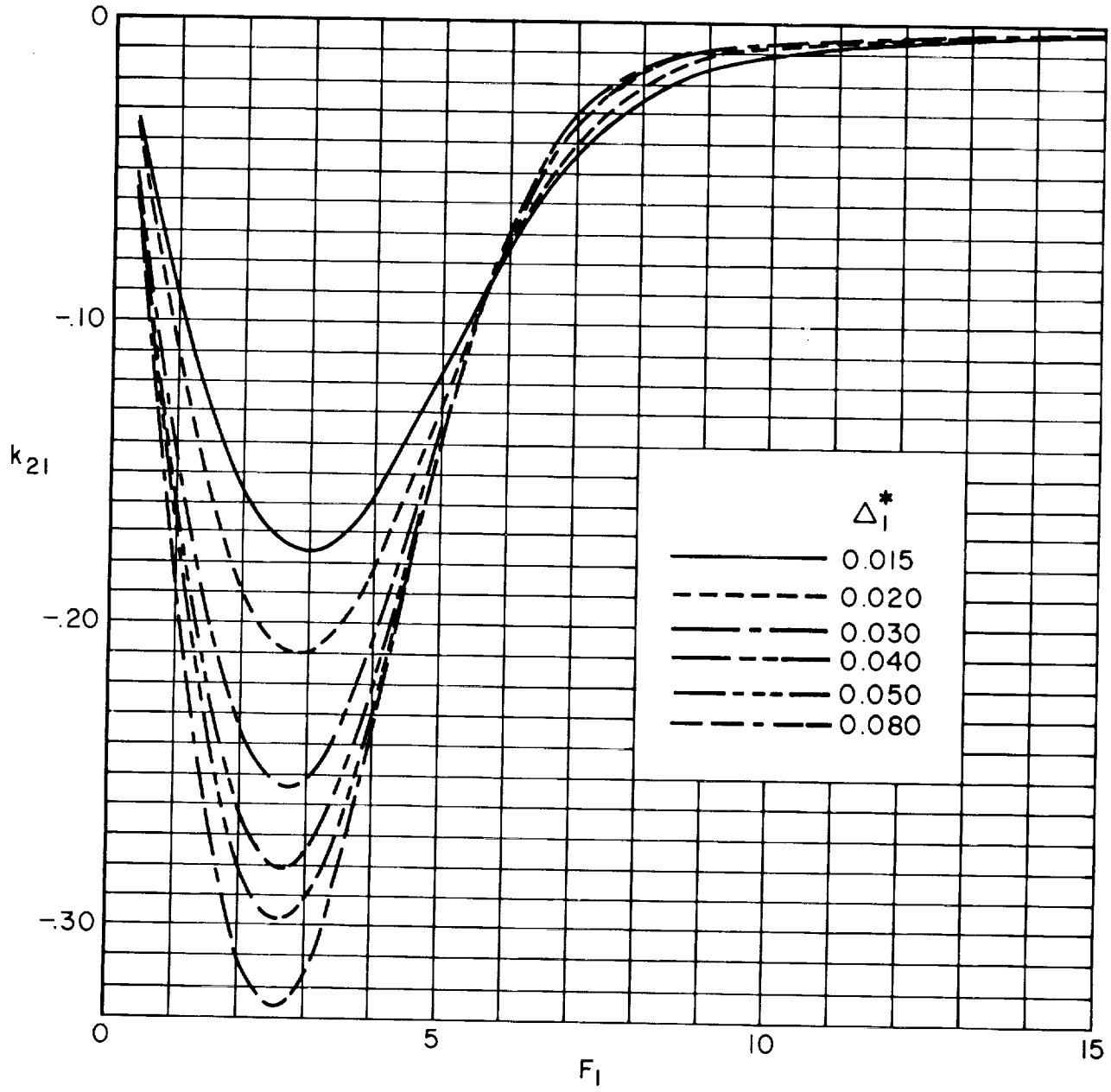

(a) k_{21}

Figure 11. – Imaginary part of longitudinal acceptance of clamped edge panels.

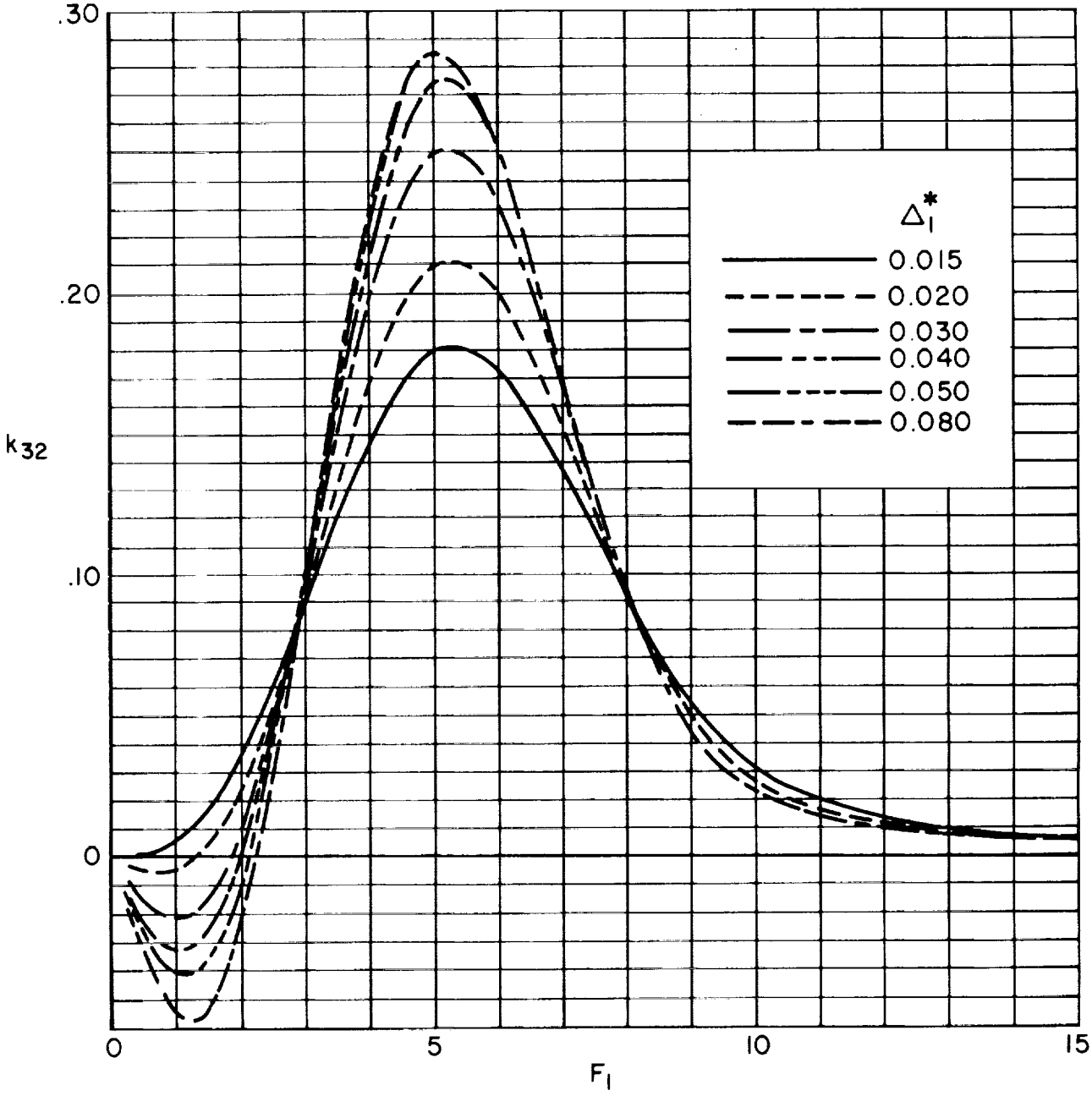

(b) k_{32}

Figure 11. – Continued.

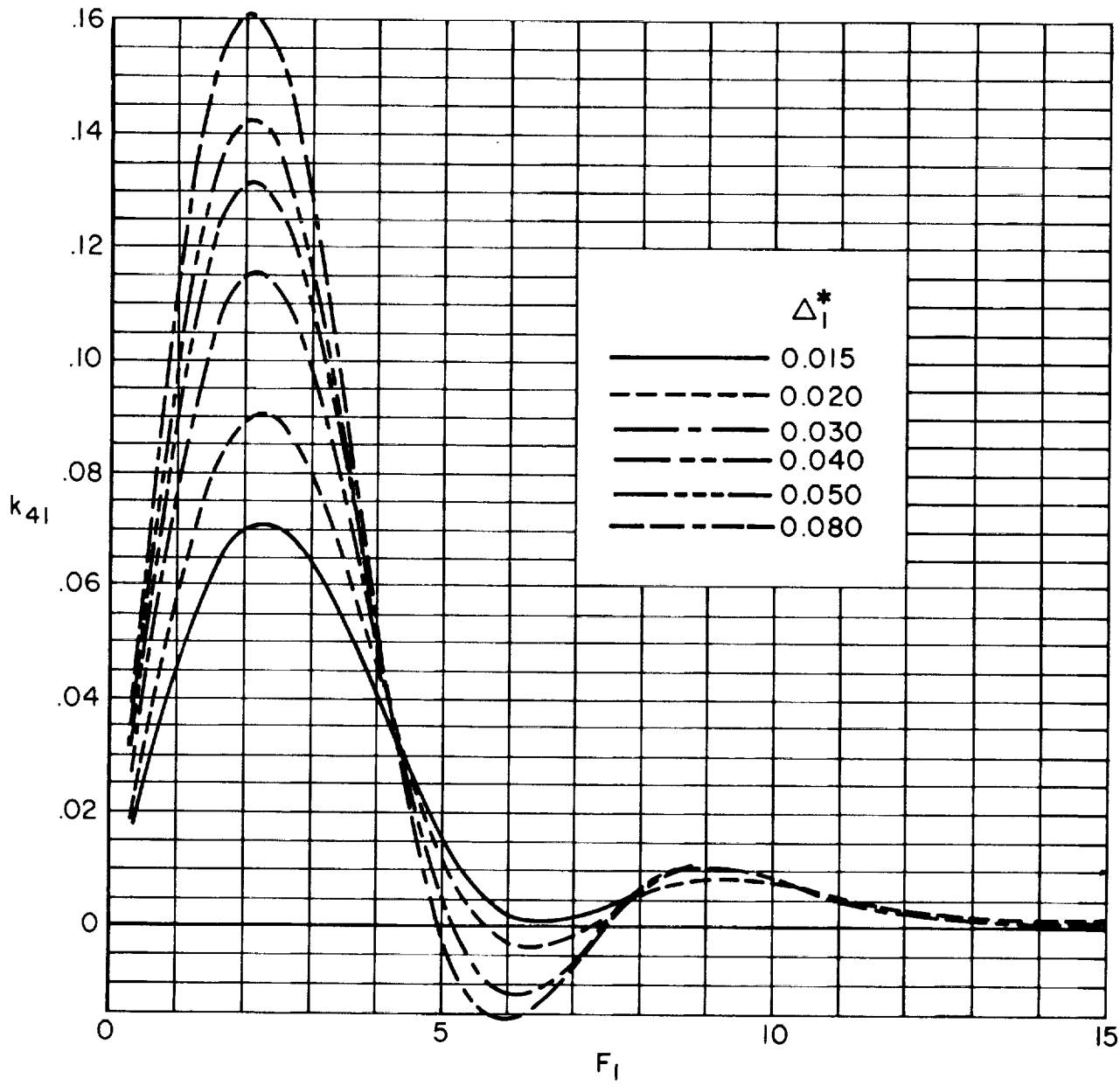

(c) k_{41}

Figure 11. – Continued.

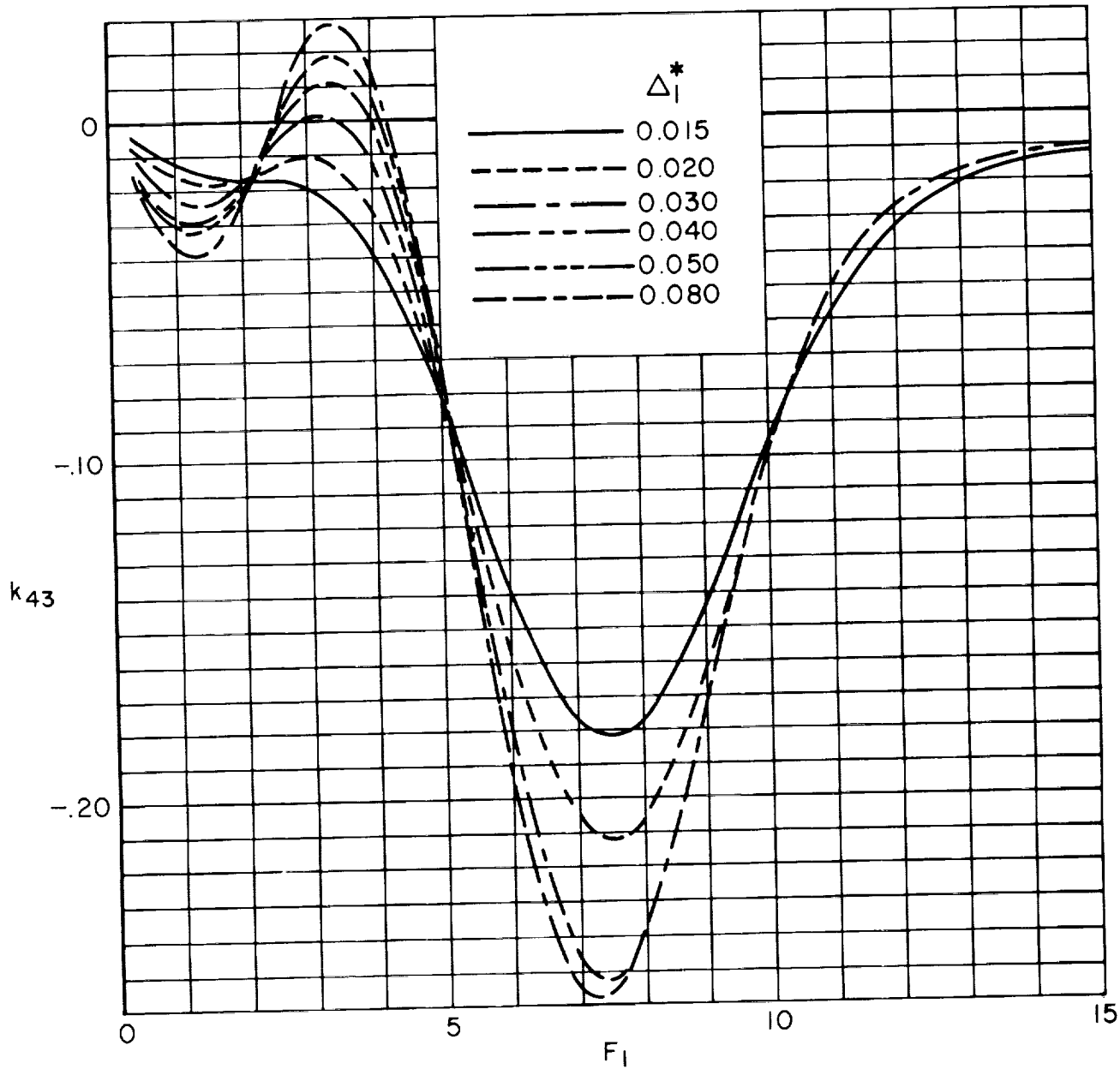

(d) k_{43}

Figure 11. – Continued.

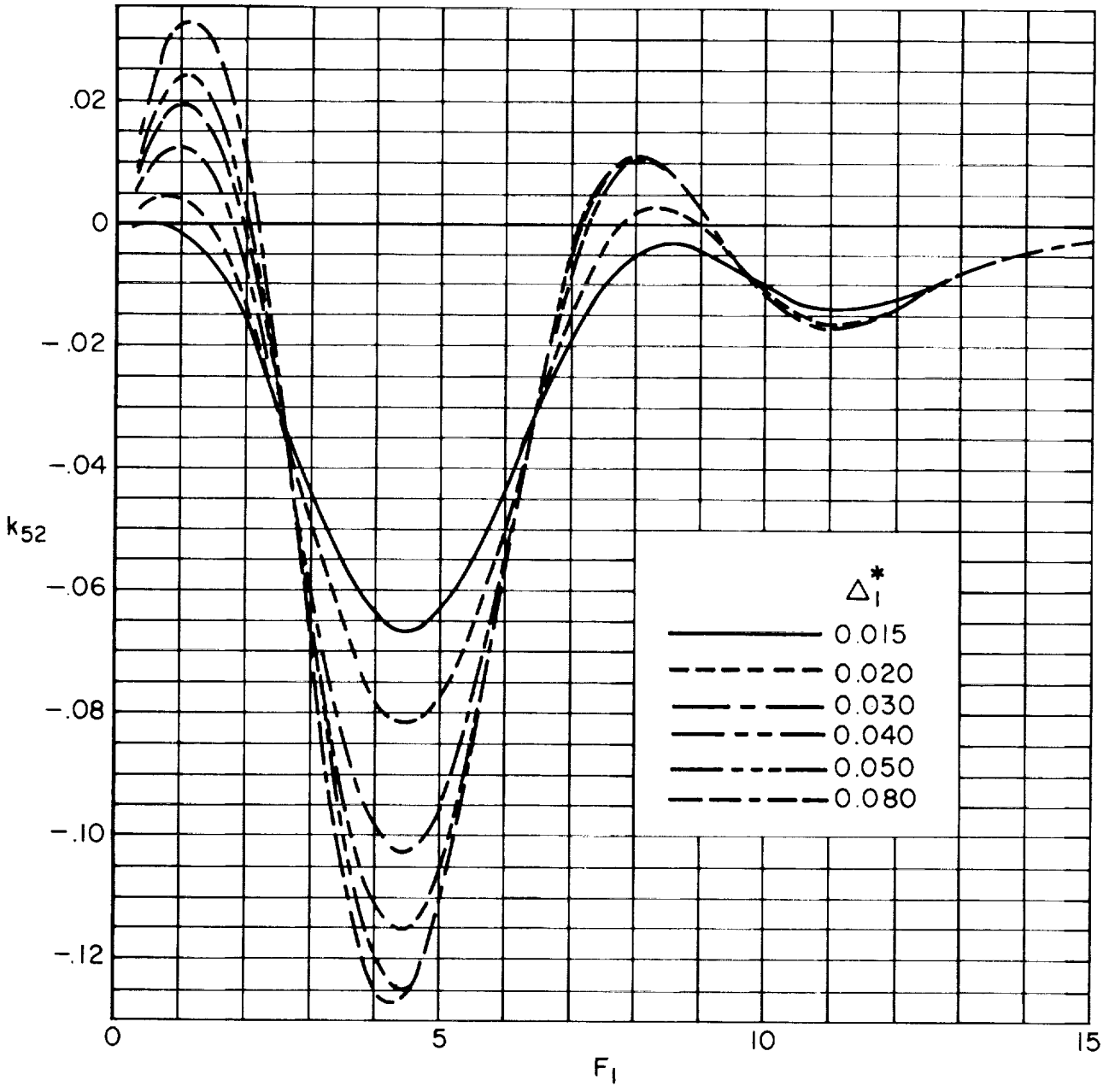

(e) k_{52}

Figure 11. – Continued.

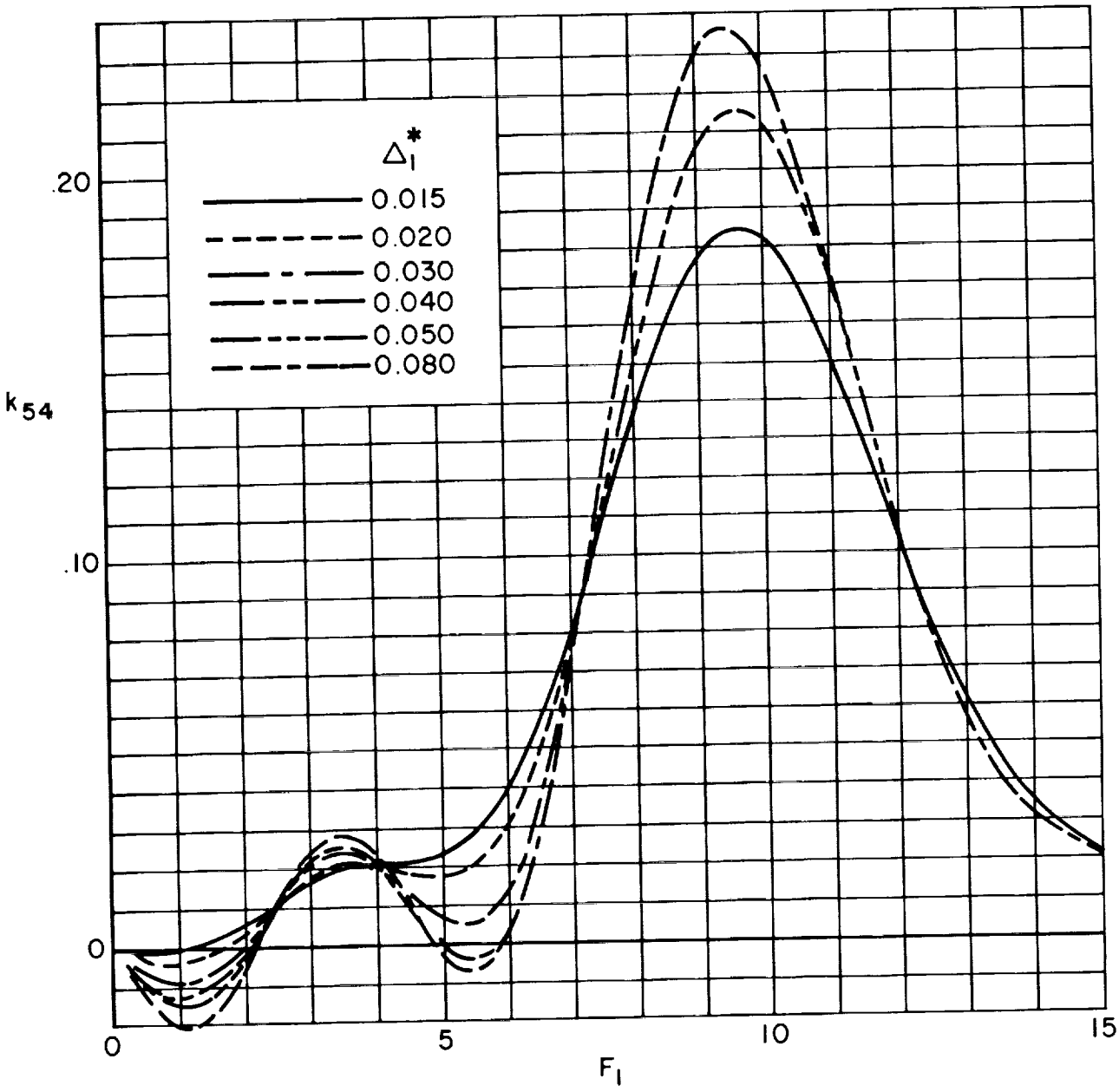

(f) k_{54}

Figure 11. – Continued.

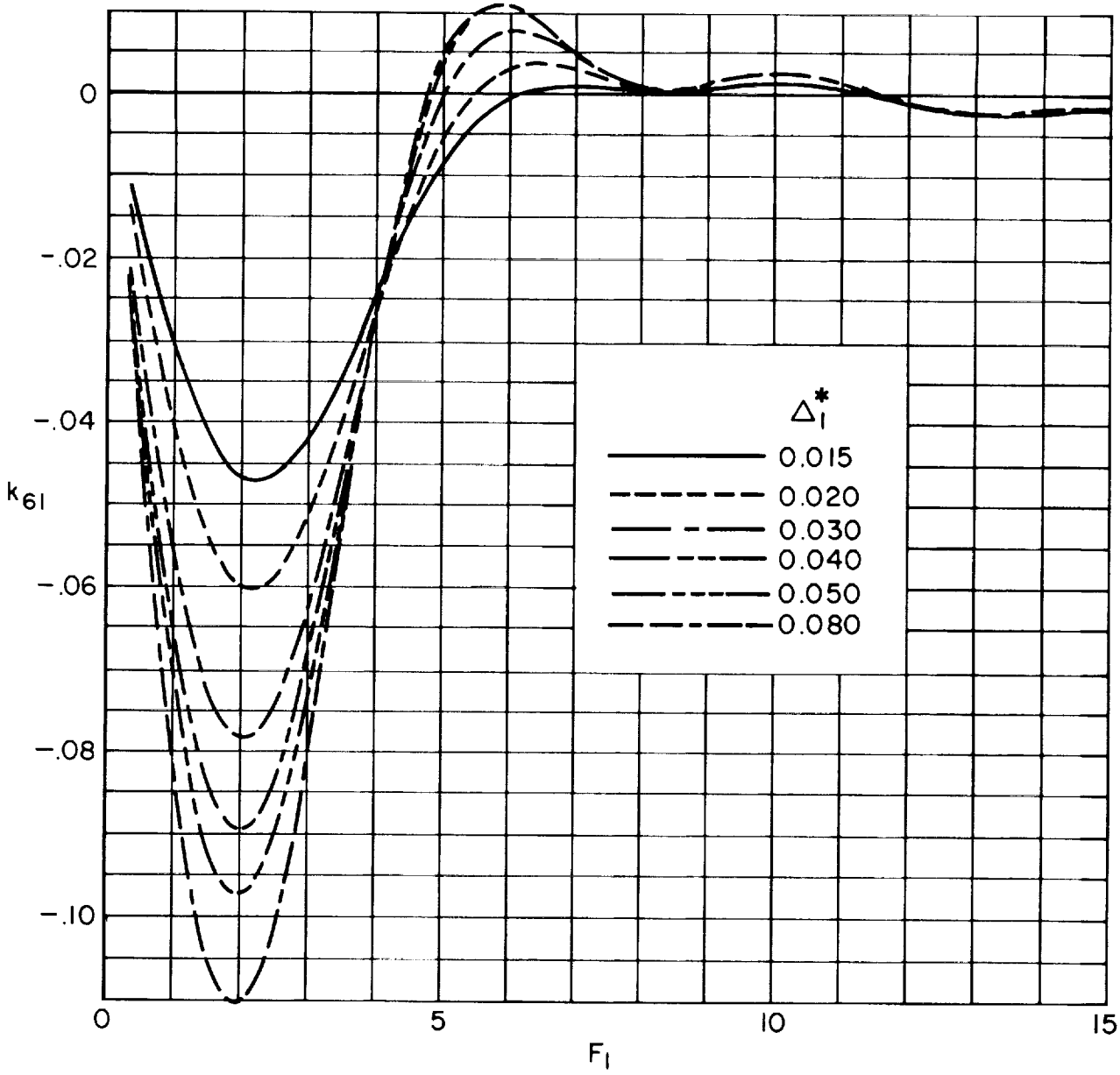

(g) k_{61}

Figure 11. – Continued.

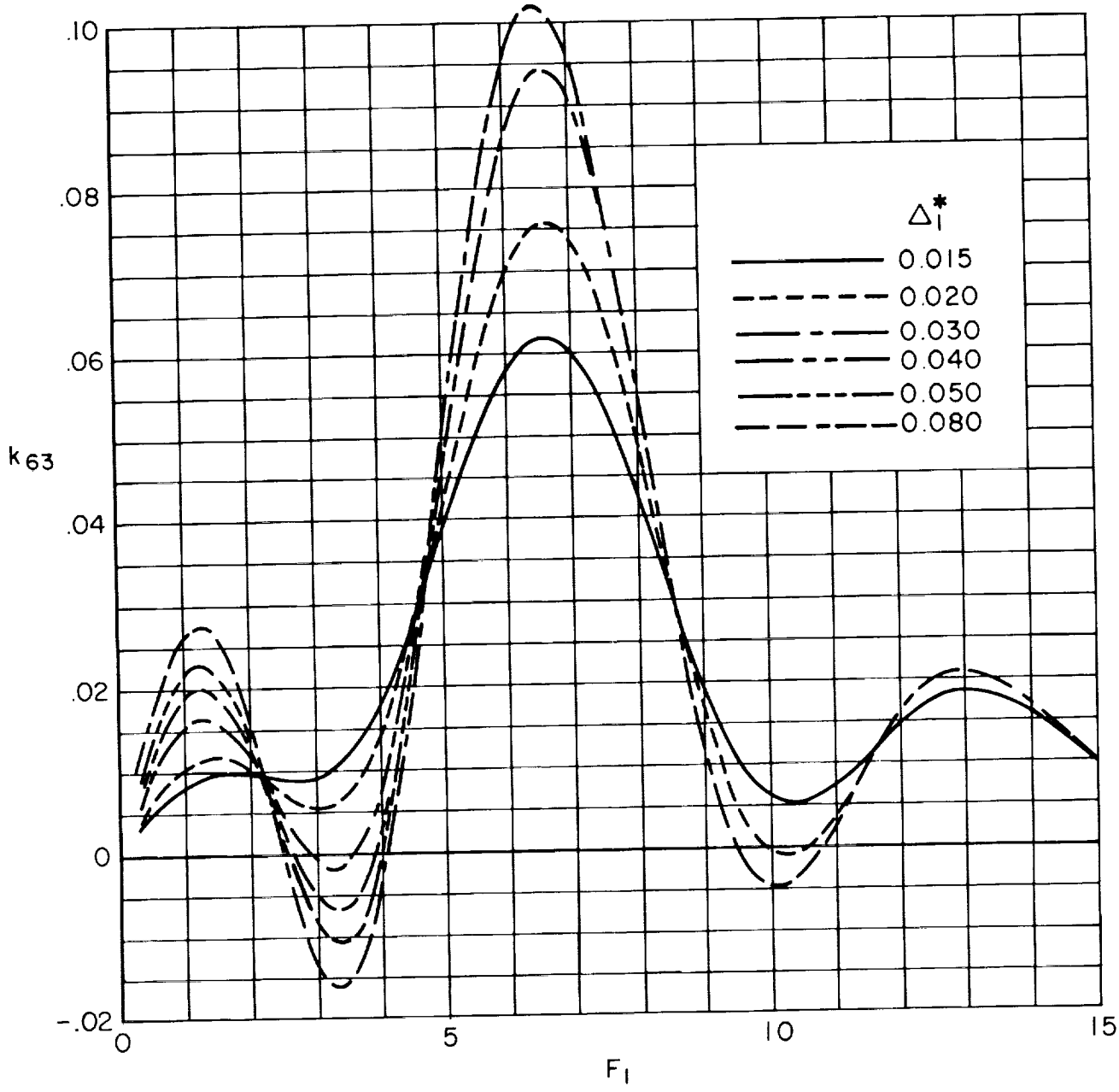

(h) k_{63}

Figure 11. – Continued.

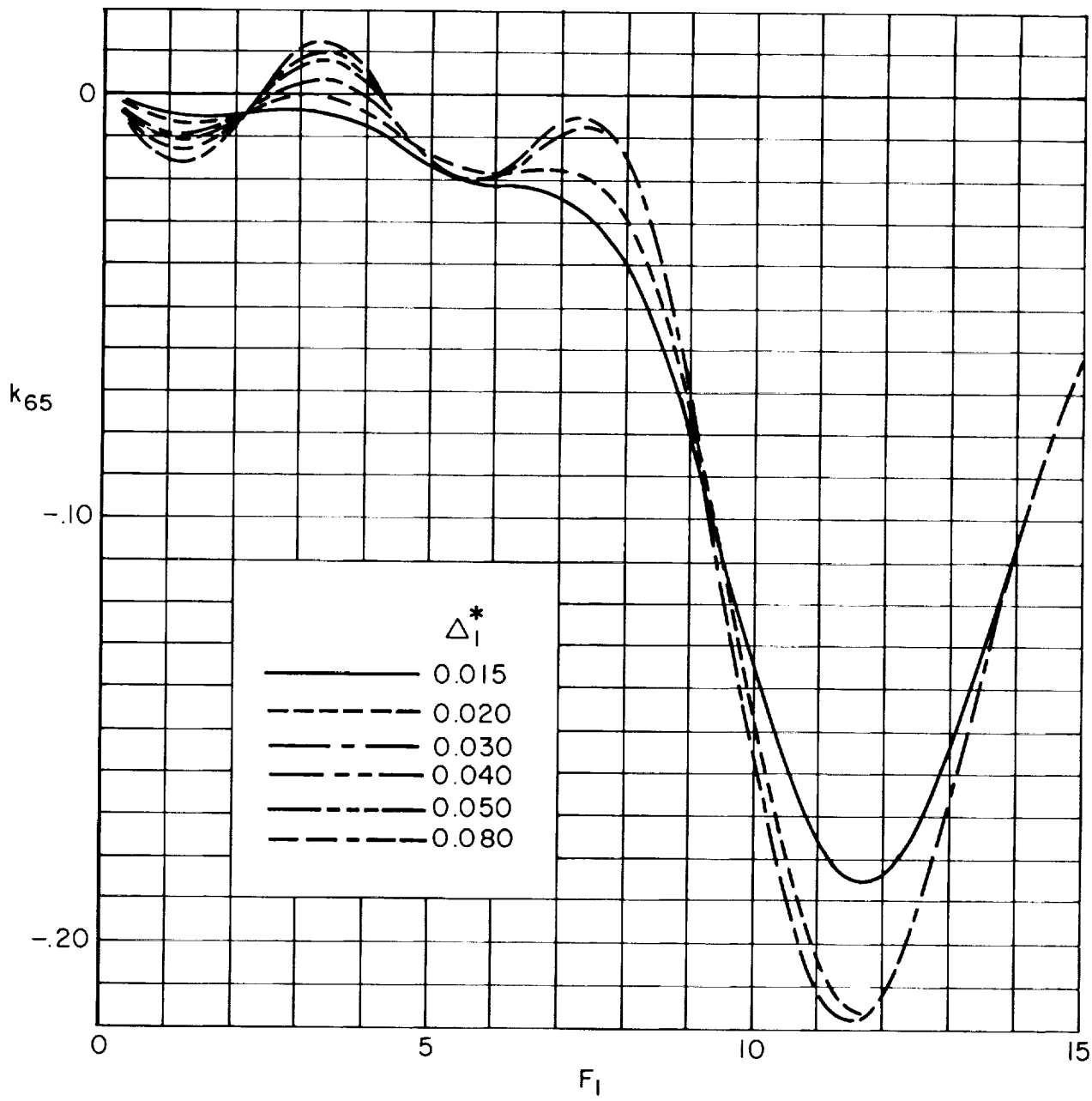

(i) k_{65}

Figure 11. – Continued.

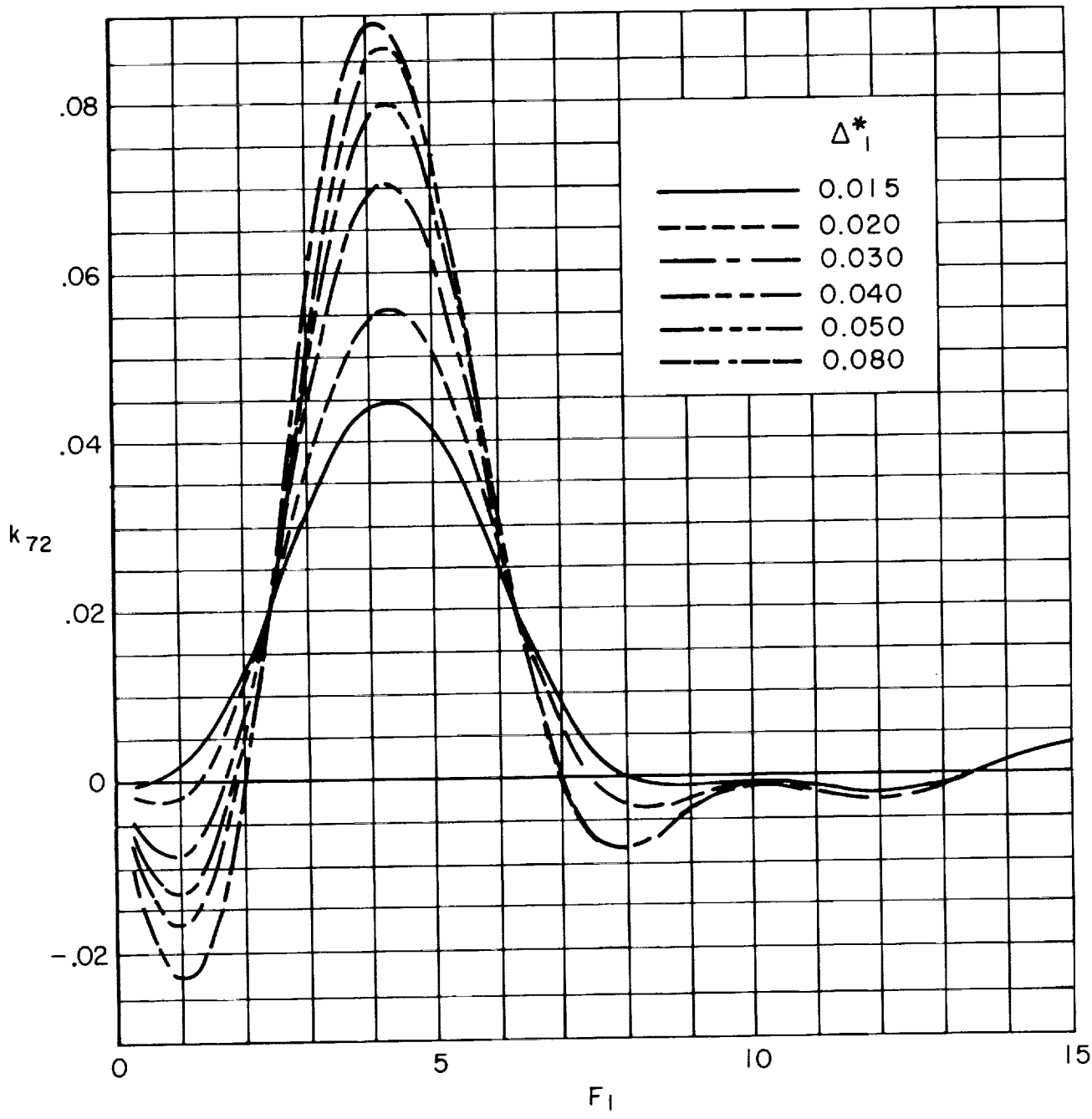

(j) k_{72}

Figure 11. – Continued.

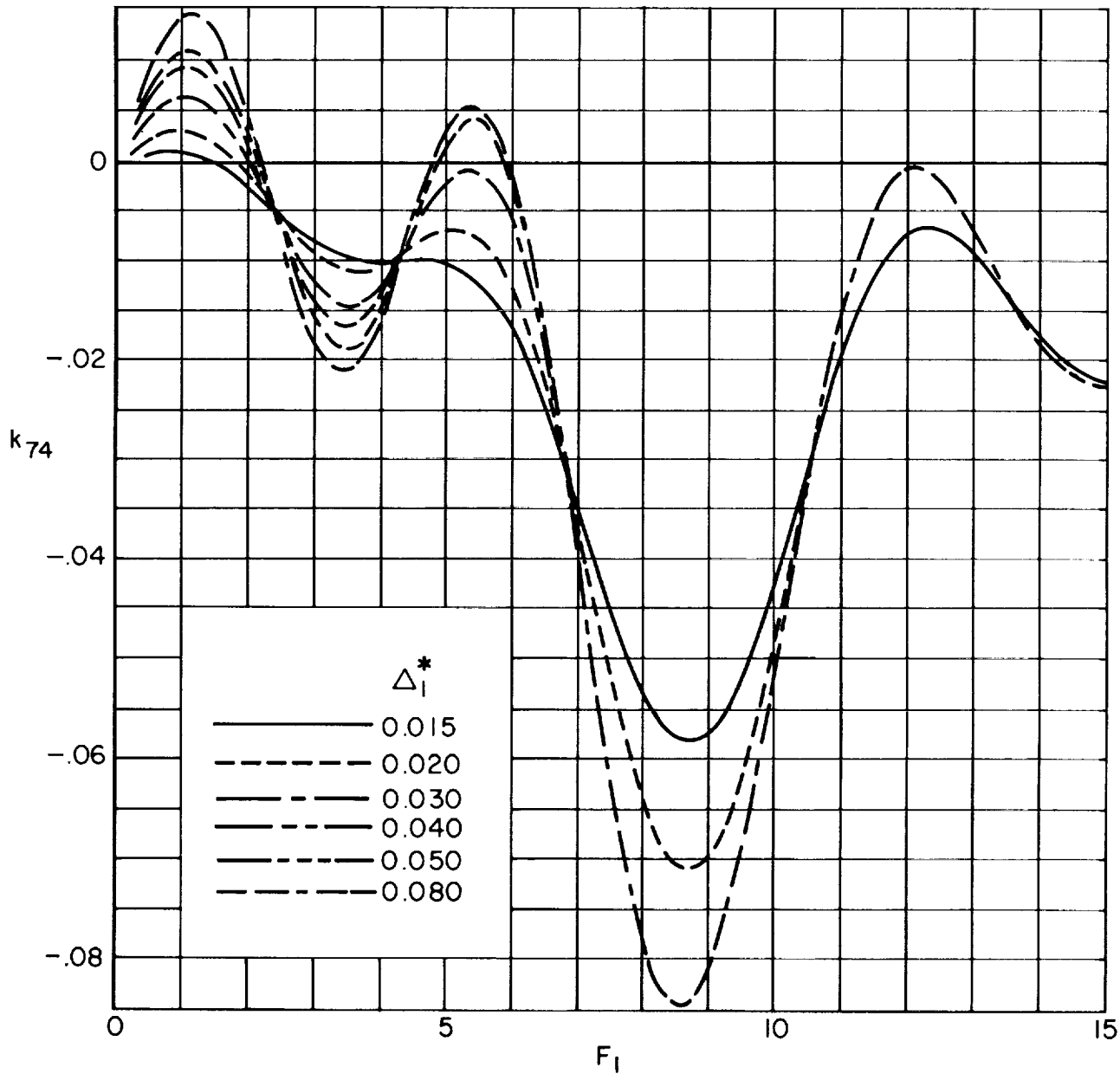

(k) k_{74}

Figure 11. – Continued.

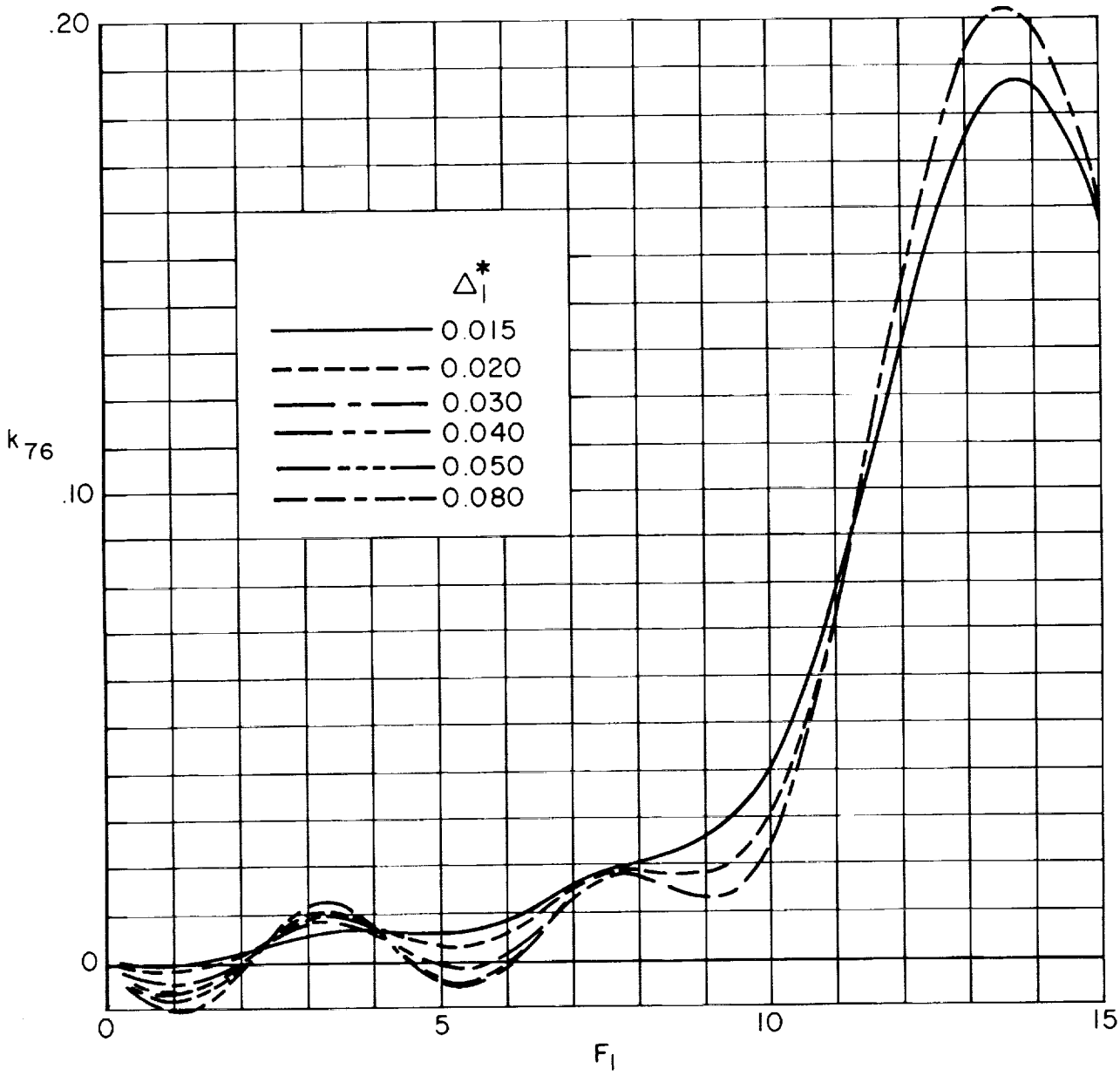

(l) k_{76}

Figure 11. – Concluded.

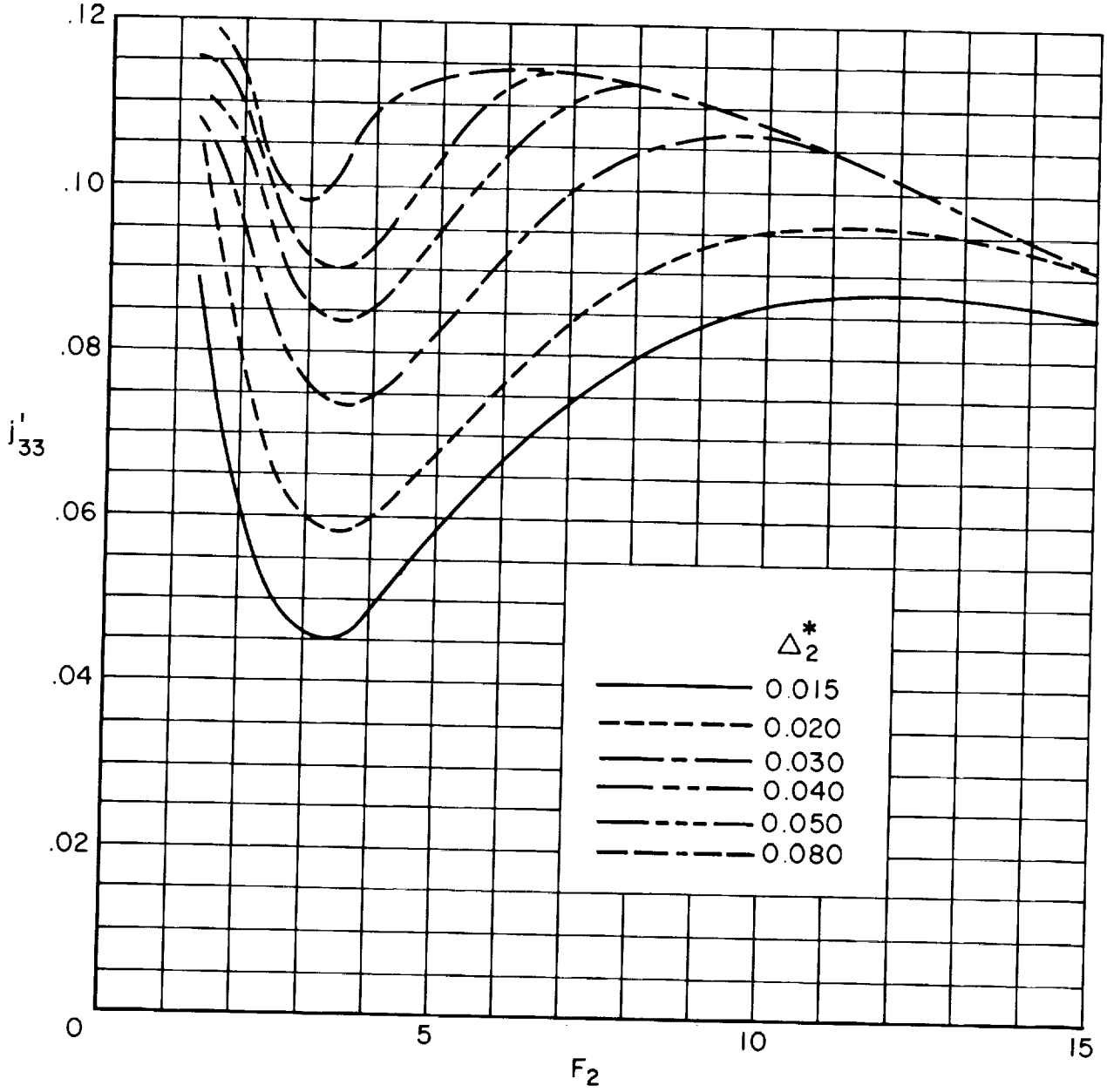

(c) j'_{33}

Figure 12. – Continued.

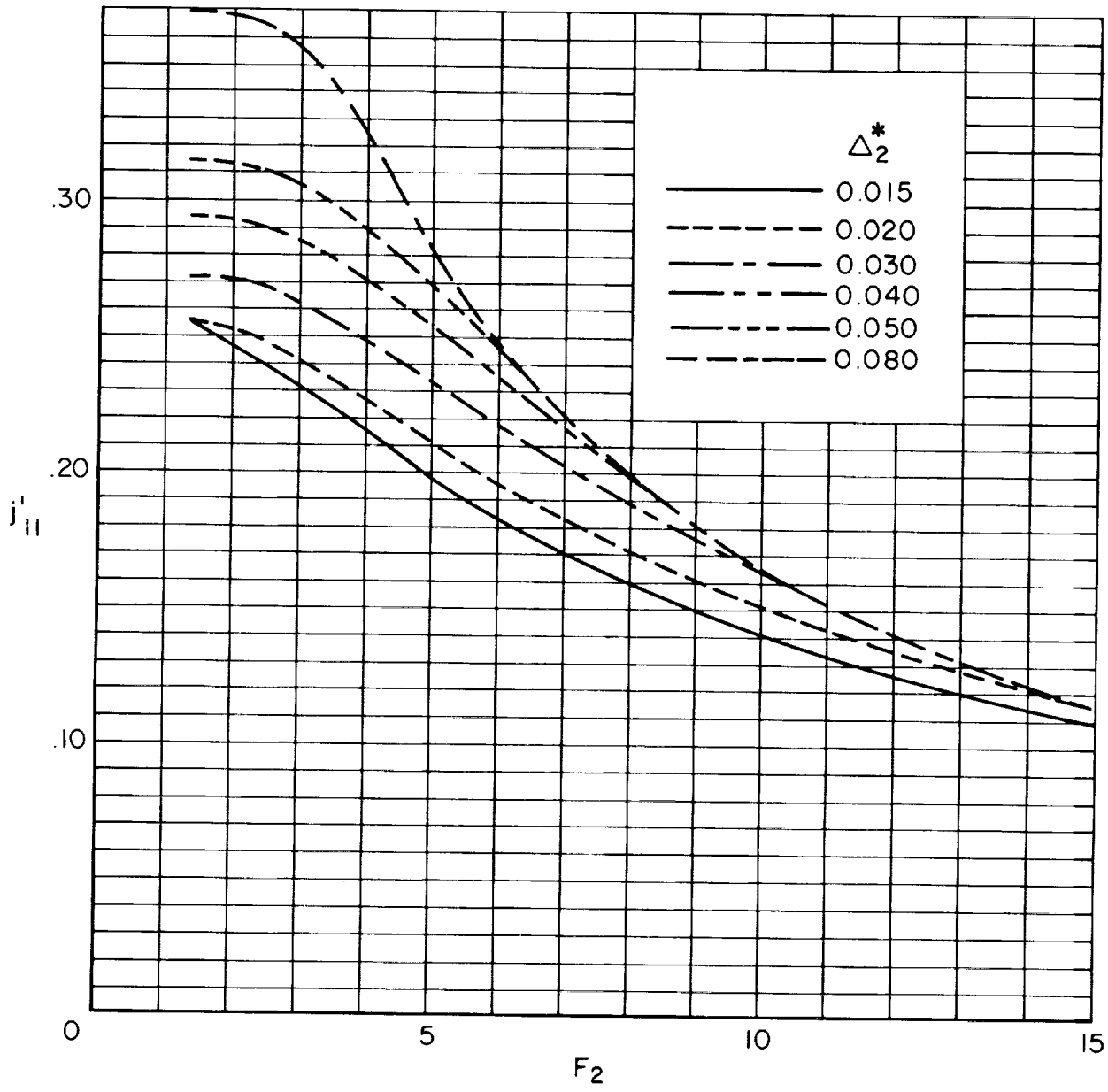

(a) j'_{11}

Figure 12. – Lateral acceptance of clamped edge panels.

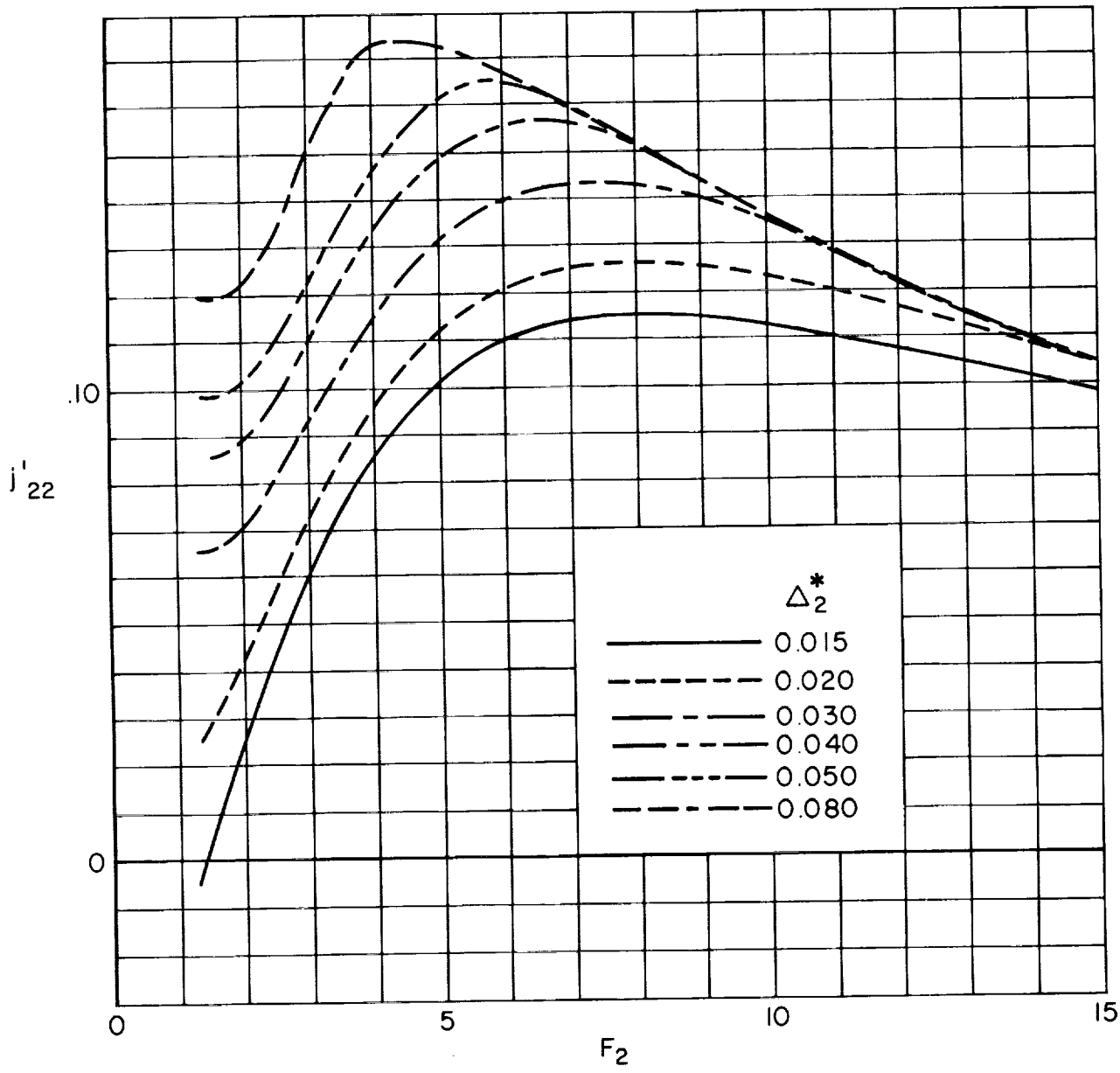

(b) j'_{22}

Figure 12. – Continued.

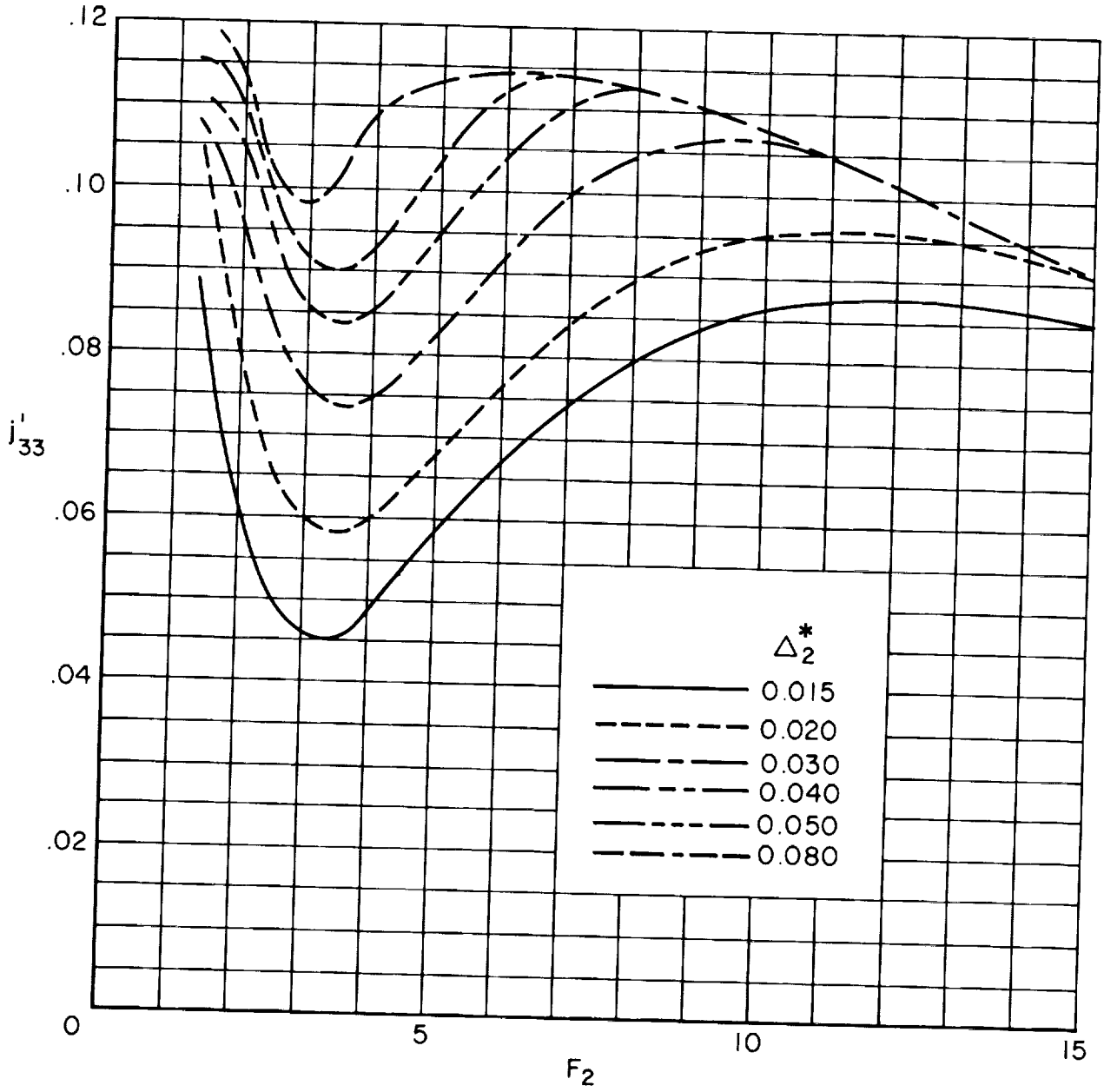

(c) j'_{33}

Figure 12. – Continued.

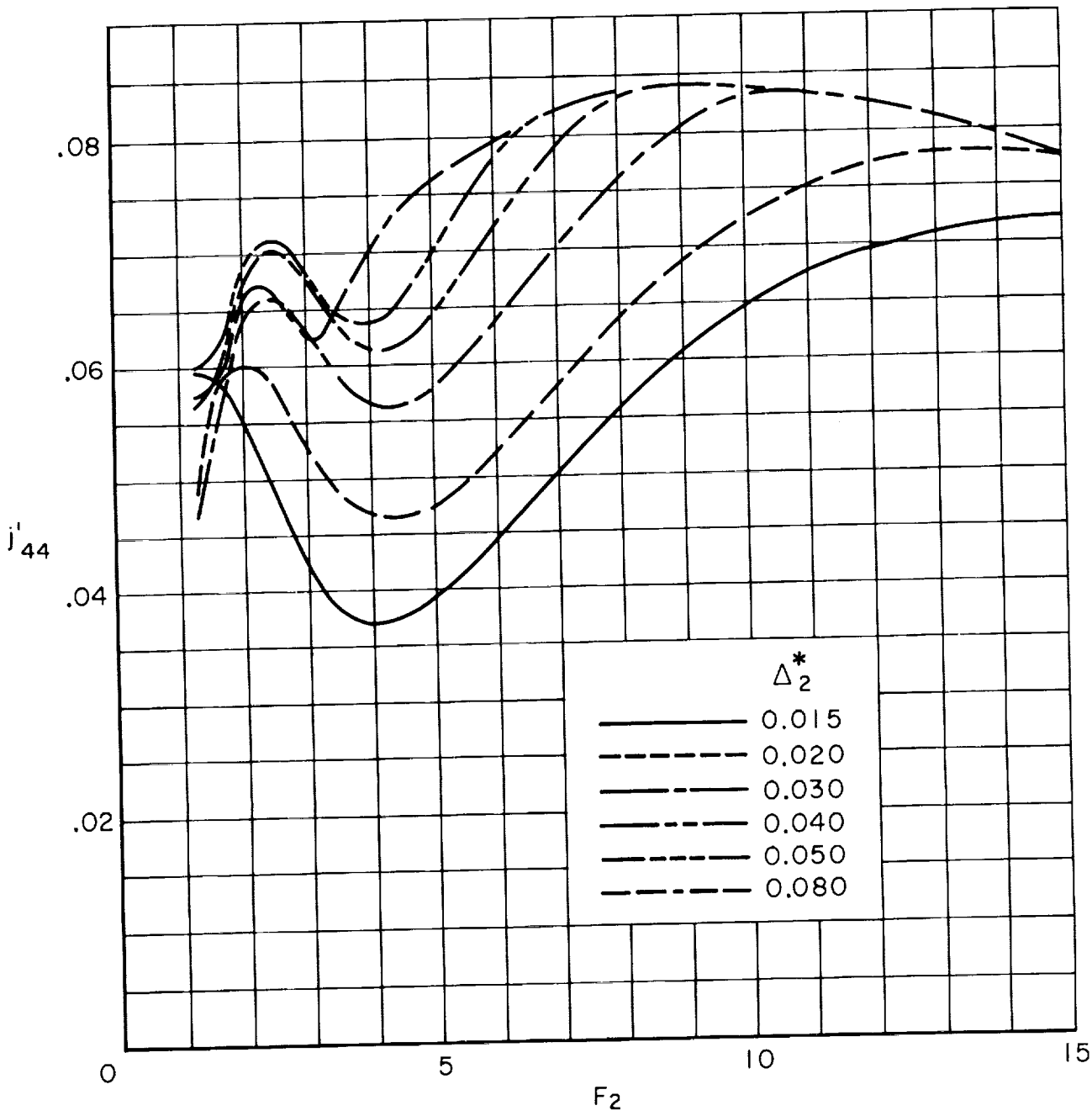

(d) j'_{44}

Figure 12. – Continued.

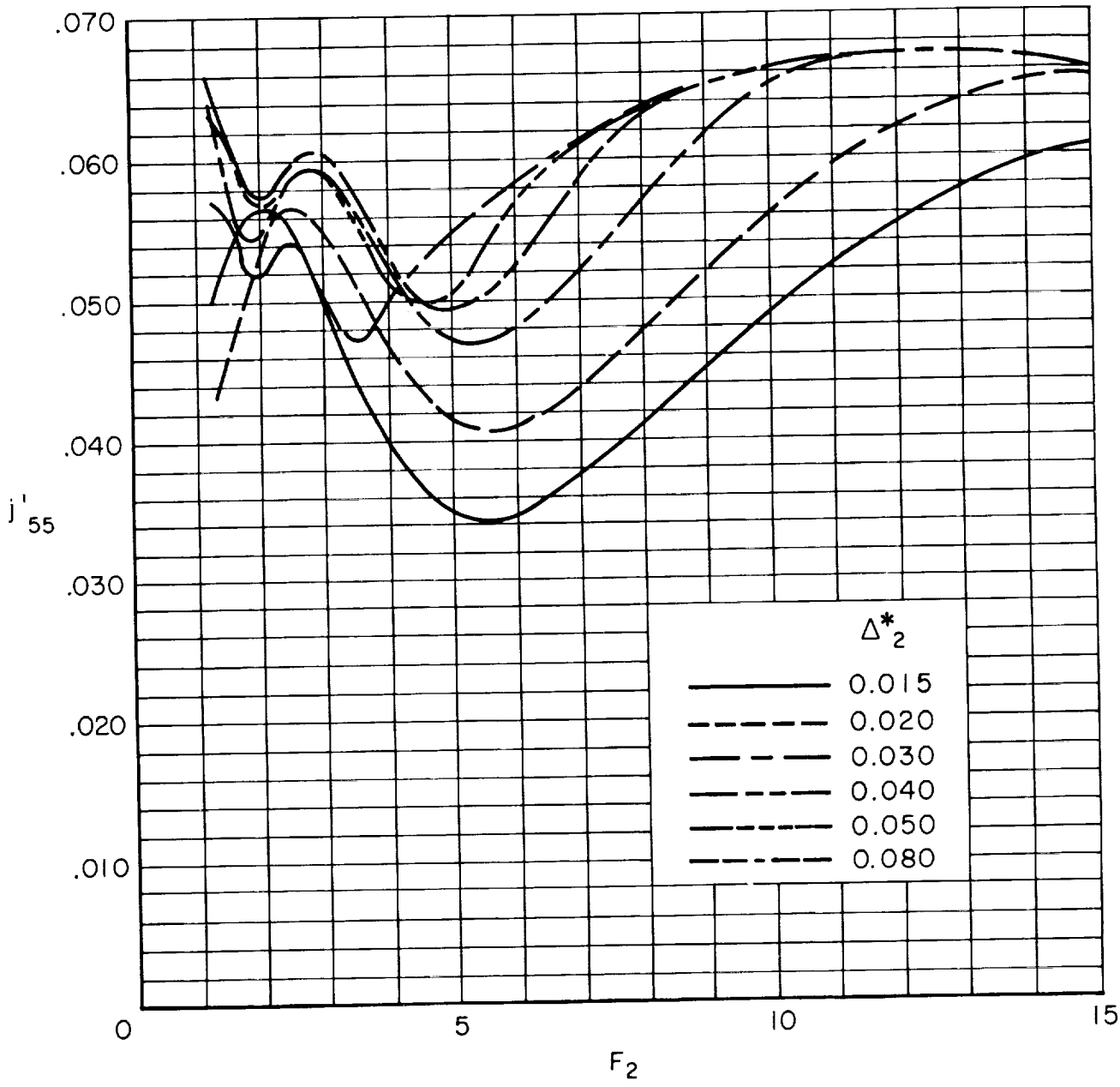

(e) j'_{55}

Figure 12. – Continued.

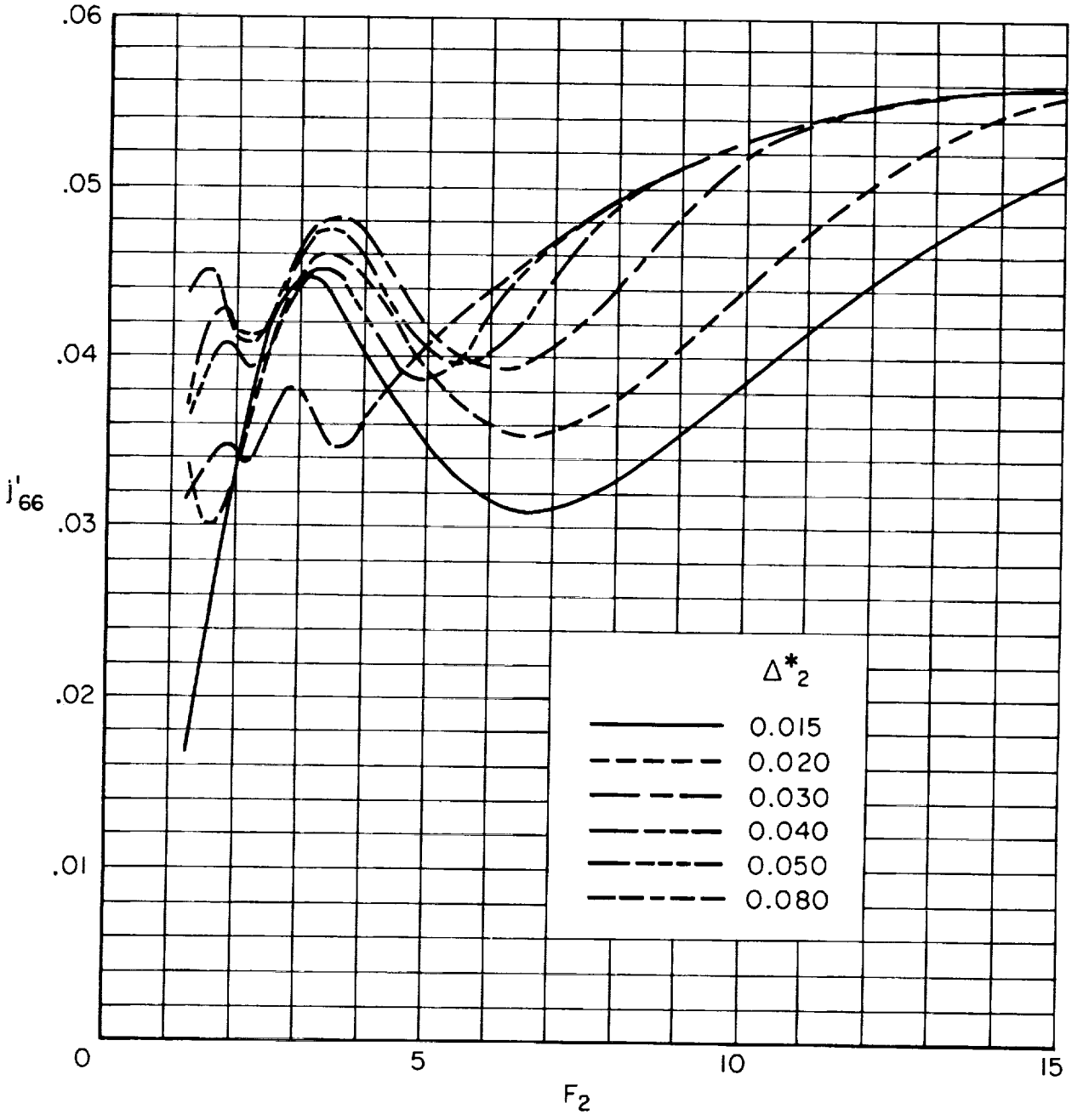

(f) j'_{66}

Figure 12. – Continued.

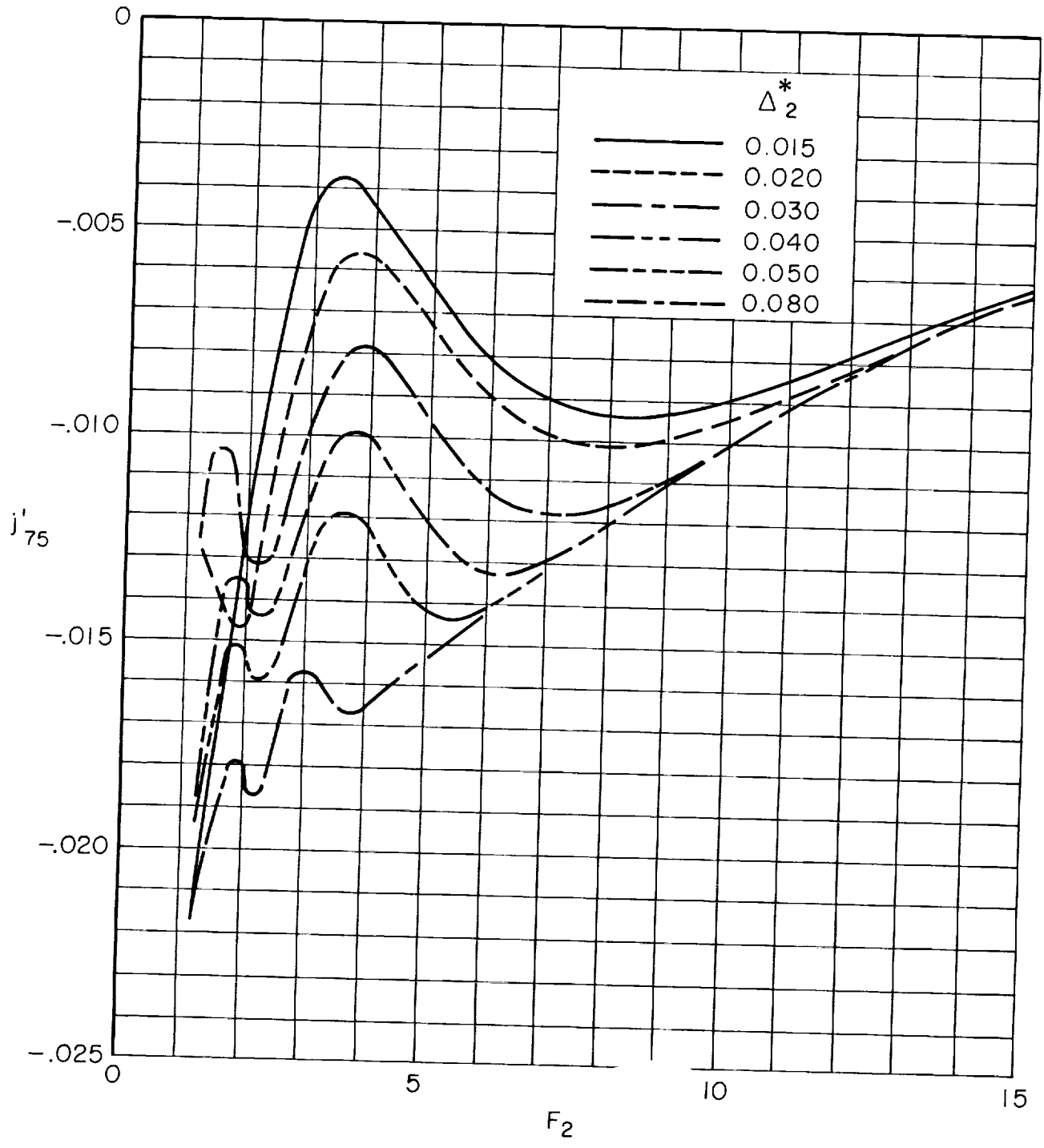

(p) j'_{75}

Figure 12. – Concluded.

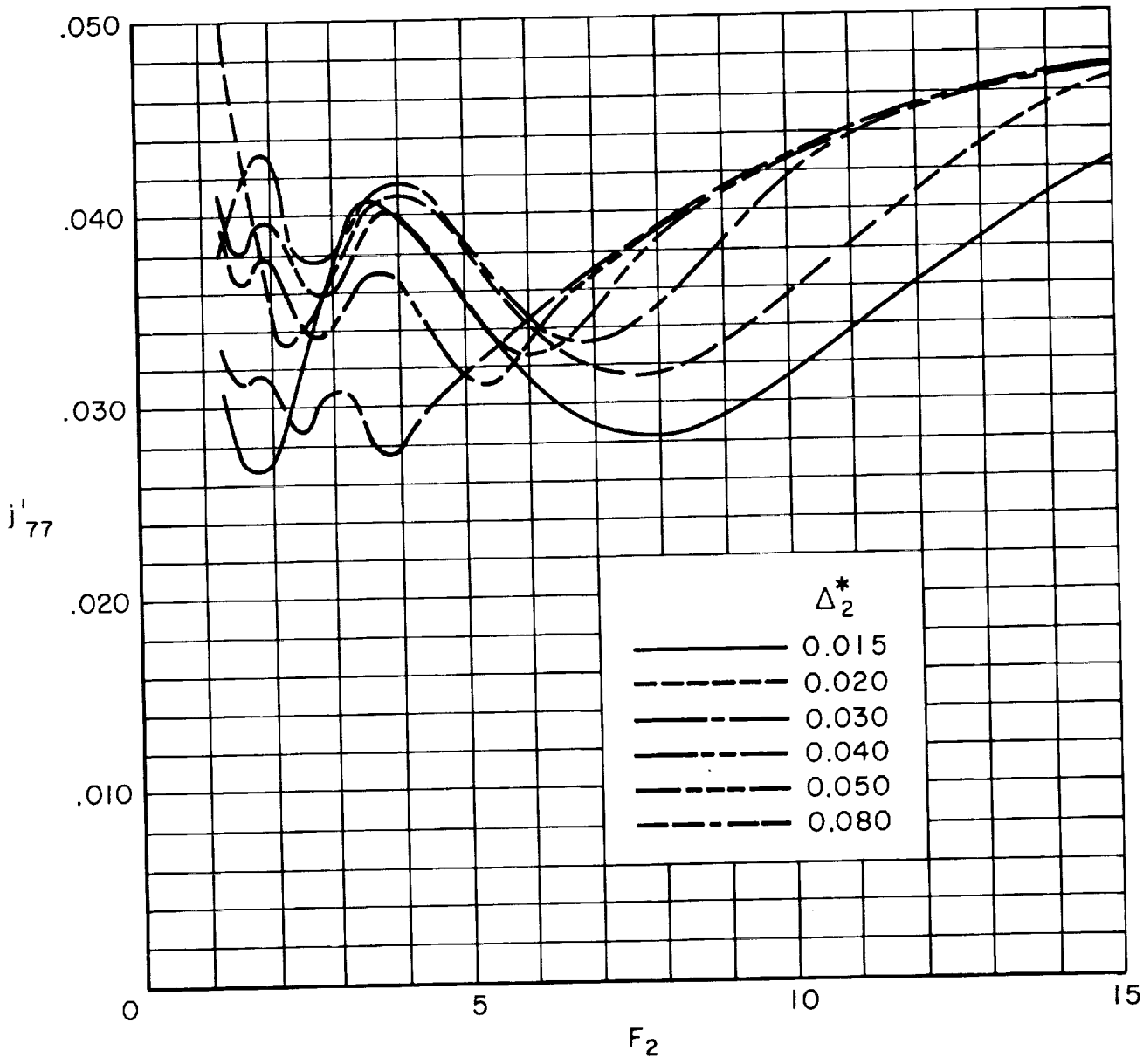

(g) j'_{77}

Figure 12. – Continued.

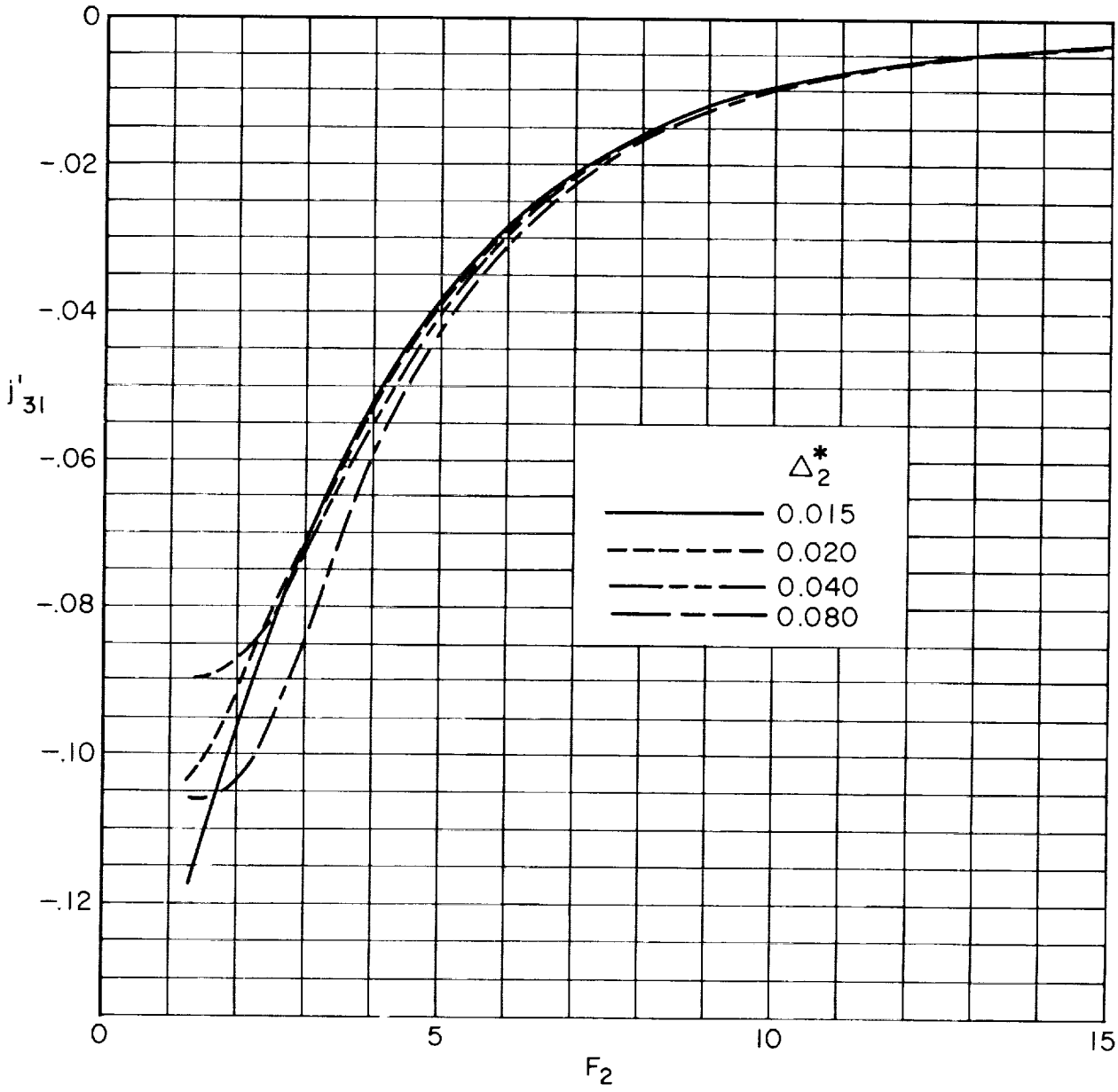

(h) j'_{31}

Figure 12. – Continued.

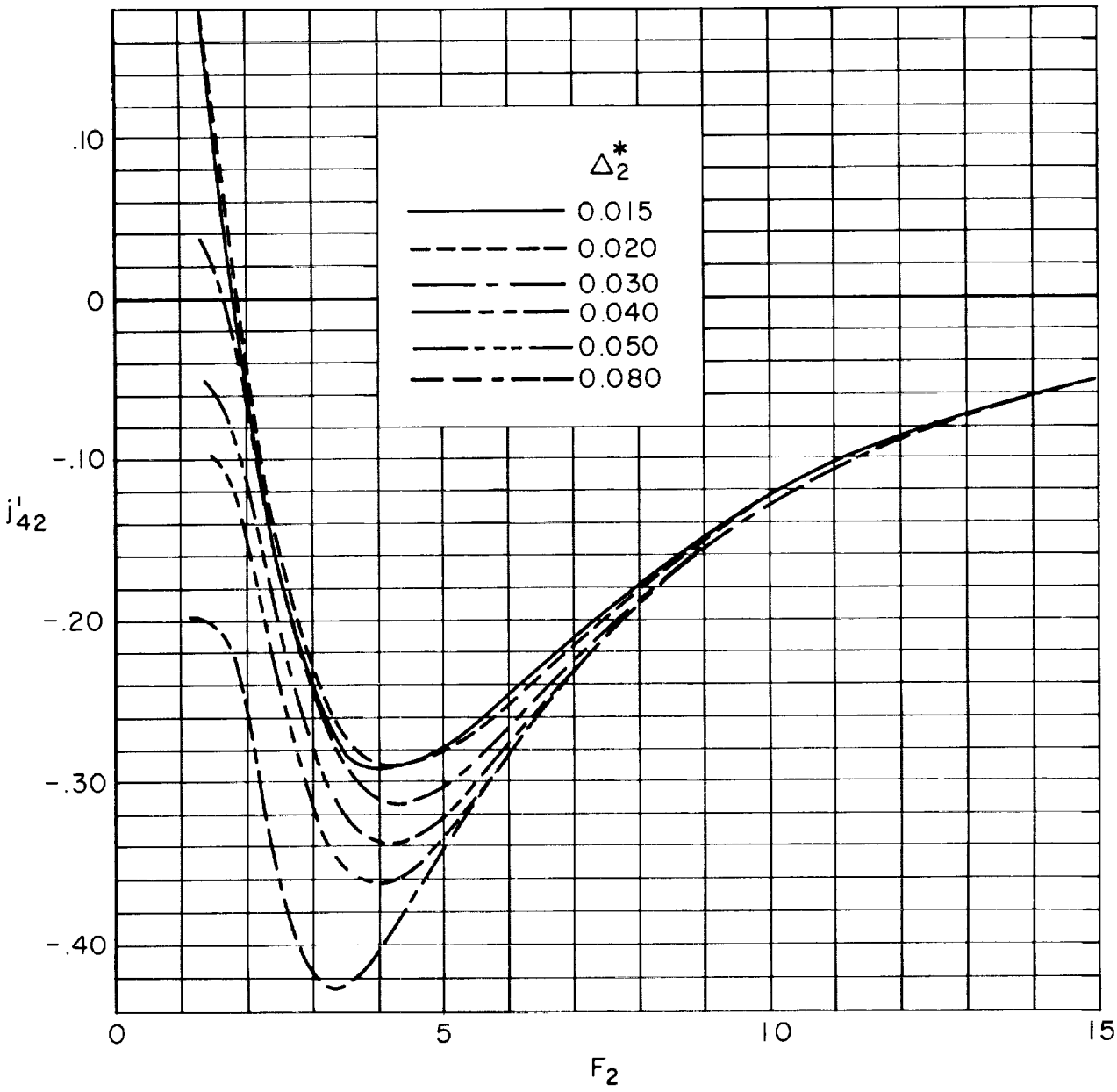

(i) j'_{42}

Figure 12. – Continued.

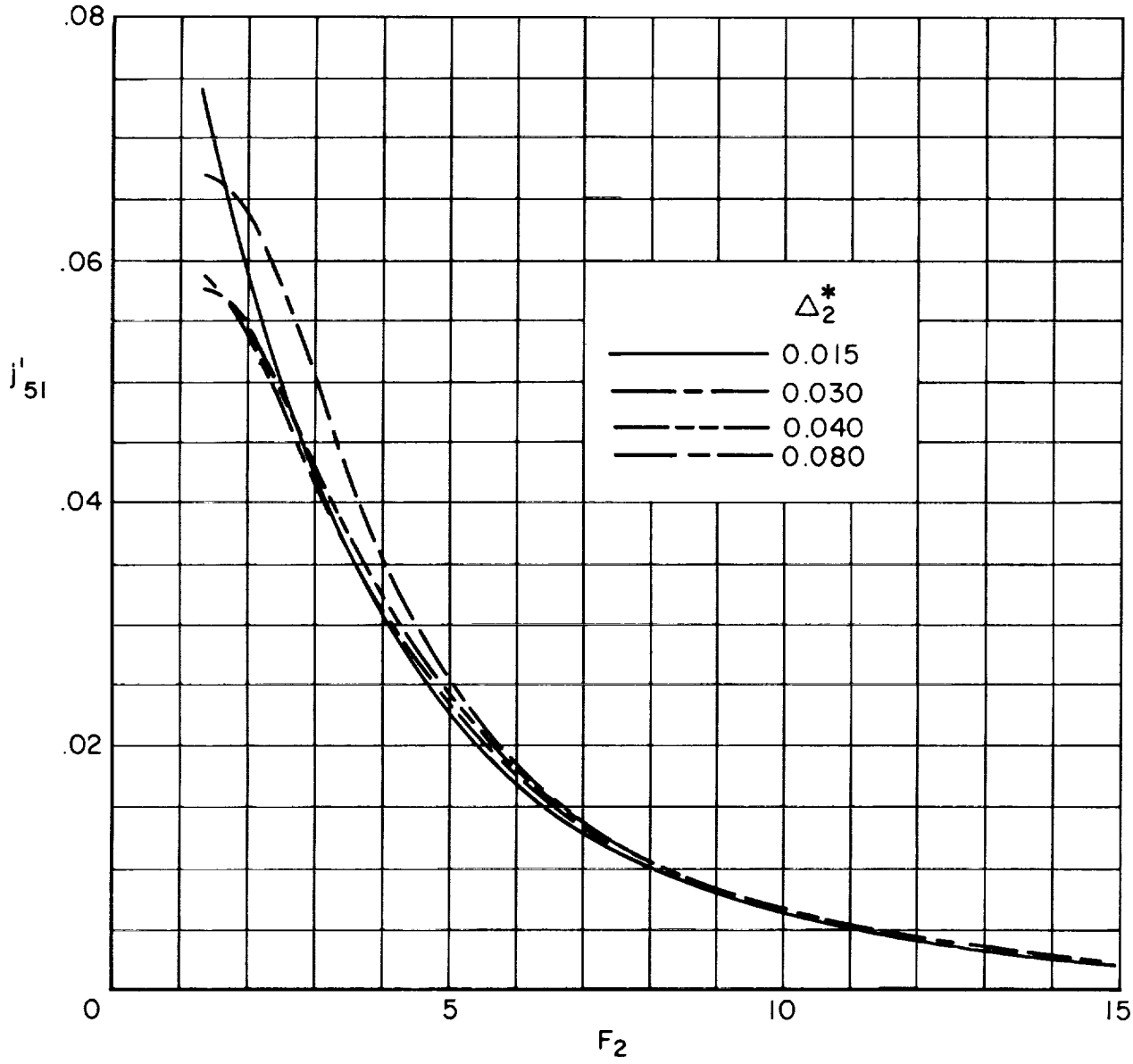

(j) j'_{51}

Figure 12. – Continued.

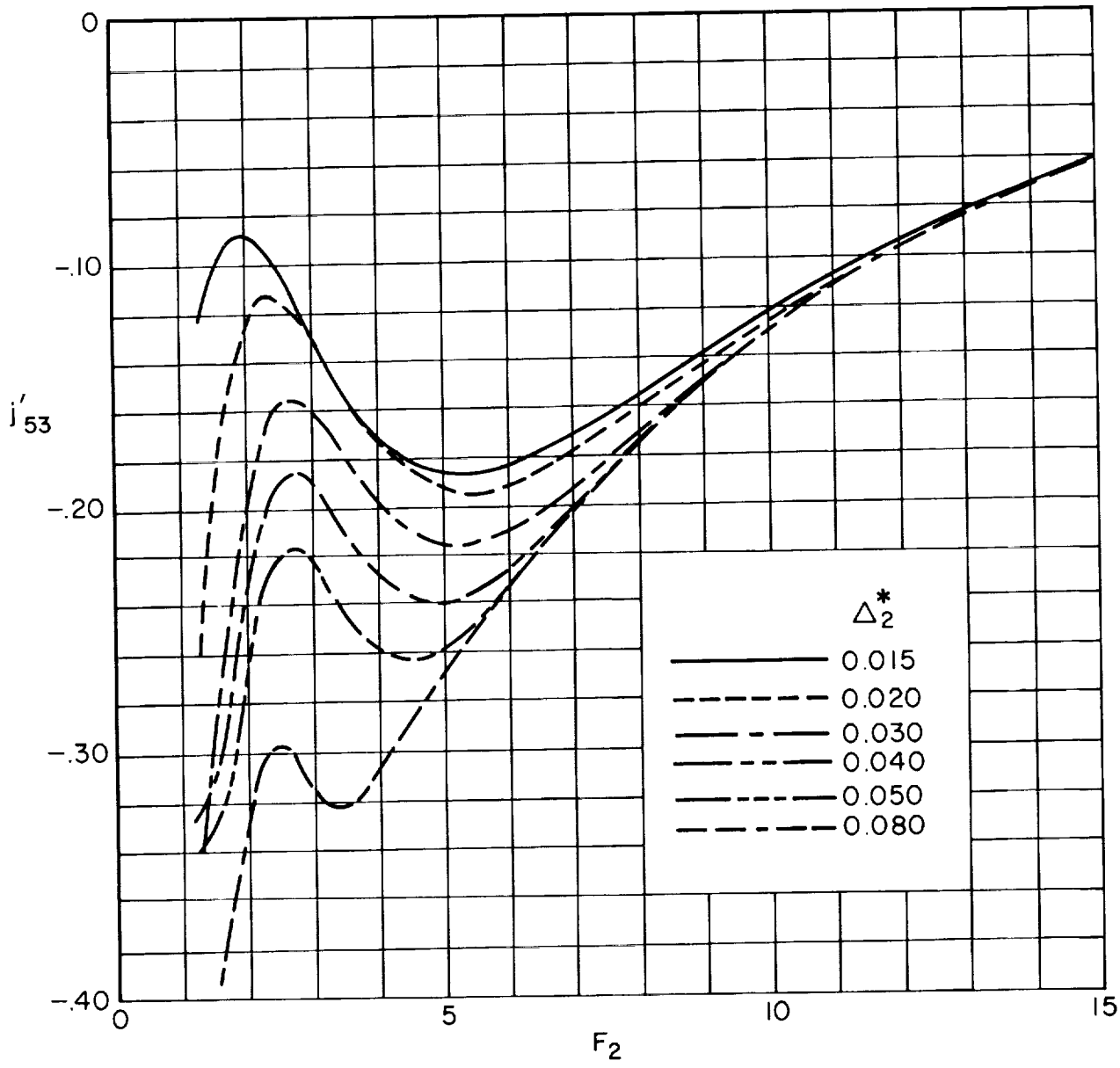

(k) j'_{53}

Figure 12. – Continued.

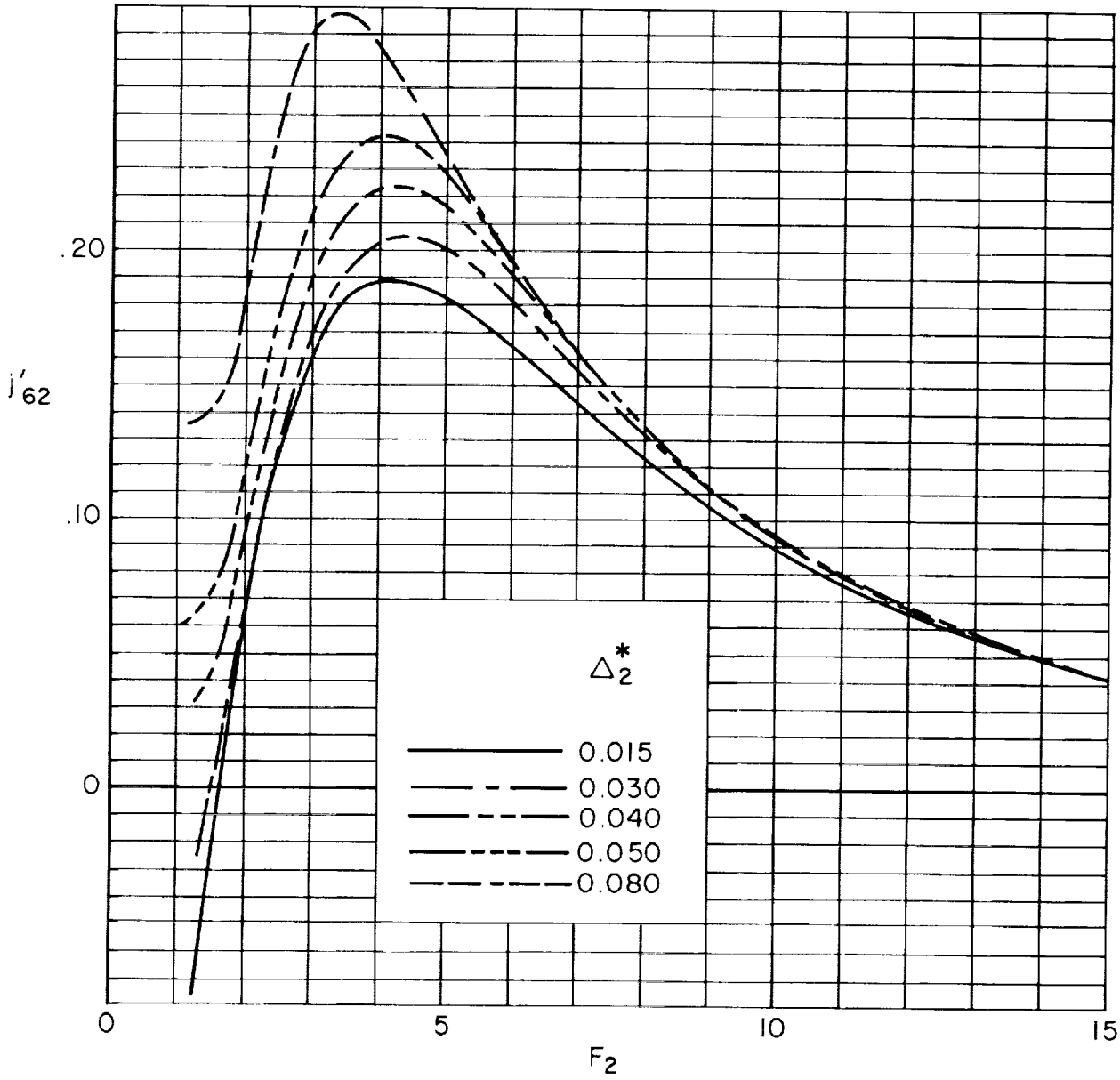

(l) j'_{62}

Figure 12. – Continued.

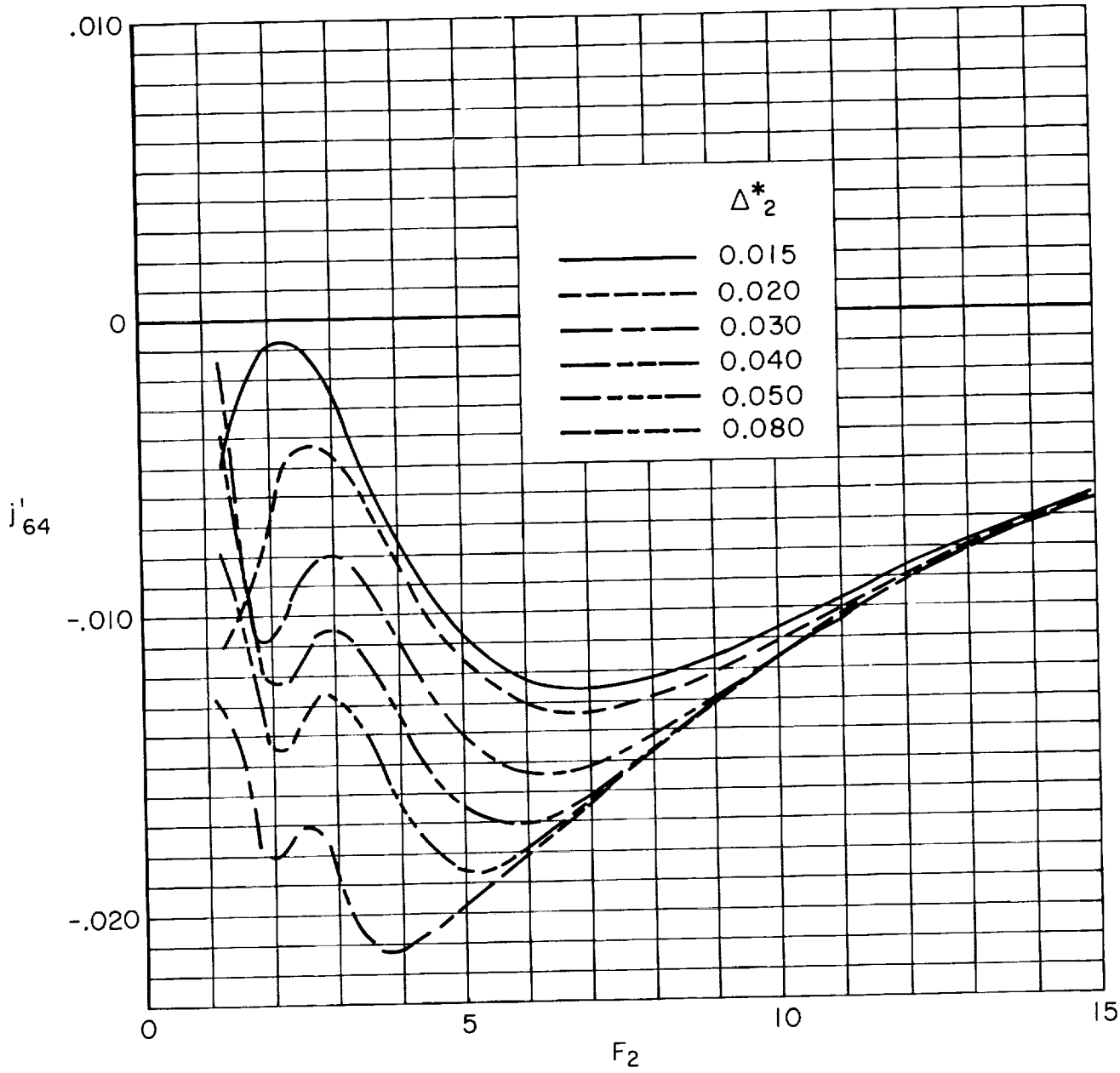

(m) j'_{64}

Figure 12. – Continued.

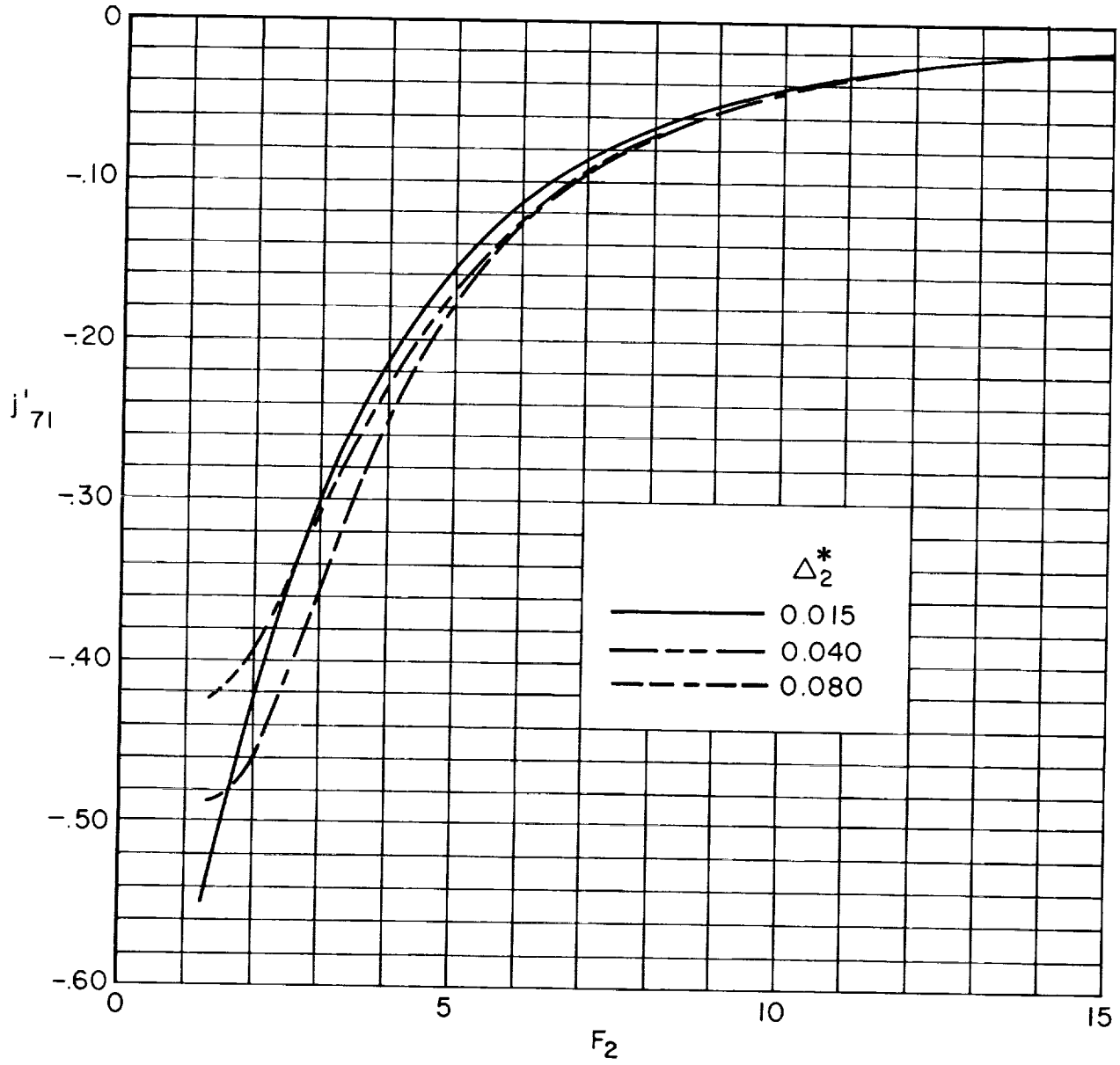

(n) j'_{71}

Figure 12. – Continued.

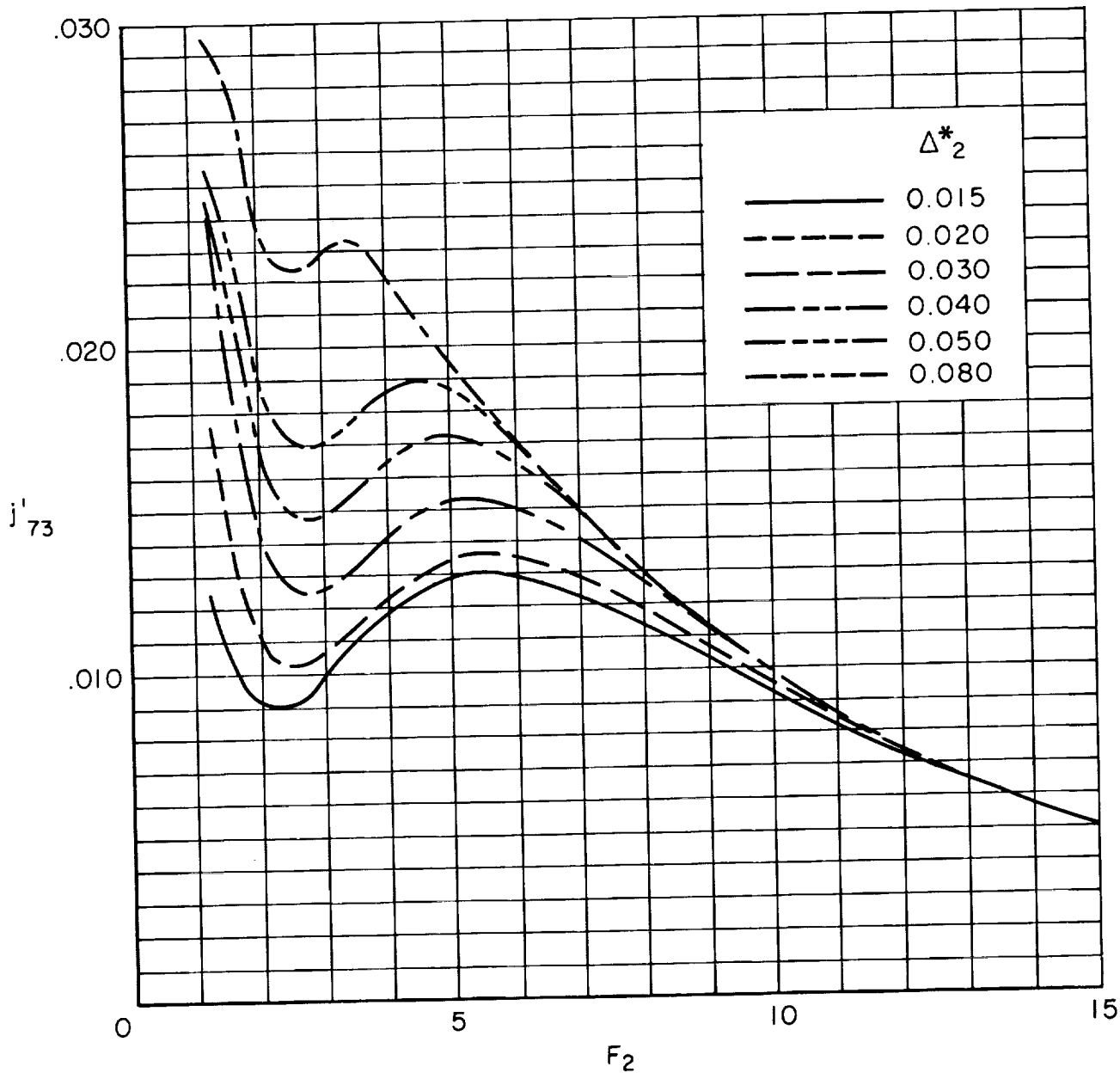

(o) j'_{73}

Figure 12. – Continued.

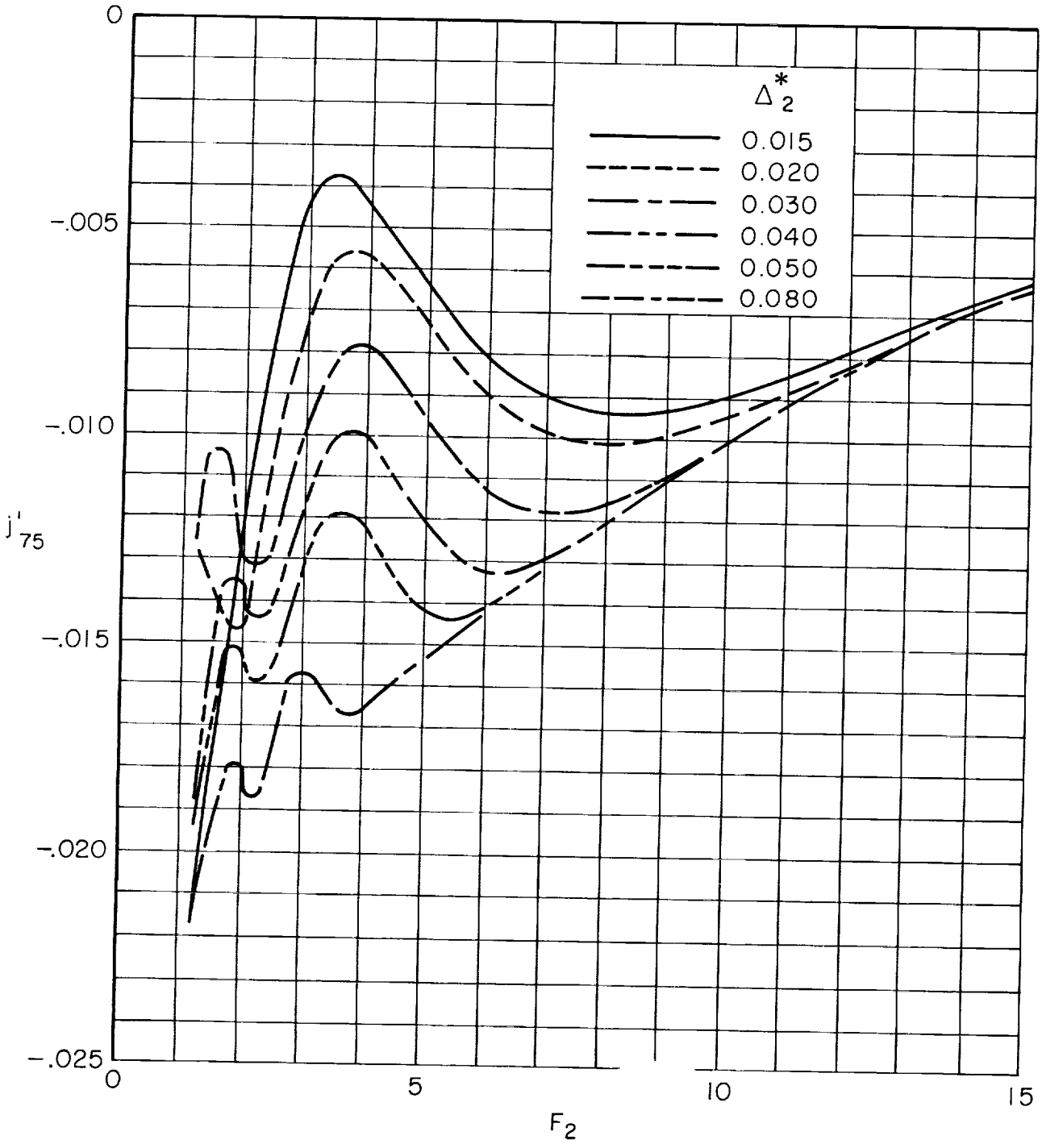

(p) j'_{75}

Figure 12. – Concluded.